Advances in Civil Engineering

Stability Analysis of Underground Rock Structures: from Design to Application

Lead Guest Editor: Hadi Hasanzadehshooiili
Guest Editors: Ali Lakirouhani, Pooya Hamdi, and Reza Mahinroosta

Stability Analysis of Underground Rock Structures: from Design to Application

Advances in Civil Engineering

Stability Analysis of Underground Rock Structures: from Design to Application

Lead Guest Editor: Hadi Hasanzadehshooiili
Guest Editors: Ali Lakirouhani, Pooya Hamdi, and Reza Mahinroosta

Contents

Hindawi
Advances in Civil Engineering
Volume 2021, Article ID 2237918, 13 pages
https://doi.org/10.1155/2021/2237918

Research Article

Parametric Evaluation of Simultaneous Effects of Damaged Zone Parameters and Rock Strength Properties on GRC

Ali Ghorbani,[1] **Hadi Hasanzadehshooiili**,[2] **and Amin Eslami**[1]

[1]*Department of Civil Engineering, University of Guilan, Rasht, Iran*
[2]*Department of Civil and Water Engineering, Université Laval, Quebec, Canada*

Correspondence should be addressed to Hadi Hasanzadehshooiili; h.hasanzadeh.shooiili@gmail.com

Received 30 April 2021; Accepted 13 August 2021; Published 29 August 2021

Academic Editor: Wei Shen

The convergence-confinement method via the ground reaction curve (GRC) is used as the common practice of tunnel design which demands accurate determination of the stress state and material strength behavior in different zones around the tunnel section. Besides, formation of the excavation/blast-induced damaged zone (EDZ/BDZ) adds more complexity to the problem due to variation of elasticity modulus of the rock mass in this zone. As a result, advanced numerical methods via finite element/difference commercial packages or user-coded, semi-numerical techniques are required to develop the GRC, which demands a high degree of proficiency and knowledge of computational plasticity and geomechanics. In this study, a new, simple, and accurate method is proposed for prediction of GRC of circular tunnels constructed in the damaged, elastoplastic rock masses obeying softening in the plastic zone. The effects of deterioration caused by the drilling/blast in the EDZ were taken into account by assuming a reduced and varying Young's modulus using the disturbance factor, in the form of Hoek–Brown failure criterion and the Geological Strength Index (GSI). Besides, effects of intermediate principal stress and the exponential decaying dilation parameter are taken into account thanks to adoption of the unified strength criterion (USC) as the material strength criteria. To do so, genetic algorithm (GA) via the method of evolutionary polynomial regression (EPR) is used to find a relationship between a number of 19 affecting parameters on the GRC as the input, and the internal support pressure as the target of prediction. Verification analysis was performed to verify the validity of the results using field measurements data as well as other advanced numerical studies found in the literature. Lastly, variation of the support pressure with simultaneous changes in the affecting input parameters was investigated using multivariable parametric study.

1. Introduction

The ground reaction curve (GRC) in the framework of convergence-confinement method (CCM) can be assumed as the most common method of tunnel design due to its simplicity while keeping the accuracy in engineering practice. The main advantages of this method lie in turning the 3-dimensional problem of tunnel's face advancement into a 2-dimensional problem by relating the distance from tunnel face to the inner pressure in GRC. Besides, a factor of safety can be estimated using the ratio between the support capacity and the load demand. The calculations can be made using closed-form solutions, numerical methods, or some combinations of each to develop the appropriate curves. However, there are some limitations in using the GRC which mainly stem from its assumptions: homogenous rock mass, isotropic stress field, circular cross section of the tunnel, and plain-strain condition [1]. In order to accurately calculate the appropriate time for the installation of support system of underground tunnels, also, to restrict the occurring deformations, the ground reaction curve (GRC) of underground openings should be correctly characterized. Development of GRC is conducted based on the required support pressure corresponding to the formation of an arbitrary convergence value. Hence, the state of stress and the material strength play a key role in the determination of such curve [2–13]. In this framework, the behavior of tunnels constructed in the rock mass is generally assessed based on the elastoplasticity

theory and the principles of convergence-confinement method [5–7, 11–14]. There are different strength criteria for the rock mass material, such as the Mohr–Coulomb [3, 8, 15, 16], the Hoek–Brown [2, 7, 10, 17], and the unified strength criterion [18–22]. To make the calculations even more accurate, the softening behavior is also taken into the consideration accounting for the variation of material strength parameters from the peak strength parameters to the residual ones (referring to the distance from the tunnel center) [4, 5, 8–10, 13, 23].

In addition of the formation of a softening zone around the tunnels, depending on the amount of blasting/excavation damage induced to the surrounding rock mass, a damaged zone will be formed. True characterization of this blast/excavated induced damage zone (BIDZ/EIDZ) is carried out based on the deterioration of material strength parameters, consideration of the variation of Young's modulus, and the weight of this zone into the problem. The effect of EDZ has been studied numerously [24–36]. However, there is limited, available solutions, which consider the effects of both softening material behavior in the plastic zone and the existence of BIDZ/EIDZ around the tunnel [26, 37–40]. To this end, complicated finite element/difference commercial packages should be adopted. User-coded, semi-numerical techniques are other possible solution approaches to the problem [4, 5, 9, 12, 15–17, 25, 37, 41–45]. Described methods need professional numerical modeling proficiency and the knowledge of computational plasticity and geomechanics. On the other hand, design engineers need a simple, efficient, and timely method for accurate prediction of GRC to make a preliminary design for their underground tunneling projects. Hence, the availability of an accurate, timely, and simple method will be a significant aid to the practitioners and design engineers.

As described, the objective of the research is to propose a new, simple, and accurate method for the prediction of GRC of circular tunnels constructed in the damaged, elastoplastic rock masses obeying softening in the plastic zone. It should be described that the adoption of appropriate material strength criteria and dilation functions are two other important parameters affecting on the developed curves. In this study, the unified strength criterion (USC) (selected to consider the effects of intermediate principal stress (b) on the strength of rock mass) and an exponential decaying dilation parameter for showing a better performance are used for the modeling purpose.

The proposed method is based on the development of an evolutionary polynomial regression (EPR) technique, which uses the best features of the genetic algorithm (GA) and the least squared method to predict new target functions based on their previous learning of the relationship between input and output parameters. In this study, as the first step, the results of previous solutions for the GRC development were gathered to generate a database using the algorithm proposed by Ghorbani and Hasanzadehshooiili [26]. Material strength parameters in elastic, plastic, and damaged states, the radius of tunnel, and all other affecting parameters along with arbitrary convergence values were considered as the input parameters. The corresponding internal support pressure, which is the target of predictions, is the output parameter. Hence, first, the problem was solved and validated for different strength and geometry parameters. As the second step, an evolutionary polynomial regression (EPR) code, available in the MATLAB environment, was used to train the neural network based on the gathered database, in order to find a mathematical model for forecasting the internal support pressure (P_i) values.

In this study, the EPR models are proposed based on the well-validated solutions of the problem of GRC development for tunnels constructed in the damaged, elastoplastic rock mass. The accuracy of the proposed model is shown through the high value of coefficient of determination (COD) and the acceptable value for the root mean squared error (RMSE). The developed model is then applied as the basis for the complementary studies. Sensitivity analysis based on the cosine amplitude method (CAM) has then shown the strength of relationship between the internal support pressure and concerning input parameters. Besides, variation of the support pressure with the simultaneous changes in the affecting input parameters is investigated using the multivariable parametric study.

The proposed evolutionary-based approach is introduced as a capable, timely, and accurate method for the prediction of the internal support pressures for the tunnels constructed in the BID/EID, elastoplastic rock mass obeying the USC criterion and showing the softening behavior in the plastic zone. In addition, the importance of material strength parameters, damaged zone's factors (D), and the tunnel's radius and their roles in the variation of support pressure is fully characterized using both sensitivity and a three-dimensional, multivariable, graphical parametric study on the input parameters.

2. Problem Definition and Methodology

A full description of the proposed algorithm along with the formulation and governing equations is presented in Ghorbani and Hasanzadehshooiili [26]. However, in this part, a summary of the procedure of stress-strain formulation, required to derive the GRC, is presented. Figure 1 illustrates definition of the problem's geometry. The tunnel has a circular section with radius of b_i, circumscribed by an isotropic elastic-plastic rock mass including the excavation/blast-induced damage zone (EDZ/BDZ). The tunnel section is under hydrostatic pressure of s_0 while its boundaries are under pressure of the internal support pressure (P_i). The radius of the plastic zone and that of the excavation damaged zone are represented by R_p and R_{EDZ}, respectively. Decreasing of the internal support pressure (P_i) results in initiation of the radial displacements. The deformations can be of either elastic or plastic type, distinguished by the critical value of the internal support pressure (P_{ic}). The deformations are considered as elastic, provided that they are formed in a pressure higher than the critical value of the support pressure (P_{ic}) [9, 10]. More decreasing of the internal support pressure leads to formation of the plastic stresses and strains, which are initiated with softening behavior and continue to a residual one. The transition

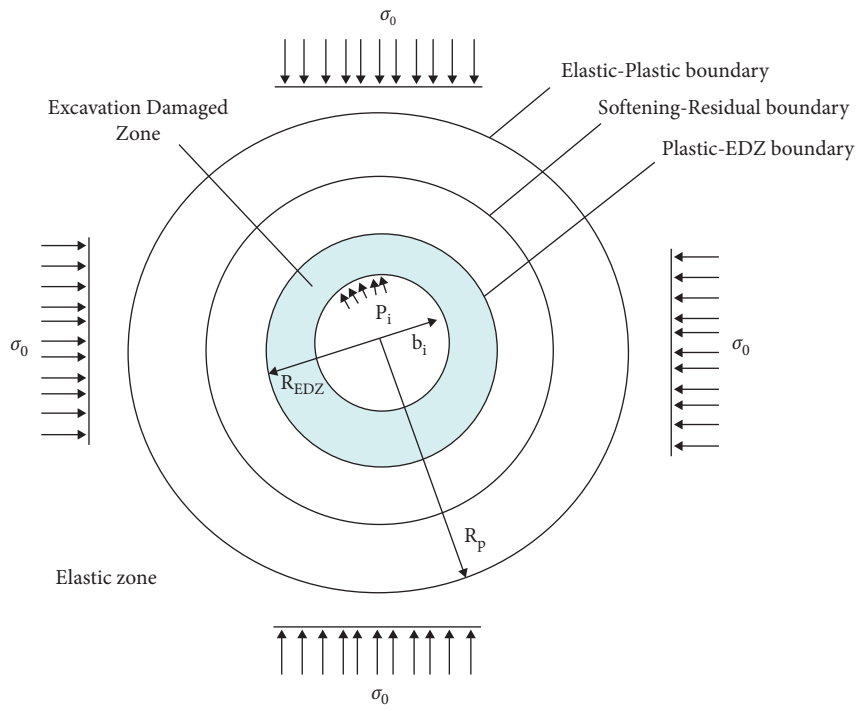

Figure 1: Problem definition.

between softening and residual behavior is governed using a parameter called the critical deviatoric plastic strain parameter (γ^{p*}) [2, 4, 9, 10, 17, 25, 46].

On the other hand, adoption of a proper plastic potential function is crucial for the progress of the plastic strains. In addition, a flow rule, which can be of either the associated or nonassociated flow rules, governs the material's plastic behavior in the plastic zone. In fact, considering an associated or nonassociated flow rule can significantly affect the material's plastic behavior in the plastic zone as the relationship between radial and tangential plastic strain increments is defined by the flow rule. In this paper, the nonassociated flow rule is put into practice to model the relationship between radial and tangential plastic strain increments.

Determination of the P_{ic} is dependent on the utilized strength criteria, such that it can be obtained by a closed-form solution in the case of linear Mohr–Coulomb strength criterion [5] or by numerical solution via the Newton–Raphson algorithm in the case of Hoek–Brown criterion [9, 10, 47] as well as the unified strength criterion (USC) [26].

In this study, the unified strength criterion (USC) is put into practice to obtain the P_{ic} using the Newton–Raphson method. Adoption of USC was due to its advantage in tracking the principal stress-strain incremental paths in a nonlinear way, which yields more accurate results in prediction of the rock mass behavior [2, 4, 10, 47, 48]. Moreover, using USC makes it possible to take the effect of the intermediate principal stress (b), which is believed to have a significant effect on the radius of the EDZ [19–21].

The EDZ is developed by approaching the tunnel's face. The radial stresses within the plastic-EDZ boundary are found numerically using the Runge-Kutta-Fehlberg (RKF) method [49] which also governs the stages of the solution. The problem is considered in the plastic zone provided that the radial stress is larger than the plastic-EDZ boundary's radial stress, (s_r^{P-E}). However, for the radial stress values lower than the (s_r^{P-E}), the output of the last step is used as the initial condition to obtain a new solution for the EDZ.

Calculation of the stresses and strains in different points around the tunnel boundary is made using different methods depending on which zone/boundary they are located. Figure 2 presents the different zones formed around the tunnel section area. In this problem, there are three main types of boundaries with different calculation approaches:

(1) The elastic-plastic boundary (=outer plastic boundary) which is represented by the radius of plastic zone (R_p).

(2) The outer boundary of the EDZ (=inner plastic boundary).

(3) The inner boundary of the EDZ (=tunnel surface).

In order to calculate the stresses and strains of the points located in the elastic-plastic boundary, the Newton–Raphson (NR) method of root finding is used to calculate the radial stress ($\sigma_r = s_R$), which is also equal to the critical support pressure (P_{ic}). The stresses located on the outer boundary of the EDZ are calculated using the Runge-Kutta-Fehlberg (RKF) method. On the elastic-plastic boundary, i.e., the external boundary of the plastic zone, the radial stress (s_r) is equal to s_R and is also equal to the critical support pressure (P_{ic}). Besides, on the internal plastic boundary, i.e., the plastic-EDZ boundary, the stresses are calculated using the Runge-Kutta-Fehlberg (RKF) method.

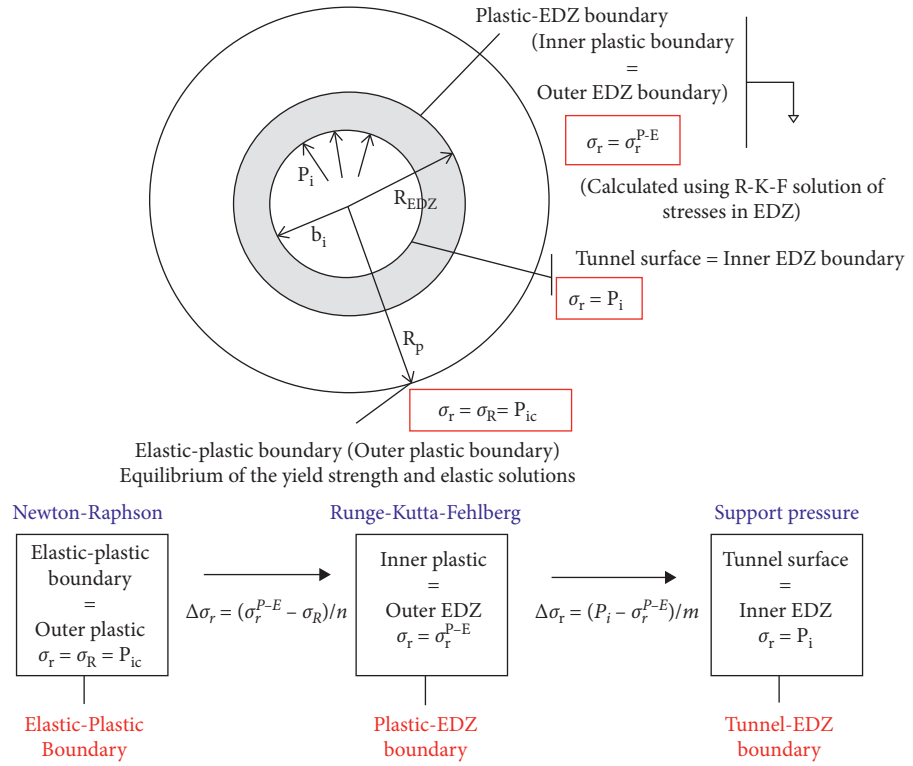

FIGURE 2: Stresses at different regions and boundaries, after Ghorbani and Hasanzadehshooiili [26].

Lastly, the radial stress on the inner boundary of the EZD is equal to the tunnel's support pressure (P_i).

The stresses are first calculated on the boundaries to be used as the initial values for the rest of areas between the boundaries. Lee and Pietruszczak [9] calculated the radial stress within the plastic zone area assuming a linear variation for the radial stress from its initial value at $r = R_p$, $s_r = s_R$ to its value on the tunnel surface $r = b_i$, $s_r = P_i$, considering a rock mass with elastic-plastic material.

In this study, in summary, the following procedure has been taken for analysis of the plastic zone: first, the Runge-Kutta-Fehlberg method is put into practice to determine the radial stress on the on the plastic-EDZ boundary (s_r^{P-E}). The region is separated into two zones, namely, the plastic zone and the EDZ. The stresses within the plastic zone can be calculated using the predetermined stresses on the boundaries as the priori, i.e., s_R (the radial stresses on the elastic-plastic boundary) and s_r^{P-E} (the radial stress on the plastic-EDZ boundary). Besides, the stresses and strains within the EDZ are calculated using the known radial stress on the plastic-EDZ (s_r^{P-E}) and the tunnel surface (P_i). In order to perform the calculations, the plastic and EDZ are divided into m and n number of zones, respectively. Thickness of each annulus is determined so that the corresponding governing equation of equilibrium is satisfied.

The most important distinction of consideration of the EDZ into the problem is to assume a reduced and varying Young's modulus for this zone rather than a constant one, to take the effects of gradual deterioration caused by the drilling/blast around the tunnel. Herein, the relationship by Hoek and Diederichs [50] was used to calculate Young's modulus on the tunnel surface:

$$E_m' = 100000\left(\frac{1 - (D'/2)}{1 + e^{(75+25D'-GSI')/11}}\right), \quad (1)$$

where D' is the disturbance factor, in the form of Hoek–Brown failure criterion and GSI is the Geological Strength Index. The "prime" superscript denotes that the parameter belongs to the excavation damaged zone (EDZ). The disturbance factor was assumed to be zero ($D' = 0$) for calculation of Young's modulus in the plastic-EDZ boundary [51]. Assuming a linear interpolation between the values of Young's modulus at the plastic-EDZ boundary and the tunnel surface, Young's modulus within the different radiuses of the EDZ was calculated using the following equation [51]:

$$E_{(j)}' = E_0' + \frac{E_m' - E_0'}{R_{EDZ}}\left[\left(\rho_{(j)}' \times R_{EDZ}\right) - b\right], \quad (2)$$

where $E_{(j)}'$, E_0' E_m' represent Young's modulus of j^{th} annulus in the EDZ, on the plastic-EDZ boundary ($D' = 0$), and on the tunnel's surface (with a proper value for the disturbance factor), respectively. $\rho_{(j)}'$ is the radius of the j^{th} annulus normalized by R_{EDZ} and b is the parameter of the intermediate principal stress. Figure 2 illustrates a summary of the procedure to find the stresses and strains in different zones/boundaries around the tunnel. Furthermore, Figure 3 represents the algorithm proposed by Ghorbani and Hasanzadehshooiili [26] which was used in the calculation of

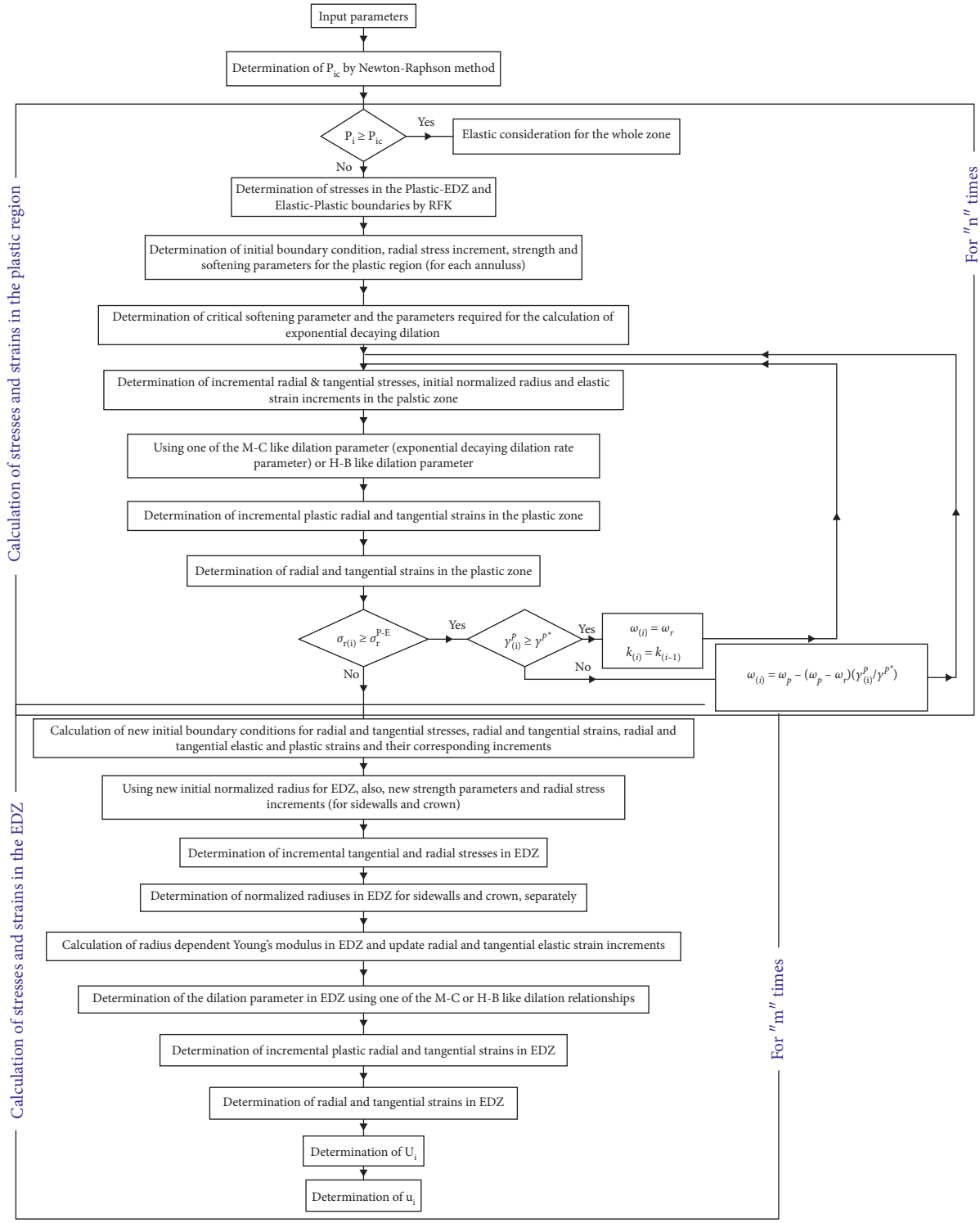

Figure 3: The algorithm used in generation of the database of GRCs used in this study. After Ghorbani and Hasanzadehshooiili [26].

the support pressure (P_i) to generate the database of GRCs used in this study.

3. Developing a Relationship

3.1. Gathering Database for Model Development. The first step in finding a relationship for the GRC is to gather a database among the available sources to be used as training data for the neural network. Each GRC is constructed by a number of input-output datasets. The value of the internal support pressure (P_i) was taken as the target of prediction, which is function of different input parameters. Ghorbani and Hasanzadehshooiili [26] proposed a comprehensive algorithm for determination of GRC for circular tunnels in

elastoplastic rock mass considering the EDZ and softening behavior. Besides, they utilized the unified strength criteria (USC) so that the effect of intermediate principal stress (b) and the exponential decaying dilation behavior can be taken into consideration. In order to verify and validate the proposed algorithm, they used a wide range of different sources including different GRCs under various conditions. In this study, the same data sources used in Ghorbani and Hasanzadehshooiili [26] were gathered as the database and then were used as the training data in the evolutionary polynomial regression (EPR) via the framework of genetic algorithm (GA). The summary of the data sources is as follows: a case of field measurements regarding the Hanlingjie tunnel in Hunan, China, at a depth of 146 m [17], two cases of Elastic-plastic rock mass considering strain softening [4, 9], a case of strain softening rock mass considering exponential decaying post-peak dilation parameter [52], and a case of elastic-perfect-plastic behavior of a rock mass considering EDZ [43]. Besides, Ghorbani and Hasanzadehshooiili [26] utilized the problem originally solved by Zareifard and Fahimifar [43] in order to cover the effects of new features of their proposed algorithm, such as the effects of the intermediate principle stress (b), the weight of the damaged rock mass and existence of a softening zone, and the exponential decaying dilation behavior. The data regarding these newly solved problems were also added to the database. All in all, a list of the input parameters included in the database along with their range of variation is presented in Tables 1 and 2, respectively.

3.2. Sensitivity Analysis. The cosine amplitude method (CAM) can be used to find the strength of relationship between two parameters [25, 53]. Herein, this method is used to determine the degree of importance of each of the 19 input parameters in variation of the target (output) parameter, which is the internal support pressure (P_i).

All the data pairs (each of the input parameters pairing with the target parameter) would form an X-array, such as $X = \{x_1, x_2, x_3, \ldots, x_i, x_n\}$ where each element, x_i, is a vector of the length of m:

$$x_i = \{x_{i1}, x_{i2}, x_{i3}, \ldots, x_{im}\}. \tag{3}$$

By defining each parameter as dimensionless normalized vectors, the strength of relationship between the input and target parameters is given by

$$r_{ij} = \frac{\left|\sum_{k=1}^{m} x_{ik} x_{jk}\right|}{\sqrt{\left(\sum_{k=1}^{m} x_{ik}\right)\left(\sum_{k=1}^{m} x_{jk}\right)}}, \quad \text{where } i, j = 1, 2, \ldots, n, \tag{4}$$

where x_{ik} and x_{jk} are the normalized vectors of the input and target parameter and r_{ij} denotes the strength of relationship which would take a value between 0 and 1, where 0 implies no relationship and 1 shows the highest relationship. The name of this method, CAM, is taken from the fact that the result of the inner product of two vectors would be 0 if they are orthogonal vectors (meaning there is no relationship between them), while the result would be 1 if the two vectors are codirectional (meaning full relationship). It should be noted that the convergence (displacement) value was omitted from this analysis since it is as a fictional input parameter to the GRC.

The results of CAM analysis are presented in Figure 4. As can be seen, there are numerous parameters with relatively high contribution in the GRC. According to the results, the in situ hydrostatic pressure (s_0) as well as the geometry of the tunnel (radius of the tunnel b_i) presents a high strength of relationship in GRC. Interestingly, the properties of the excavation damaged zone make equal or even relatively higher contribution in the internal support pressure (P_i) than those of the intact rock mass. In fact, m', s', and a' (the constant parameters of the Hoek–Brown failure criterion taken for the EDZ) with 77.9, 78.9, and 75.1% of contribution, the range of Young's modulus assumed for the EDZ (E_i', E_0') with 78.3 and 77.8%, and the extent of formation of the EDZ (R_{EDZ}) with 75.4 as well as its disturbance factor (D) with 75.5% of contribution are placed amongst the most important parameters in the GRC. This highlights the importance of considering the EDZ in design of tunnel as well as taking proper values for the material's stiffness and strength of this zone.

On the other hand, the properties of the intact rock mass (E, ν, m_{i}, GSI_p) have shown 77.1, 72.4, 69.1, and 76.5% of strength relationship, respectively. In contrast, the softening parameters (φ_p, φ_r, γ^p, and γ^{p*}) made the least strength of relationship with 9.8–37.2%. Besides, it can be inferred that the role of material properties parameters of the rock mass and the EDZ is shown to be more meaningful in the value of support pressure, compared to that of the intermediate principal stress (b).

3.3. Evolutionary Polynomial Regression (EPR). In this study, the genetic algorithm (GA) via the evolutionary polynomial regression (EPR) method is used to make a correlation between a number of 19 affecting parameters on the ground reaction curve (GRC), as the input parameters, and the internal support pressure of the tunnel (P_i), as the output parameter, i.e., the target of prediction. This method has successfully been used in developing mathematical models in different applications, especially in civil engineering [25, 54–61].

Evolutionary polynomial regression (EPR), developed by Giustolisi and Savic [62], is known as a hybrid data-driven method. This method takes advantage of optimization in fitness to training data, yet by keeping the efficiency of mathematical expression, which is thanks to using a multiobjective search algorithm to establish multiple models. Hence, various optimal models are compared to pick the best fit such that the governing pattern can be created in a timely manner [63]. EPR applies different functions, components, forms, number of terms, and gens to present models in logarithmic, exponential, trigonometric, and inverse trigonometric sentences simultaneously by minimizing the error of prediction.

In this study, the EPR was implemented in MATLAB environment. EPR provides a multiobjective genetic

Table 1: List of affecting parameters on the GRC included in the database.

b_i	Radius of the tunnel	m'	Material constant of the EDZ
N	Poisson ratio of the rock mass	s'	Material constant of the EDZ
m_i	Material constant of intact rock	a'	Material constant of the EDZ
σ_0	In situ hydrostatic confining pressure	γ^p	Strain softening parameter
GSI_p	Peak Geological Strength Index of the rock mass	E_i'	Young's modulus in the inner annulus of the EDZ
D	Disturbance factor	E_0'	Young's modulus in the outer annulus of the EDZ
E	Young's modulus of rock mass	R_{EDZ}	Radius of the excavation-induced damaged zone
ϕ_p	Peak friction coefficient	b	Intermediate principal stress parameter
ϕ_r	Residual friction coefficient	U_i	Convergence (displacement)
γ^{p*}	Critical deviatoric plastic strain parameter	P_i	Internal support pressure

Table 2: Range of variation of input and output parameters of the database.

Parameter	$b_i^{(m)}$	ν	m_i	$\sigma_0^{(MPA)}$	GSI_p	D	$E^{(MPa)}$	ϕ_p	ϕ_r	γ^{p*}
Max.	5.5	0.35	17.7736	30	50	0.6	5500	12	5	1
Min.	5	0.25	10	4.8	41.88	0.6	4000	0	0	0
STD.	0.14	0.03	2.25	7.30	2.35	0.00	434.79	3.51	1.63	0.25
Mean	5.05	0.26	10.72	27.67	49.25	0.60	5361.11	1.51	0.82	0.07
Parameter	m'	s'	a'	γ^p	$E_i'^{(MPA)}$	$E_0'^{(MPA)}$	$R_{EDZ}^{(m)}$	b	$U_{i(m)}$	$P_i^{(MPA)}$
Max.	0.8	0.001	0.527	30	3800	5500	8	1	0.439184	7
Min.	0.428	$3.95E-05$	0.5	0	277.18	1257.18	6.5	0	0.021	0
STD.	0.11	0.00	0.01	14.16	1053.54	986.46	0.37	0.35	0.06	2.60
Mean	0.77	0.00	0.50	10.43	3313.98	3784.92	7.14	0.21	0.09	3.00

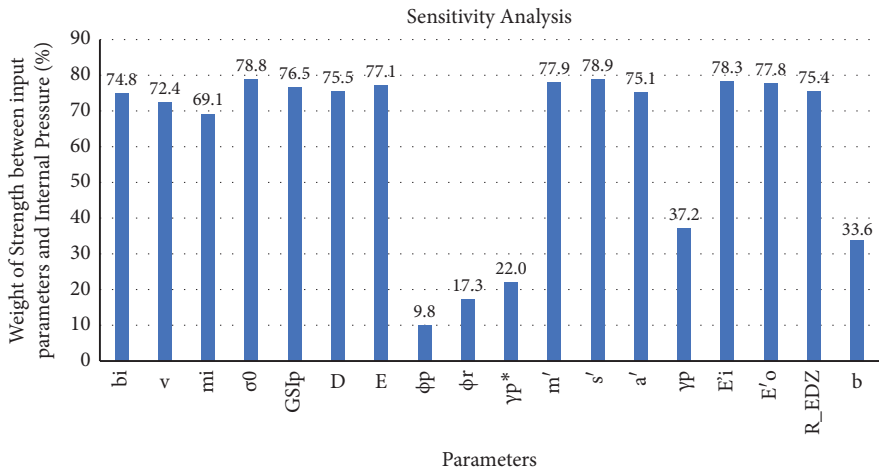

Figure 4: Results of sensitivity analysis using CAM.

algorithm (MOGA) strategy in order to increase the regression's parsimony.

This strategy performs optimization of the model based on minimization of the number of inputs, number of terms, the error of prediction, or any combination of them. Herein, in order to maximize the model's parsimony, the optimization was made with the target of least possible number of inputs and number of terms, along with the least sum of squared errors (SSE). Therefore, amongst the 19 input parameters, a number of 7 parameters (m_i, GSI^p, E, s', a', γ^{p*}, E_i') were automatically excluded from the model. This is probably because such parameters are interdependent variables where their effect can be incorporated by other parameters. The program automatically removes the less important or interdependent variables to increase the model's parsimony via a procedure of trial and error to find the most efficient parameters to be used in the model. Also, as some parameters have similar effects on the GRC, it is believed that the program relies on the variation of P_i with some of them aiming at accurate predictions. Although some of the deleted parameters are still important to the problem, the remaining parameters with similar natures were enough to predict different values of P_i based on the concerning input parameters for the whole range of studied input parameters. As the proposed relationship is efficient for the development of GRCs of rock masses with input parameters, which lie in the range of parameters studied in this paper, some other deleted parameters may be still required for the

representation of a new formula for other input ranges (useful for other stress, and material states/strength values). Hence, it is suggested to employ the proposed relationship for cases with adequate consistencies to the problem defined in this paper. Numerous functions in various forms were examined to find a relationship with the highest parsimony. The final relationship to predict the internal support pressure (P_i) of the tunnel is presented by the following equation:

$$\begin{aligned} P_i\,(\mathrm{MPa}) = {} & 1.3746\times10^{-11}\left[\left(\nu^{-2}\right)\left(\sigma_0^3\right)\left(D^{-1}\right)\left(m'\right)\right. \\ & \left.\cdot\left(R_{\mathrm{EDZ}}^3\right)\left(U_i^{-3}\right)\right] \\ & -3.431\times10^{-9}\left[\left(\varphi_p^{-0.5}\right)\right]+0.00056024 \\ & \times\left[\left(\varphi_r^{-0.25}\right)\left(R_{\mathrm{EDZ}}^{-0.25}\right)\right] \\ & -3.9274\times10^{-6}\left[\left(\varphi_r^{-0.25}\right)\left(b^{0.75}\right)\left(U_i^{-1}\right)\right] \\ & +1.704\times10^{-13}\left[\left(\gamma^{p^{-0.5}}\right)(b)\left(U_i^{-3}\right)\right] \\ & -3.2565\times10^{-10}\left[(b_i)\left(\nu^{-1}\right)\left(\sigma_0^3\right)\left(E_0^{'0.5}\right)\right. \\ & \left.\cdot\left(R_{\mathrm{EDZ}}^{-1}\right)\left(U_i^{-3}\right)\right]+0.16224. \end{aligned} \tag{5}$$

Figure 5 illustrates a comparison of the predicted values of the support pressure verses the original values existing in the database. The quality of regression can be assessed by statistical measurements such as the coefficient of determination (COD = R^2), the sum of squared errors (SSE), and the mean of squared errors (MSE). The COD was obtained as 90.33% which shows the good performance of the obtained mathematical model. Moreover, the SSE and MSE are obtained as 0.63% and 0.58%, respectively, verifying the decent precision of the proposed model. However, as Figure 5 suggests, the error of prediction mostly occurred in the range of support pressure less than 3 MPa. Therefore, it can be inferred that the model gives the best results in the range of 3–8 MPa, which is also the most common range of support pressure in practice.

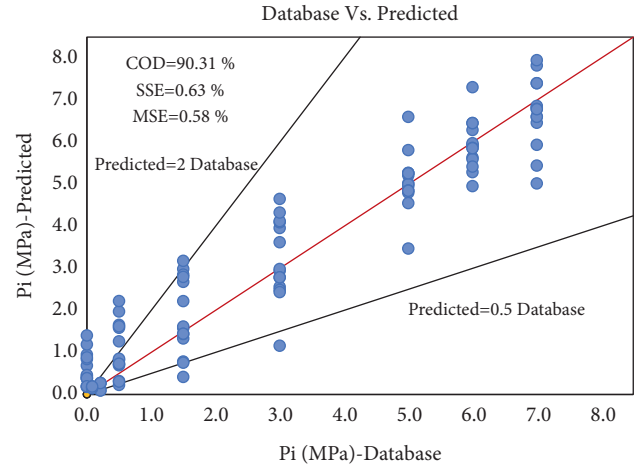

Figure 5: Comparison of the predicted support pressure with those of the database.

Table 3: Values of the parameters used in the verification analysis.

Parameter	Zou et al. [17]	Lee and Pietruszczak [9]
b_i (m)	5.5	3
ν	0.35	0.25
m_i	17.77	5.88
s_0 (MPa)	4.8	15
GSI_p	41.88	55.25
D	0.6	0.6
E (MPa)	4000	5700
ϕ_p	12	15
ϕ_r	5	5
γ^p	0.008	0.01
m'	0.428	0.6
s'	$3.95E-05$	0.002
a'	0.527	0.5
γ' (kN/m^3)	28.65	2.5
E_i' (MPa)	277.18	5700
E_0' (MPa)	1257.18	5700
R_{EDZ}	7.5	4
b	0, 0.5, 1	0.5

3.4. Verification and Comparison. In order to verify the validity of the obtained equation (equation (5)), a verification analysis was performed using two sets of available data in the literature. The first case was the results of field measurements at the crown of Hanlingjie tunnel in Hunan, China, reported by Zou et al. [17]. The tunnel is located at the depth of 146 m with the radius of 5.5 meters. It should be noted that some of the required data were back-calculated using proper relationships and correlations found in the literature, due to lack of data, especially regarding the EDZ. Moreover, the effect of intermediate principal stress was also investigated by varying parameter (b) in the range of 0–1. Table 3 presents a summary of the used parameters and Figure 6 depicts the results of calculations in the form of variation of radial displacements (U_i) against the internal support pressure. As can be seen, a meaningful consistency is observed as the required support pressure to restrict the displacement to a defined value can be acceptably predicted by the proposed relationship. It should be noted that some damaged parameters were not specified in this real case and the required values are calculated based on the available relationships. Therefore, the accuracy of predictions can be even higher while accessing to all the required in-field/laboratory measured parameters.

The second case is the study by Lee and Pietruszczak [9], in which the effect of strain softening was taken into account for the problem of circular tunnel in an elastic-plastic rock mass. The effects of EDZ and the intermediate principal stress were not considered in Lee and Pietruszczak [9]. Therefore, the proposed relationship is more practical for the cases of elastic-plastic-EDZ rock masses with strain softening in the plastic region. Hence, equivalent damaged parameters must be calculated prior to the analysis since the original studied case did not consider the occurred damaged zones. In this regard, damaged zone parameters are assumed to be identical to the residual zone parameters and the radius of the damaged zone is assumed to be 1 m (according to the

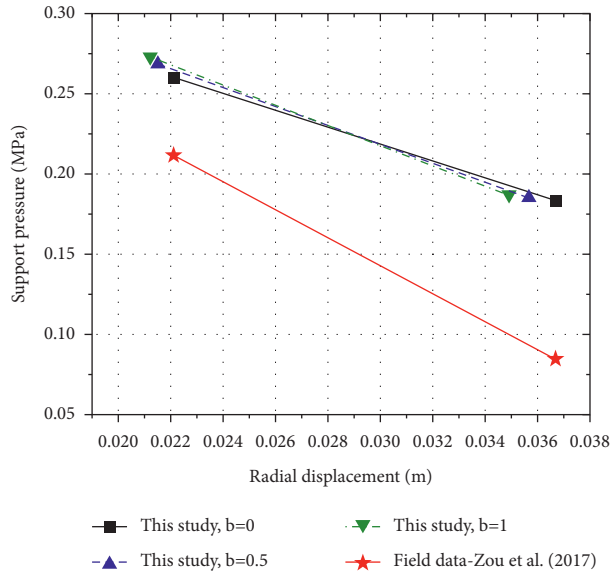

Figure 6: Verification analysis using field measurements data reported by Zou et al. [17].

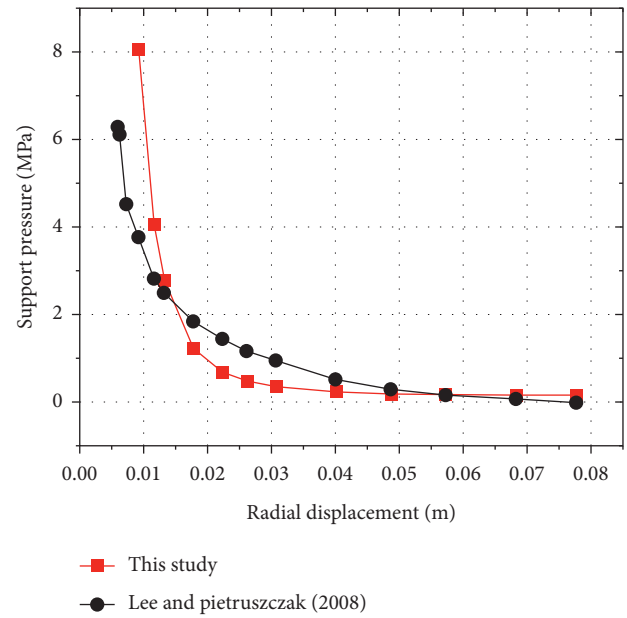

Figure 7: Comparison of the results in this study with Lee and Pietruszczak [9].

values proposed in the literature). Other affecting and missing parameters are calculated using the relationships presented in Ghorbani and Hasanzadehshooiili [26]. The parameters used in this analysis are presented via Table 3 while Figure 7 depicts the results of comparison. As can be seen, a good consistency is observed between two studies which shows the strength and validity of the obtained equation by evolutionary polynomial regression (EPR) in this study while keeping simplicity and ease of use. This is important as the obtained equation can be used as a robust tool in the preliminary stages of design and construction in engineering practice by considering the state-of-the-art features of the problem such as strain softening, the intermediate principal stress, and the degradation caused by excavation damaged zone in the problem.

4. Multiple-Variable Parametric Study

In this part, using the obtained relationship (equation (5)), a multivariable parametric study is conducted to investigate the simultaneous effects of various parameters such as the extent of excavation damage zone (R_{EDZ}) as well as its properties such as Young's modulus at the EDZ-plasticity boundary and the constant parameter of m' on the ground reaction curve. Besides, the effect of the intermediate principal stress parameter (b) is investigated. Such analysis is also helpful in verifying the obtained formula, by illustrating its sensitivity to variation of different parameters. In order to perform this analysis, all the variables were assumed to be constant equal to their default values, except the one being investigated.

4.1. Effects of R_{EDZ} on GRC. Figure 8 shows the effect of considering different values for the extent of the excavation damaged (EDZ) zone on the GRC by varying the R_{EDZ} between 6.5 and 8 meters. The same figure is represented in two different views for better observation. As can be seen, the internal support pressure (P_i) increases with increase of the R_{EDZ}. However, a critical boundary can be identified for displacements (obtained as 5–7 cm in this case), above which the R_{EDZ} has no effect on the internal support pressure.

Conversely, in the case of restricting the tunnel's convergence to displacements lower than the critical boundary value (5–7 cm), the effect of R_{EDZ} will be more considerable. In fact, this is implying that the effects of the extent of the damaged zone around the tunnel can be neglected provided that the installation time of the support system can have an enough delay, and the associated displacements are higher than the critical value. On the contrary, a special consideration should be paid to the extent of the damaged zone where only low displacements are allowed for the support system.

4.2. Simultaneous Effects of E_0' and R_{EDZ}. Figure 9 is presented to investigate the effects of both the extent of the damage zone (R_{EDZ}) and its strength properties, simultaneously. This figure shows the ground reaction curve with regard to the different radius of the damaged zone while three different values are taken for the elasticity modus at the EDZ-plastic boundary (E_0'), namely, 1257, 3800, and 5500 MPa. As depicted, with increasing E_0', GRC drops. As can be seen, (4–6) cm is a critical boundary value for the tunnel's convergence. For all cases, a higher internal pressure is needed to restrict displacements to values lower than 4 cm. The required internal support pressure increases for higher radiuses of the damaged zone. Such value will be even higher for a rock medium with lower E_0'. On the other hand, the effect of E_0' on the GRC decreases as the tunnel's

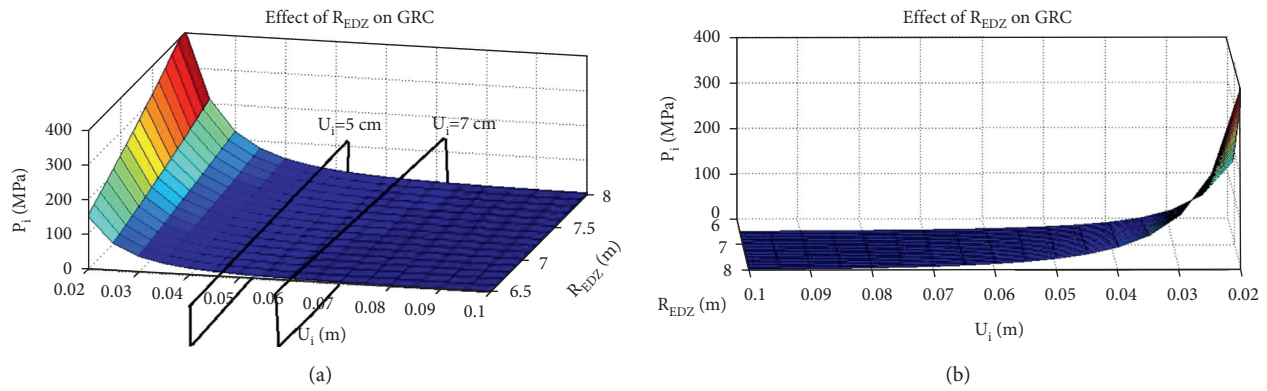

Figure 8: Effect of R_{EDZ} on GRC: (a) first view, (b) second view.

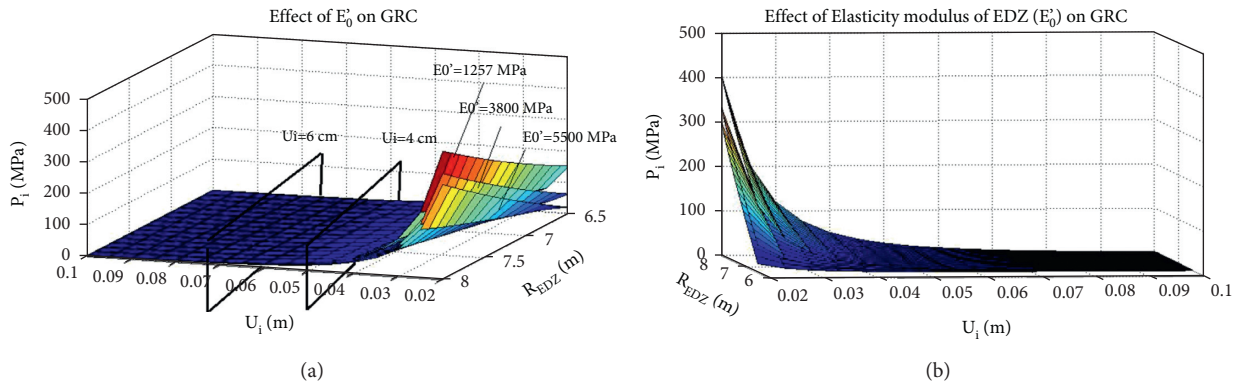

Figure 9: Effect of variation of Young's modulus of the EDZ on the GRC: (a) first view, (b) second view.

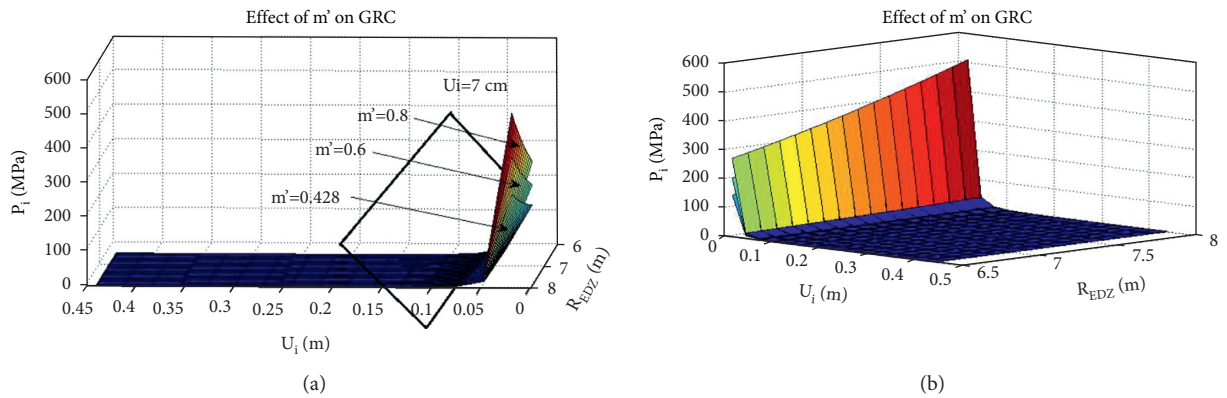

Figure 10: Effect of variation of m' on the GRC: (a) first view, (b) second view.

displacement increases. Indeed, for displacements higher than (4–6) cm, effects of E_0' on the GRC will be negligible.

4.3. Simultaneous Effects of m' and R_{EDZ}. Figure 10 presents the simultaneous effect the extent of the excavation damage zone (R_{EDZ}) and m' which represents the material's constant of the excavation damaged zone. m' was varied by taking three values: $m' = 0.428$, 0.6, and 0.8 regarding the values available in the database. It can be said the GRC is sharply surged by increasing m' even by small steps, leading to severe increase of the support pressure. This verifies the high contribution of the EDZ properties on the ground reaction curve of tunnel, as already suggested by the CAM analysis. Besides, the boundary value of the convergence is found to be 7 cm, after which the GRC would be constant.

4.4. Simultaneous Effects of b (the Roll of Intermediate Principal Stress) and R_{EDZ}. Figure 11 is presented to show the simultaneous effect of the intermediate principal stress (b)

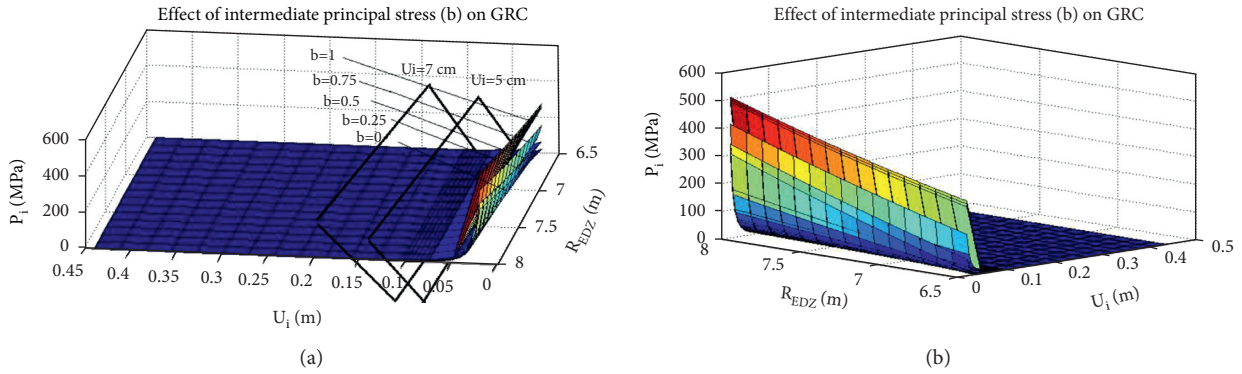

Figure 11: Effect of intermediate principal stress and R_{EDZ} on the GRC: (a) first view and (b) second view.

and R_{EDZ} on the GRC. For this purpose, the intermediate principal stress factor was varied between 0 and 1 taking five values in the steps of 0.25. As can be seen, the critical boundary value of convergence is (5–7) cm. Besides, it can be inferred that the value of b has a significant effect on the GRC, such that ignoring this parameter leads to overestimation of displacements and an overdesign supporting system, consequently. Similarly, increasing b-values result in decreasing displacements.

5. Conclusion

In this study, an attempt was made to present a simple, yet accurate and comprehensive method using the genetics algorithms (GA), to construct the ground reaction curve (GRC) of circular tunnels in elastoplastic rock mass considering the state-of-the-art feature of the problem including strain softening, effect of excavation damaged zone (EDZ), the effect of principal stress parameter, and the exponential decaying dilation behavior via the unified strength criterion (USC) framework as the material strength criteria. Incorporating such advanced issues into the problem usually demands advanced numerical analysis in a time-consuming procedure and a high level of knowledge of rock mechanics, constitutive models, etc. The results of this study can be beneficial in the preliminary stages of tunnel design in a simple, yet accurate and comprehensive manner.

A database was gathered from the available data sources available in the literature including various tunnels in different conditions with different assumptions. Besides, the database was enriched by adding some new advanced features such as the effect of the intermediate principal stress, weight of EDZ, and the exponential decaying dilation parameter obtained by a newly developed algorithm. A relationship was produced using evolutionary polynomial regression (EPR) technique, which uses the best features of the genetic algorithm (GA) and the least squared method to predict new target functions based on their previous learning of the relationship between input and output parameters. This relationship can be used, via a design spreadsheet, for preliminary design of the supporting system of the tunnel in a timely manner and high accuracy. Validity of the results was confirmed using verification against field measurements data and comparison to other advanced numerical solutions. Sensitivity analysis of the database using the cosine amplitude method showed firstly the importance of taking EDZ into account in the design procedure and secondly choosing proper values for stiffness and strength of this zone. Besides, a multivariable parametric study was performed to show the simultaneous effects of the extent of excavation damage zone (R_{EDZ}) and taking proper properties such as m' (material's constant for the EDZ) and E' (Young's modulus of the EDZ) for this zone on the GRC. In addition, the effect of intermediate principal stress on the GRC was significant, such that ignoring this parameter results in an overdesign supporting system. The boundary values of the tunnel convergence were obtained 5–7 cm for the R_{EDZ}, 4–6 cm for Young's modulus of the EDZ-plasticity boundary (E_0'), 7 cm for the material constant of EDZ (m'), and 5 cm for the intermediate principal stress (b). Most importantly, the boundary value of the tunnel convergence showed a relatively strong dependency on the extent of EDZ. Therefore, in case of restricting convergence conditions, i.e., where a small value of tunnel convergence (lesser than the aforementioned boundary values) is desired for the tunnel, the radius of the excavation damaged zone (R_{EDZ}) should be determined with cautious.

Last but not least, it should be remembered that the method originated from the ground reaction curve in the framework of the confinement convergence method. Therefore, the same assumptions and limitations are applied, as mentioned above (homogenous rock mass, isotropic stress field, circular cross section of the tunnel, plain-strain condition, and neglecting the gravity forces). Besides, the rock quality should be in the same range with the values considered in this study (medium quality rock mass) and the small strain condition is applied.

Data Availability

The data that supported the findings of this study are available on request from the corresponding author.

Conflicts of Interest

The authors declare that they have no conflicts of interest.

References

[1] D. L. Álvarez, "Limitations of the ground reaction curve concept for shallow tunnels under anisotropic in-situ stress conditions," Master's thesis, The Royal Institute of Technology—KTH, Stockholm, Sweden), 2012.

[2] L. Alejano, E. Alonso, A. Rodriguez-Dono, and G. Fernandez-Manin, "Application of the convergence-confinement method to tunnels in rock masses exhibiting Hoek-Brown strain-softening behaviour," *International Journal of Rock Mechanics and Mining Sciences*, vol. 47, no. 1, pp. 150–160, 1997.

[3] L. R. Alejano, A. Rodriguez-Dono, E. Alonso, and G. Fdez-Manín, "Ground reaction curves for tunnels excavated in different quality rock masses showing several types of post-failure behaviour," *Tunnelling and Underground Space Technology*, vol. 24, no. 6, pp. 689–705, 2009.

[4] E. Alonso, L. R. Alejano, F. Varas, G. Fdez-Manin, and C. Carranza-Torres, "Ground response curves for rock masses exhibiting strain-softening behaviour," *International Journal for Numerical and Analytical Methods in Geomechanics*, vol. 27, no. 13, pp. 1153–1185, 2003.

[5] E. T. Brown, J. W. Bray, B. Ladanyi, and E. Hoek, "Ground response curves for rock tunnels," *Journal of Geotechnical Engineering*, vol. 109, no. 1, pp. 15–39, 1983.

[6] C. Carranza-Torres, "Elasto-plastic solution of tunnel problems using the generalized form of the Hoek-Brown failure criterion," *International Journal of Rock Mechanics and Mining Sciences*, vol. 41, no. 1, pp. 1–11, 2004.

[7] C. Carranza-Torres and C. Fairhurst, "The elasto-plastic response of underground excavations in rock masses that satisfy the Hoek-Brown failure criterion," *International Journal of Rock Mechanics and Mining Sciences*, vol. 36, no. 6, pp. 777–809, 1999.

[8] Z. Guan, Y. Jiang, and Y. Tanabasi, "Ground reaction analyses in conventional tunnelling excavation," *Tunnelling and Underground Space Technology*, vol. 22, no. 2, pp. 230–237, 2007.

[9] Y.-K. Lee and S. Pietruszczak, "A new numerical procedure for elasto-plastic analysis of a circular opening excavated in a strain-softening rock mass," *Tunnelling and Underground Space Technology*, vol. 23, no. 5, pp. 588–599, 2008.

[10] K.-H. Park, B. Tontavanich, and J.-G. Lee, "A simple procedure for ground response curve of circular tunnel in elastic-strain softening rock masses," *Tunnelling and Underground Space Technology*, vol. 23, no. 2, pp. 151–159, 2008.

[11] S. K. Sharan, "Elastic-brittle-plastic analysis of circular openings in Hoek-Brown media," *International Journal of Rock Mechanics and Mining Sciences*, vol. 40, no. 6, pp. 817–824, 2003.

[12] S. K. Sharan, "Exact and approximate solutions for displacements around circular openings in elastic-brittle-plastic Hoek-Brown rock," *International Journal of Rock Mechanics and Mining Sciences*, vol. 42, no. 4, pp. 542–549, 2005.

[13] M. R. Zareifard, "Ground response curve of deep circular tunnel in rock mass exhibiting Hoek-Brown strain-softening behaviour considering the dead weight loading," *European Journal of Environmental and Civil Engineering*, pp. 1–31, 2019.

[14] Q. Jiang, X. Liu, F. Yan, Y. Yang, D. Xu, and G. Feng, "Failure performance of 3DP physical twin-tunnel model and corresponding safety factor evaluation," *Rock Mechanics and Rock Engineering*, vol. 54, no. 1, pp. 109–128, 2021.

[15] K. H. Park, "Large strain similarity solution for a spherical or circular opening excavated in elastic-perfectly plastic media," *International Journal for Numerical and Analytical Methods in Geomechanics*, vol. 39, no. 7, pp. 724–737, 2015.

[16] M. R. Zareifard and A. Fahimifar, "Elastic–brittle–plastic analysis of circular deep underwater cavities in a Mohr-Coulomb rock mass considering seepage forces," *International Journal of Geomechanics*, vol. 15, no. 5, Article ID 04014077, 2015.

[17] J.-f. Zou, C. Li, and F. Wang, "A new procedure for ground response curve (GRC) in strain-softening surrounding rock," *Computers and Geotechnics*, vol. 89, pp. 81–91, 2017.

[18] H. Mohammadi, M. A. E. Farsangi, H. Jalalifar, and A. Reza, "Influence of gravity loading on the ground reaction curve at tunnel crown based on the nonlinear unified strength criterion," *The International Research Journal of Applied and Basic Sciences*, vol. 6, no. 5, pp. 563–571, 2013.

[19] S.-Q. Xu and M.-H. Yu, "The effect of the intermediate principal stress on the ground response of circular openings in rock mass," *Rock Mechanics and Rock Engineering*, vol. 39, no. 2, pp. 169–181, 2006.

[20] M.-H. Yu, Y.-W. Zan, J. Zhao, and M. Yoshimine, "A unified strength criterion for rock material," *International Journal of Rock Mechanics and Mining Sciences*, vol. 39, no. 8, pp. 975–989, 2002.

[21] C. Zhang, J. Zhao, Q. Zhang, and X. Hu, "A new closed-form solution for circular openings modeled by the unified strength theory and radius-dependent Young's modulus," *Computers and Geotechnics*, vol. 42, pp. 118–128, 2012.

[22] C.-g. Zhang, Q.-h. Zhang, J.-h. Zhao, F. Xu, and C.-z. Wu, "Unified analytical solutions for a circular opening based on non-linear unified failure criterion," *Journal of Zhejiang University - Science*, vol. 11, no. 2, pp. 71–79, 2010.

[23] A. Fahimifar and M. R. Zareifard, "A theoretical solution for analysis of tunnels below groundwater considering the hydraulic-mechanical coupling," *Tunnelling and Underground Space Technology*, vol. 24, no. 6, pp. 634–646, 2009.

[24] S. R. Carlson and R. P. Young, "Acoustic emission and ultrasonic velocity study of excavation-induced microcrack damage at the underground research laboratory," *International Journal of Rock Mechanics and Mining Science & Geomechanics Abstracts*, vol. 30, no. 7, pp. 901–907, 1993.

[25] A. Ghorbani and H. Hasanzadehshooiili, "A novel solution for ground reaction curve of tunnels in elastoplastic strain softening rock masses," *Journal of Civil Engineering and Management*, vol. 23, no. 6, pp. 773–786, 2017.

[26] A. Ghorbani and H. Hasanzadehshooiili, "A comprehensive solution for the calculation of ground reaction curve in the crown and sidewalls of circular tunnels in the elastic-plastic-EDZ rock mass considering strain softening," *Tunnelling and Underground Space Technology*, vol. 84, pp. 413–431, 2019.

[27] R. Holmberg, "Design of tunnel perimeter blasthole patterns to prevent rock damage," in *Proceedings of the 2nd International Symposium Tunnelling*, London, England, March 1979.

[28] S. Kruschwitz and U. Yaramanci, "Detection and characterization of the disturbed rock zone in claystone with the complex resistivity method," *Journal of Applied Geophysics*, vol. 57, no. 1, pp. 63–79, 2004.

[29] W. S. Pettitt, C. Baker, R. P. Young, L.-O. Dahlström, and G. Ramqvist, "The assessment of damage around critical engineering structures using induced seismicity and ultrasonic techniques," *The Mechanism of Induced Seismicity*, Springer, Berlin, Germany, 2002.

[30] D. Saiang, *Damaged Rock Zone Around Excavation Boundaries and its Interaction with Shotcrete*, Luleå Tekniska Universitet, Luleå, Sweden, 2004.

[31] S. Singh, "Prediction and determination of explosive induced damage," in *Proceedings of the 4th International Symposium*

On Rock Fragmentation By Blasting, pp. 5–8, Vienna, Austria, July 1993.

[32] L. X. Xie, W. B. Lu, Q. B. Zhang, Q. H. Jiang, G. H. Wang, and J. Zhao, "Damage evolution mechanisms of rock in deep tunnels induced by cut blasting," *Tunnelling and Underground Space Technology*, vol. 58, pp. 257–270, 2016.

[33] Y. Zhang, X. Ding, S. Huang, Y. Qin, P. Li, and Y. Li, "Field measurement and numerical simulation of excavation damaged zone in a 2000 m-deep cavern," *Geomechanics & engineering*, vol. 16, no. 4, pp. 399–413, 2018.

[34] Q. Xie and K. Peng, "Space-time distribution laws of tunnel excavation damaged zones (EDZs) in deep mines and EDZ prediction modeling by random forest regression," *Advances in Civil Engineering*, vol. 2019, Article ID 6505984, 13 pages, 2019.

[35] J. Yang, X.-G. Yang, J.-W. Zhou, Y. Liu, B.-S. Dong, and H.-B. Li, "Comparative study of the excavation damage and rockburst of the deeply buried jinping II diversion tunnels using a TBM and the drilling-blasting method," *Advances in Civil Engineering*, vol. 2020, Article ID 8876214, 14 pages, 2020.

[36] Z.-q Yin, Z.-x Hu, Z.-d Wei et al., "Assessment of blasting-induced ground vibration in an open-pit mine under different rock properties," *Advances in Civil Engineering*, vol. 2018, Article ID 4603687, 10 pages, 2018.

[37] J. González-Cao, F. Varas, F. G. Bastante, and L. R. Alejano, "Ground reaction curves for circular excavations in non-homogeneous, axisymmetric strain-softening rock masses," *Journal of Rock Mechanics and Geotechnical Engineering*, vol. 5, no. 6, pp. 431–442, 2013.

[38] M. R. Zareifard, "Ground reaction curve for deep circular tunnels in strain-softening mohr–coulomb rock masses considering the damaged zone," *International Journal of Geomechanics*, vol. 20, no. 10, Article ID 04020190, 2020.

[39] M. R. Zareifard, "A new semi-numerical method for elasto-plastic analysis of a circular tunnel excavated in a Hoek–Brown strain-softening rock mass considering the blast-induced damaged zone," *Computers and Geotechnics*, vol. 122, Article ID 103476, 2020.

[40] M. R. Zareifard and M. R. Shekari, "Comprehensive solutions for underwater tunnels in rock masses with different GSI values considering blast-induced damage zone and seepage forces," *Applied Mathematical Modelling*, vol. 96, pp. 236–268, 2021.

[41] A. Vrakas and G. Anagnostou, "A finite strain closed-form solution for the elastoplastic ground response curve in tunnelling," *International Journal for Numerical and Analytical Methods in Geomechanics*, vol. 38, no. 11, pp. 1131–1148, 2014.

[42] S. Wang and S. Yin, "A closed-form solution for a spherical cavity in the elastic-brittle-plastic medium," *Tunnelling and Underground Space Technology*, vol. 26, no. 1, pp. 236–241, 2011.

[43] M. R. Zareifard and A. Fahimifar, "Analytical solutions for the stresses and deformations of deep tunnels in an elastic-brittle-plastic rock mass considering the damaged zone," *Tunnelling and Underground Space Technology*, vol. 58, pp. 186–196, 2016.

[44] W. Yu and F. Liu, "Stability of close chambers surrounding rock in deep and comprehensive control technology," *Advances in Civil Engineering*, vol. 2018, Article ID 6275941, 18 pages, 2018.

[45] Y. Yuan, W. Wang, S. Li, and Y. Zhu, "Failure mechanism for surrounding rock of deep circular roadway in coal mine based on mining-induced plastic zone," *Advances in Civil Engineering*, vol. 2018, Article ID 1835381, 14 pages, 2018.

[46] B. Abbasi, M. Pierce, E. Dzik, and Y. Chugh, "Barton approach for predicting Hoek-Brown residual parameters," in *Proceedings pf the 48th US Rock Mechanics/Geomechanics Symposium*, Minneapolis, MN, USA, June 2014.

[47] M. R. Zareifard and A. Fahimifar, "A new solution for shallow and deep tunnels by considering the gravitational loads," *Acta Geotechnica Slovenica*, vol. 9, no. 2, pp. 37–49, 2012.

[48] M. Veiskarami, A. Ghorbani, and M. Alavipour, "Development of a constitutive model for rockfills and similar granular materials based on the disturbed state concept," *Frontiers of Structural and Civil Engineering*, vol. 6, no. 4, pp. 365–378, 2012.

[49] J. H. Mathews and K. D. Fink, *Numerical Methods Using MATLAB*, Pearson prentice hall Upper, Saddle River, NJ, USA, 2004.

[50] E. Hoek and M. S. Diederichs, "Empirical estimation of rock mass modulus," *International Journal of Rock Mechanics and Mining Sciences*, vol. 43, no. 2, pp. 203–215, 2006.

[51] D. Saiang, *Behaviour of Blast-Induced Damaged Zone Around Underground Excavations in Hard Rock Mass*, Luleå tekniska universitet, Luleå, Sweden, 2008.

[52] E. Katebian and H. Molladavoodi, "Practical ground response curve considering post-peak rock mass behaviour," *European Journal of Environmental and Civil Engineering*, vol. 21, no. 1, pp. 1–23, 2017.

[53] T. J. Ross, *Fuzzy Logic with Engineering Applications*, Wiley Online Library, New York, NY, USA, 2004.

[54] A. Fiore, G. Quaranta, G. C. Marano, and G. Monti, "Evolutionary polynomial regression–based statistical determination of the shear capacity equation for reinforced concrete beams without stirrups," *Journal of Computing in Civil Engineering*, vol. 30, no. 1, Article ID 04014111, 2016.

[55] A. H. Gandomi, A. Faramarzifar, P. G. Rezaee, A. Asghari, and S. Talatahari, "New design equations for elastic modulus of concrete using multi expression programming," *Journal of Civil Engineering and Management*, vol. 21, no. 6, pp. 761–774, 2015.

[56] A. Ghorbani and A. Eslami, "Energy-based model for predicting liquefaction potential of sandy soils using evolutionary polynomial regression method," *Computers and Geotechnics*, vol. 129, Article ID 103867, 2021.

[57] H. Hasanzadehshooiili, R. Mahinroosta, A. Lakirouhani, and V. Oshtaghi, "Using artificial neural network (ANN) in prediction of collapse settlements of sandy gravels," *Arabian Journal of Geosciences*, vol. 7, no. 6, pp. 2303–2314, 2014.

[58] Ł. Sadowski and J. Hoła, "ANN modeling of pull-off adhesion of concrete layers," *Advances in Engineering Software*, vol. 89, pp. 17–27, 2015.

[59] E. Sadrossadat, F. Soltani, S. M. Mousavi, S. M. Marandi, and A. H. Alavi, "A new design equation for prediction of ultimate bearing capacity of shallow foundation on granular soils," *Journal of Civil Engineering and Management*, vol. 19, no. 1, pp. S78–S90, 2013.

[60] Z.-Y. Yin, Y.-F. Jin, H.-W. Huang, and S.-L. Shen, "Evolutionary polynomial regression based modelling of clay compressibility using an enhanced hybrid real-coded genetic algorithm," *Engineering Geology*, vol. 210, pp. 158–167, 2016.

[61] N. Shariatmadari, H. Hasanzadehshooiili, P. Ghadir, F. Saeidi, and F. Moharrami, "Compressive strength of sandy soils stabilized with alkali activated volcanic ash and slag," *Journal of Materials in Civil Engineering*, vol. 33, 2021.

[62] O. Giustolisi and D. A. Savic, "A symbolic data-driven technique based on evolutionary polynomial regression," *Journal of Hydroinformatics*, vol. 8, no. 3, pp. 207–222, 2006.

[63] O. Giustolisi and D. Savic, "Advances in data-driven analyses and modelling using EPR-MOGA," *Journal of Hydroinformatics*, vol. 11, no. 3-4, pp. 225–236, 2009.

Hindawi
Advances in Civil Engineering
Volume 2021, Article ID 4901670, 12 pages
https://doi.org/10.1155/2021/4901670

Research Article

Field and Numerical Investigation on the Coal Pillar Instability of Gob-Side Entry in Gently Inclined Coal Seam

Xupeng Ta,[1,2] Zhijun Wan,[1,2] Yuan Zhang,[1,2] Peng Shi,[1,2] Zejie Wei,[1,2] Xin Sun,[1,2] and Liangliang Jia[3]

[1]*Key Laboratory of Deep Coal Resource Mining (China University of Mining & Technology), Ministry of Education of China, Xuzhou 221116, China*
[2]*School of Mines, China University of Mining & Technology, Xuzhou 221116, China*
[3]*Chensilou Coal Mine, Henan Energy Chemical Group Yongmei Company, Yongcheng 476600, China*

Correspondence should be addressed to Zhijun Wan; zhjwan@cumt.edu.cn and Yuan Zhang; zhangyuan@cumt.edu.cn

Received 30 May 2021; Accepted 14 July 2021; Published 28 July 2021

Academic Editor: Ali Lakirouhani

In order to study the coal pillar stability of gob-side entry in gently inclined coal seam, a comprehensive method including theoretical analysis, numerical modeling, and field monitoring was applied to study its fracturing and instability mechanism. The results show that the uneven horizontal stress was the internal cause of entry asymmetric deformation and failure in inclined coal seam. In gently inclined coal seam, the rotation movement of the main roof and stress distribution were closely related to inclination of the coal seam. Based on the asymmetric deformation characteristics and mechanisms of entry, a collaborative control technology of roof cutting for pressure relief and support strengthening has been put forward. The research results have practical significance for revealing the mechanism of entry damage in gently inclined coal seam mining and proposing engineering measures to prevent coal pillar damage and disaster occurrence.

1. Introduction

With the increasing energy demand and mining intensity, the shallow coal resources gradually exhausted. In order to improve recovery rate of coal resources in China, gob-side entry driving (GED) techniques are widely adopted in the process of entry excavation. The stability of coal pillar is the key of the GED technique. In recent decades, the research on mechanical properties of coal pillar mainly reveals the dynamic mechanical state of coal pillar through field observation, theoretical analysis, similar material simulation test, and numerical simulation, and then puts forward the control methods of changing the width of coal pillar, optimizing support parameters and improving the properties of surrounding rock [1–7]. Scholars have studied the relationship between ground stress distribution and roadway fracture development by using comprehensive monitoring system and borehole camera exploration device and developed a strictly calibrated numerical model to simulate the stress redistribution under different conditions [8, 9]. Das et al. [10] developed generic analytical solutions to estimate the strength of the inclined coal pillars, deriving mathematical models to obtain the confining stress in the coal pillar and the corresponding peak stress at the time of its failure. Gao and Ge [11] proposed a composite rock mass method based on the mechanical method to obtain the derived stress not only for the cohesive constraining forces of the coal pillar but also for the rock mass of the roof and floor. Prassetyo et al. [12] analyzed the effect of coal-entry friction on the strength of coal pillar by laboratory tests and modified the empirical equation for the strength of coal pillar. Dai et al. [13] studied the intelligent identification method for the stability of coal pillar in the section, analyzed load transfer law of the overlying strata in the upper part of coal pillar, and calculated the optimal value of the coal pillar using the Delphi index evaluation system. Liu et al. [14] improved the method of coal pillar fracture digitization and established the model of coal pillar stability evaluation. Gao [15] proposed a new

method to comprehensively study the stability of the strip coal pillar based on the elastic-plastic mechanics theories and the previous studies of the limiting equilibrium method.

Compared with the flat coal pillars, the stress environment of the inclined coal pillars is more complex because of the asymmetric stress distribution. Das et al. [16, 17] analyzed the failure stress states within the coal pillars having different dip angles and elucidated the procedures to estimate the strength of the inclined coal pillars by the numerical modeling technique. Zhao et al. [18] analyzed the mechanical characteristics of narrow coal pillars' gob-side entry in inclined coal seams and obtained the damage form of coal pillars with different widths during excavation. Chen and Wang [19] analyzed surrounding rock deformation characteristics of gob-side entry driving in deep inclined coal seam and revealed the asymmetric large deformation characteristics of such roadway. Zhang et al. [20] analyzed the support stress distribution law near the gob side and investigated the relationship between the surrounding rock stress distribution of the roadway and the coal pillar width by the numerical method. A review of the previous studies indicated that (1) the inclination angle of the coal seam has a significant influence on the stability of the coal pillar and (2) there was less research on the distribution pattern of coal pillar abutment pressure under the influence of dip angle of coal seam. Thus, it is necessary to take the abutment pressure, generated by roof overburden structure in gently inclined coal seam, into account in examining coal pillar stability.

In this study, numerical simulations were conducted to examine the stability of a mining entry with 2.0 m section coal pillars under the influence of dip angle of coal seam. A surrounding rock structure model was established to investigate dynamic mechanical characteristics of a coal pillar in the gently inclined coal seam. According to the theoretical and numerical results, the dynamic mechanical state of the coal pillar was studied in detail, and a method for controlling the entry stability was proposed.

2. Geological Setting and Mining Conditions

In this study, the 21015 entry with 2.0 m section coal pillars in the 21015 working face of the Chensilou coal mine, Henan Province, was used as the research object, as shown in Figure 1(a). The coal seam dip angle was 18°, and the average thickness and burial depth were 2.66 m and 400 m, respectively. According to the drilling records, the immediate roof and floor were sandy mudstone with average thickness of 2.76 m and 3.3 m, and the main roof and floor were medium-fine sandstone with average thickness of 20.4 m and 4.83 m. The 2.0 m section coal pillar was reserved between the 21015 and 21011 working faces. During the actual mining process, after the end of the 21011 working face, the 21015 entry began to excavate along the edge of the gob. The 21015 entry was supported by anchor-mesh-cable system, as shown in Figure 1(b). The roof of the entry was supported by 22×2200 mm bolts and 21.6×8300 mm cables. The pillar rib and the solid coal rib of the entry were supported by 16×2200 mm and 22×2200 mm bolts, respectively. The roof bolt and rib bolt spacings for the entry was 880 mm and 700 mm, respectively, and roof cable spacing was 1600 mm, as shown in Figure 1(c).

3. Methodology

3.1. In Situ Monitoring. To fully understand the asymmetric deformation law of the entry in the gently inclined coal seam, surface displacement monitoring stations and borehole measuring points were arranged in the tail entry, as shown in Figure 2. The borehole measurement points No. 1 and No. 2 were located at 12~15 m and 28~30 m in the advancing direction of 21015 working face, and only three of them can be fully observed. The distance between each stations was 25 ~ 30 m and the first monitoring station was located 60 m ahead the 21015 working face. According to the site situation, the borehole measurement point No. 1 was set within the advanced support range, and the borehole measurement point No. 2 was set outside the range as a comparison. As the working face advances, the observation data of each surface displacement monitoring station can be compared with the observation data of borehole measuring points.

3.2. Numerical Modeling. To fully understand the stability of a mining entry with 2.0 m section coal pillars under the influence of dip angle of coal seam, a FLAC^{3D} numerical simulation with the "Mohr–Coulomb criterion" based on the engineering geological conditions of 21015 working face was established as shown in Figure 3. The dimension of the numerical model was $150 \times 150 \times 150$ m (width × height × length). The four sides and the bottom of the model were constrained by displacement, and the top boundary was applied with a vertical stress of 12.6 MPa. The physical and mechanical rock mass parameters were obtained via laboratory tests and previously performed research works [21], as shown in Table 1. The simulation process was as follows: (1) excavate the mining entry of the 21011 working face; (2) mine the 21011 working face; (3) fill the caved zone with the double-yield model; (4) excavate the mining entry of the 21015 working face; and (5) mine the 21015 working face (Figure 3).

4. Results and Discussion

4.1. In Situ Deformation Test Results and Discussion. The observation results are shown in Figure 4. Based on the statistics of observation results shown in Figure 4(a), it was found that the internal damage of the coal pillar can be divided into three areas: relatively complete area (<40 cm), limited damage area (40~80 cm), and loose failure area (>80 cm). It can be seen that the coal pillar was relatively complete within 40 cm of the shallow part, and there were a few macroscopic cracks; the coal pillar was relatively broken within the range of 40~80 cm, the hole wall was in a fragmented state, and most of the blocks do not peel off; the area within the range of 40~80 cm appears loosely broken, mostly blocky, with large blockiness, and the small hole walls were peeled off. The roof observation results are shown in Figure 4(b); it was found that in the range of 0~22 cm, many

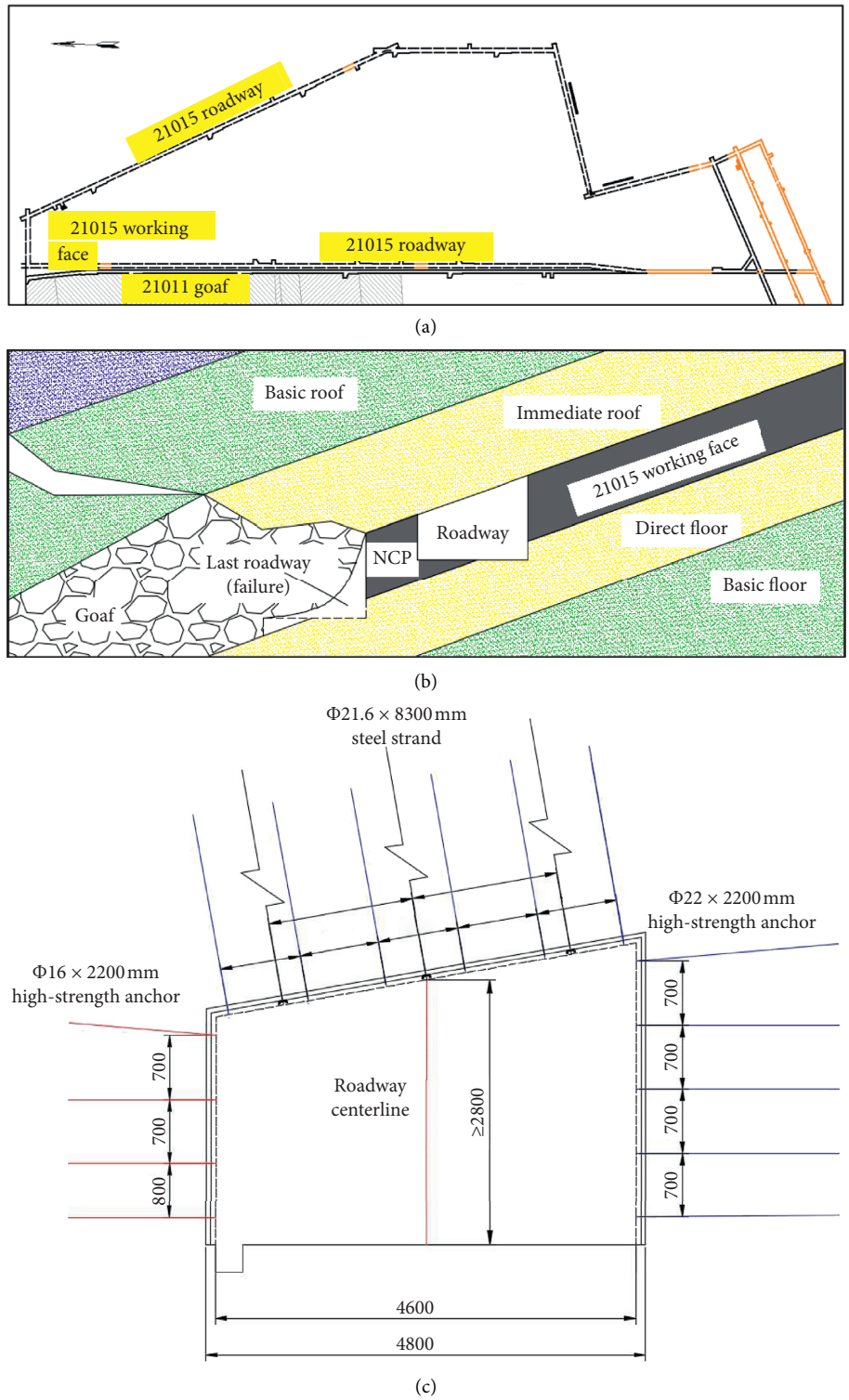

Figure 1: Position of the gob-side entry and support parameters.

cracks were distributed in the hole wall, and the roof was relatively complete; in the range of 0.68~1.56 m, longer cracks penetrated the hole wall and formed fragmentation areas; in the further range, the hole wall was completed. From the above data analysis, we can see that with the increase of observation depth, entry deformation became more and more serious, and within a certain inclination, main roof fracture line was located above the coal pillar.

Figure 5 shows deformation monitoring curve of entry. It can be seen that the deformation law of surrounding rock monitored by stations was similar. As the working face advances, the deformation of the roadway gradually

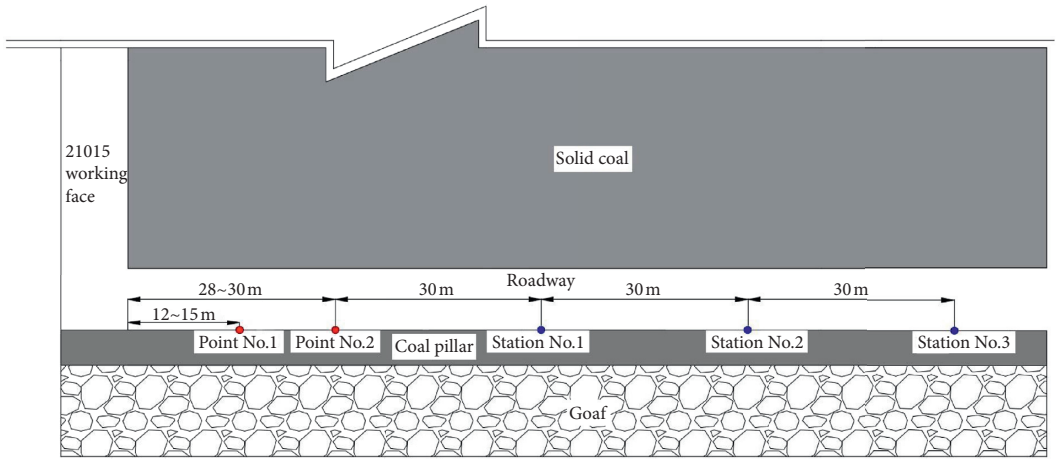

Figure 2: Monitoring stations and measuring point arrangement.

Table 1: Numerical simulation parameters.

Rock layer	Rock type	Average thickness (m)	Density (kg/m^3)	Bulk modulus (GPa)	Shear modulus (GPa)	Tensile strength (MPa)	Internal stress (MPa)	Internal friction angle (°)
Overlying strata	—	385	2500	12.00	7.8	1.6	2.4	28
Main roof	Middle-fine sandstone	4.83	2680	12.23	8.4	2.19	9.1	36
Immediate roof	Sandy mudstone	3.3	2659	2.51	1.36	1.70	1.9	21
Coal	—	3	1212	0.79	0.24	1.52	3.46	22
Immediate floor	Sandy mudstone	2.76	2659	2.51	1.36	1.70	1.9	21
Main floor	Middle-fine sandstone	20.04	2680	12.23	8.4	2.19	9.1	36

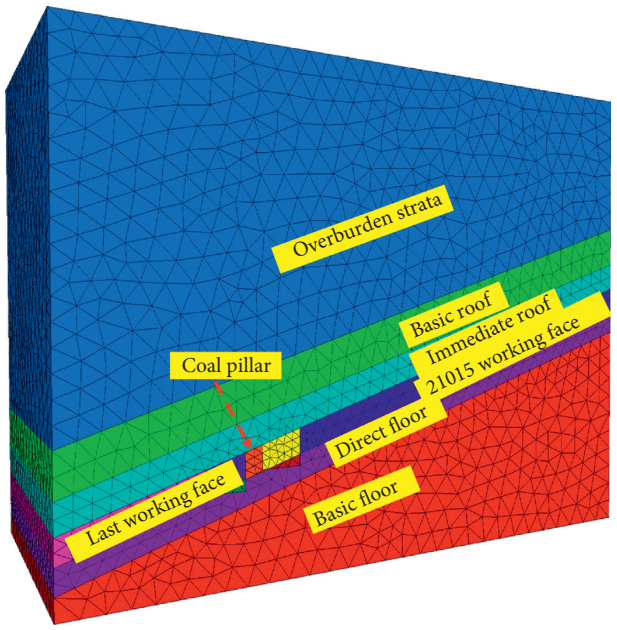

Figure 3: Sketch map of numerical model.

increases, with the deformation of the rib up to 140 mm and the deformation of the roof and floor up to 64 mm. Compared with the solid coal side, the surrounding rock deformation of coal pillar side was larger, and the deformation of the roof was slightly larger than that of the floor. The surge in deformation rate was observed at all stations and occurred 30–45 m from the working face, where the entry was subjected to front abutment pressure of working face. At a distance of about 30 m and 15 m from the working surface, the deformation of the coal pillar side and the roof was consistent with the failure of the borehole observation. From the above analysis, it can be concluded that the asymmetry deformation of entry is obviously, affected by the front abutment pressure of 21015 working face.

4.2. Structure Characteristics of Roadway Surrounding Rock in Gently Inclined Coal Seam. It is generally believed that the abutment pressure distribution significantly affects the stability of the roadway. In order to reveal the force condition of roadway under the influence of dip angle of coal seam, the structure characteristics of roadway surrounding rock were investigated, as shown in Figure 6.

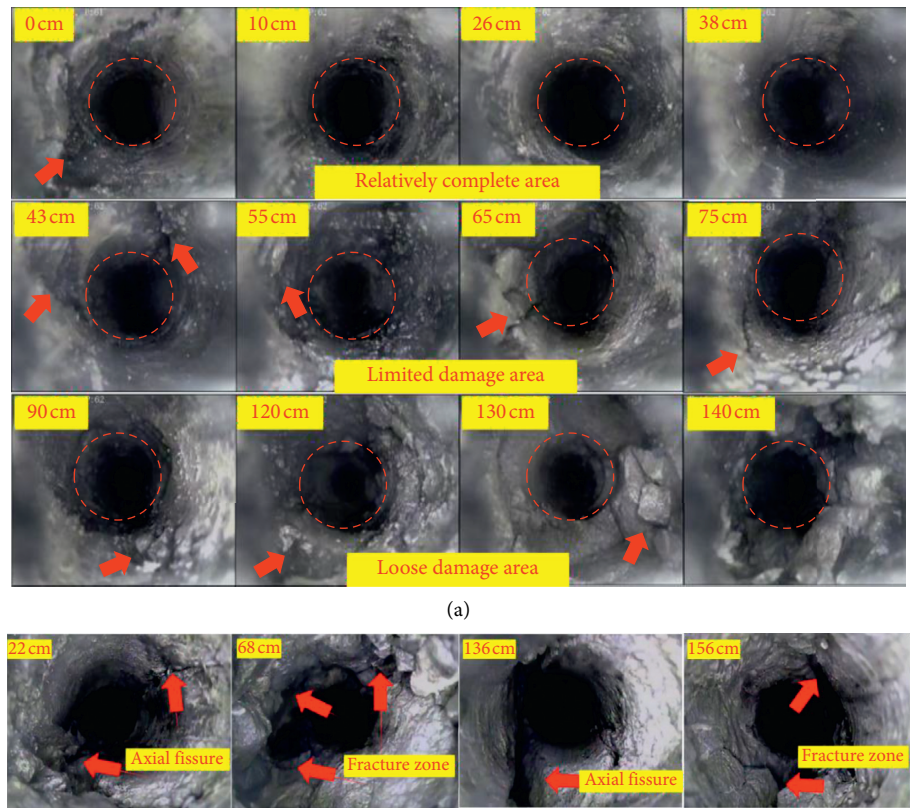

Figure 4: Observation of the inside of the coal pillar. (a) No. 1 point. (b) No. 2 point.

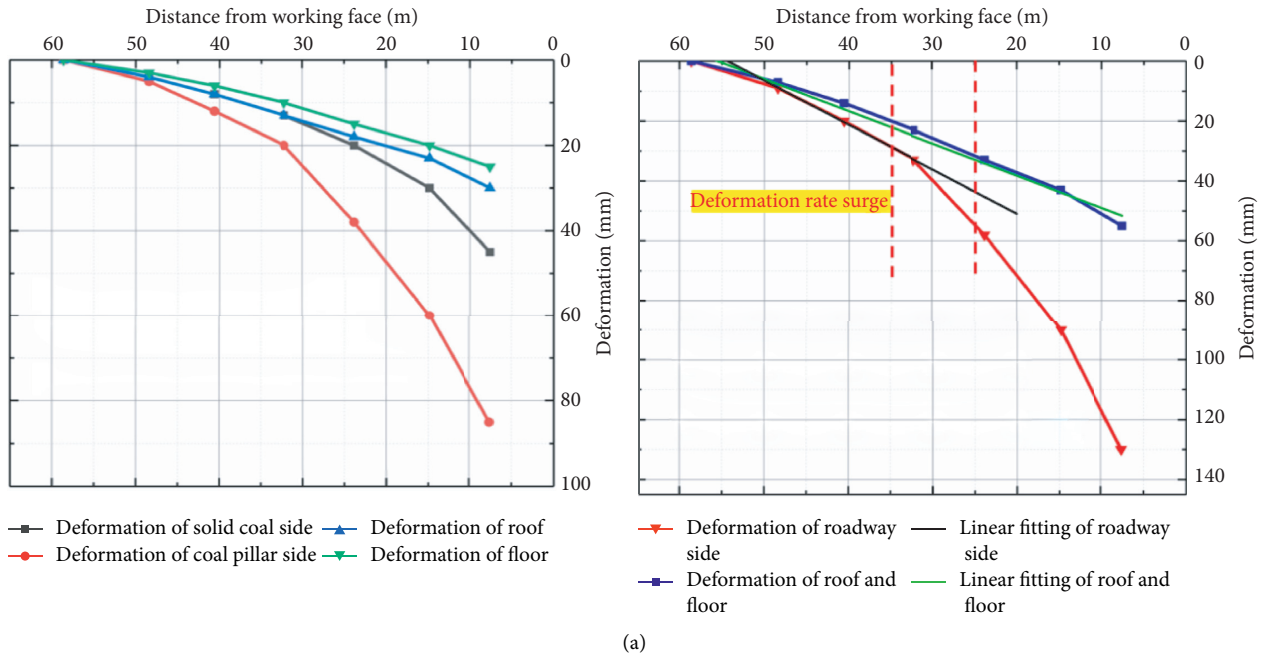

Figure 5: Continued.

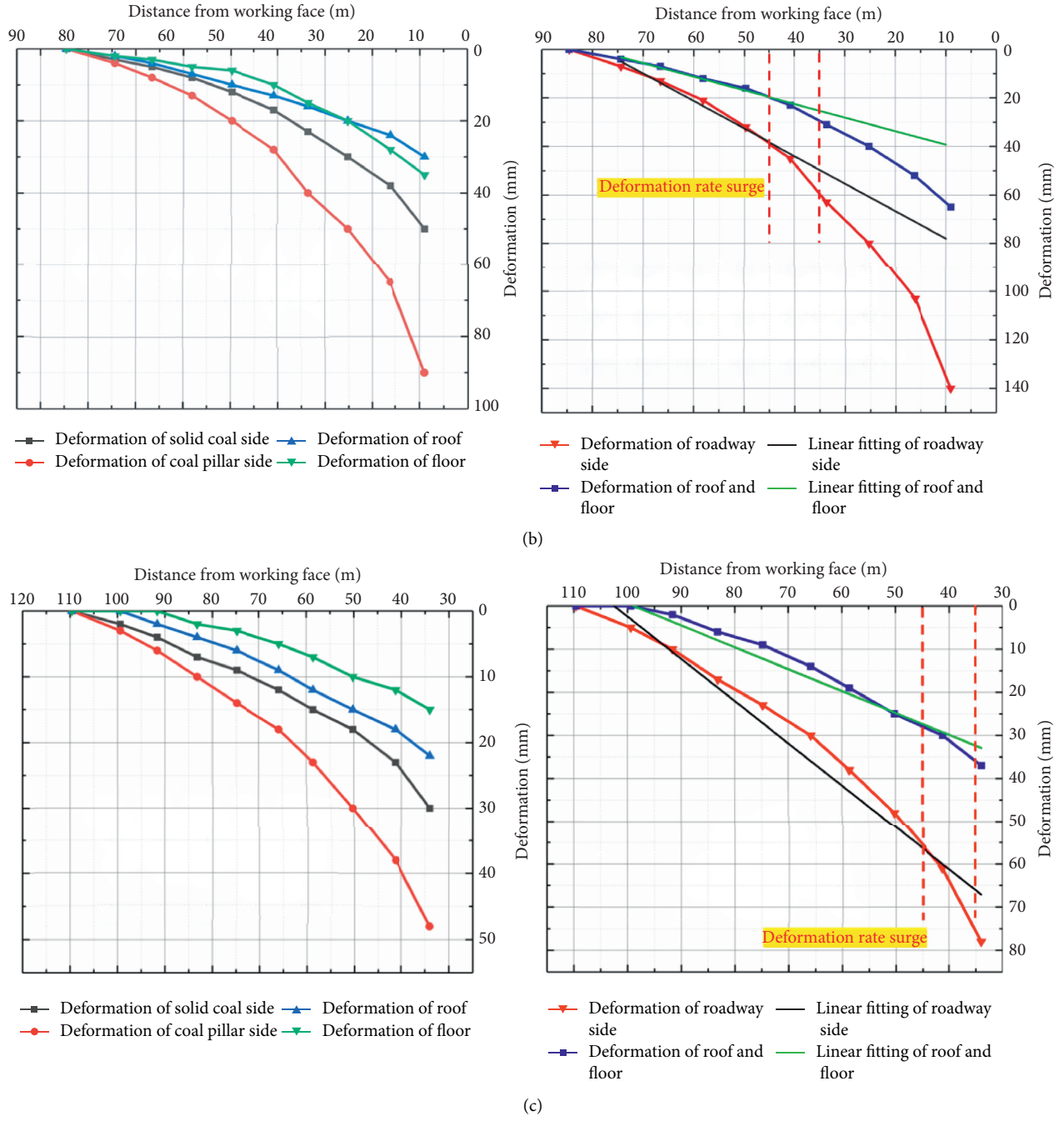

Figure 5: Entry deformation monitoring curve. (a) 1# monitoring station. (b) 2# monitoring station. (c) 3# monitoring station.

The fracture position of key block B can be obtained from the limit equilibrium theory, and the expression is as follows [22, 23]:

$$X_0 = \frac{\lambda M}{2\tan\varphi}\ln\left(\frac{k\gamma H + (c/\tan\varphi)}{(c/\tan\varphi) + (P/\lambda)}\right). \quad (1)$$

The position where the highest pressure of the coal pillar occurs can be calculated by the following formula:

$$x_0 = \frac{M\lambda}{2\tan\varphi_0}\ln\left[\frac{\lambda(k\gamma H\cos\alpha\tan\varphi_0 + 2c - m\gamma\sin\alpha)}{\lambda(2c - m\gamma\sin\alpha) + 2P\tan\varphi_0}\right], \quad (2)$$

where X_0 is the distance between the fracture line of key block B and gob, m; x_0 is the place where peak stress occurs; c is the cohesion of the coal, 3.46 MPa; φ is the inner friction angle of the coal, 22°; P is the support resistance of the coal

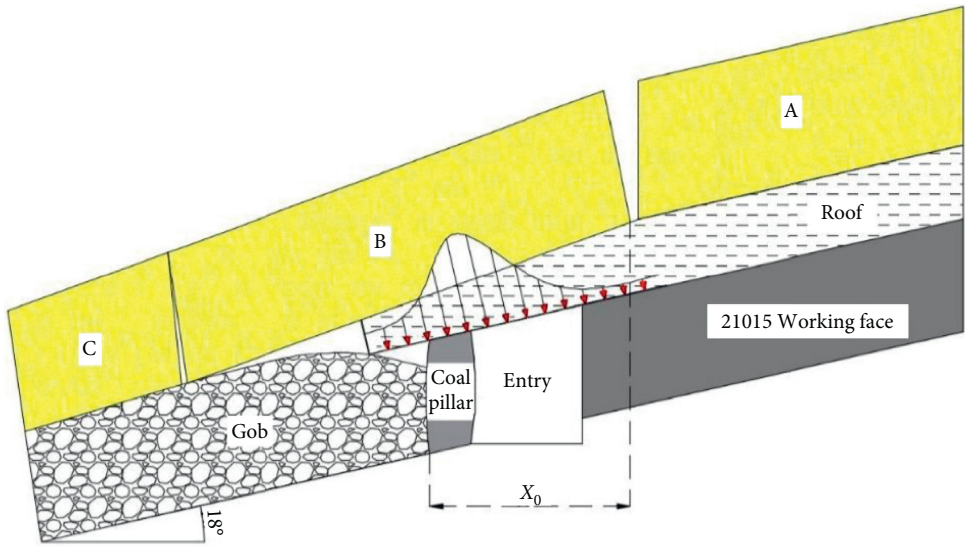

Figure 6: Structure characteristics of roof strata in gently inclined coal seam.

pillar, 0.25 MPa; λ is the side pressure coefficient, 1.2; k is the maximum stress concentration factor, 1.2~1.4; γ is the average density of the overburden, 25 kN/m^3; H is the depth of the coal seam, 400 m; and M is the coal seam thickness, 3.0 m.

According to Equation (1) and (2), X_0 was 3.83~4.19 m, and x_0 was 0.6 m. In addition, according to the rock pressure theory [22] and above field monitoring, the length of key block B is about 30 m, with an average thickness of 4.83 m.

4.3. Mechanical Principle of Stress Change of Coal Pillar in Gently Inclined Coal Seam. After the 21011 working face was mined, the stress in the surrounding rocks of the 21015 entry was redistributed, and the abutment stress was carried by gob and solid coal; when the 21015 working face was mined, the abutment stress was carried by the coal pillar and solid coal. Under the influence of inclination, the horizontal stress was transferred to the coal pillar which became the main load carrier. Figure 7 presents the distribution of abutment stress.

It can be seen that in gently inclined coal seam, with the mining of 21015 working face, the main roof gradually rotates and sinks and forms the key block B analyzed in 4.2. Within this stage, front abutment stress increases sharply, and the coal pillar is the main bearing body; therefore, the deformation and stress of the coal pillar gradually reached the peak value and were obviously greater than those of solid coal. Additionally, in the process of abutment stress rebalance, the inclination angle affects the accumulation of the gob and limits the free space of the gob-side coal pillar. Therefore, the stress and strain of the gob-side coal pillar were obviously smaller than those of the entry side.

Previous research works have shown that horizontal stress exerted on the coal pillar is closely related to the size of the key block B and the degree of rotation [24]. Furthermore, the inclination significantly affects the stability of the coal pillar. Generally, with the increase of dip angle, the horizontal force will inevitably lead to a sharp increase. The above proves that in inclined coal seam, the inclination angle affects the uneven distribution of horizontal stress, and this uneven horizontal stress environment is the internal cause of entry asymmetric deformation failure.

In Figure 6, τ_{xy} is the shear stress at the interface between coal seam and roof and floor; σ_y is the y-direction stress; P_x is the gob-side resistance.

4.4. Analysis of Numerical Simulation Results. After the entry was excavated, the original structure of the stratum was destroyed. Surrounding rock asymmetric deformation was related to rotary horizontal extrusion of key block B influenced by inclination. Figure 8 shows horizontal stress distribution of coal pillar in gently inclined coal seam. It can be seen that the horizontal stress in the coal pillar generally shows a trend of decreasing and then increasing with height changes. The specific performance is as follows. (1) Entry excavation stage: the horizontal stress in the middle of the coal pillar was significantly lower than that of the top and bottom, and the stress of the entry-side coal pillar was obviously greater than that of the goaf-side coal pillar. (2) Mining stage: similar to the entry excavation stage, the horizontal stress in the middle of the coal pillar was significantly lower than that of the top and bottom, and the stress on both sides of coal pillar was basically the same.

In order to further comprehend the effect of inclination on coal pillar asymmetric deformation failure, Figure 9 presents the displacement distribution of coal pillar in gently inclined coal seam. It can be seen that the horizontal displacement of gob side of coal pillar generally shows a decreasing trend, while the entry side generally increases and then decreases with height changes. The specific performance is as follows. (1) Entry excavation stage: the deformation of the upper and middle part of the coal pillar is significantly larger

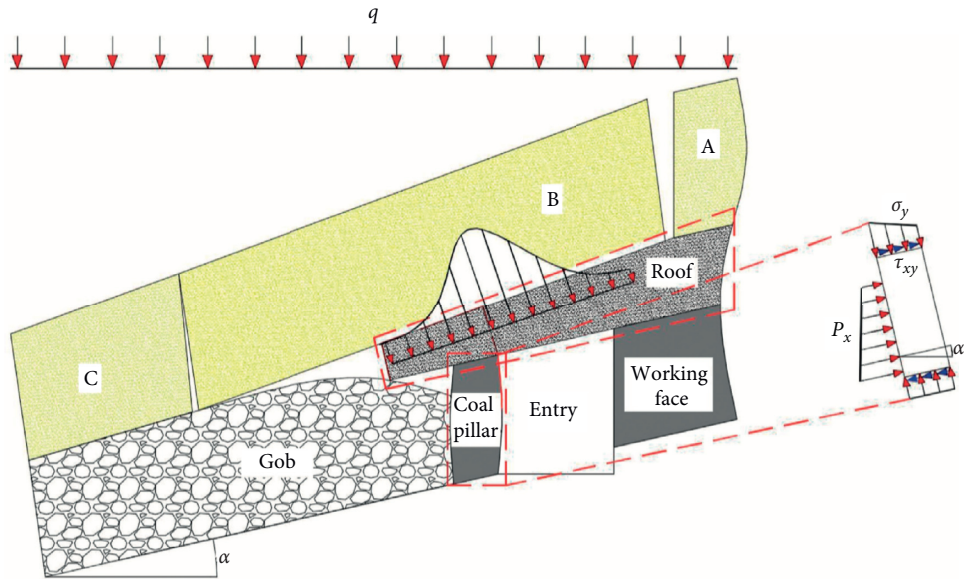

Figure 7: Distribution of side abutment stress.

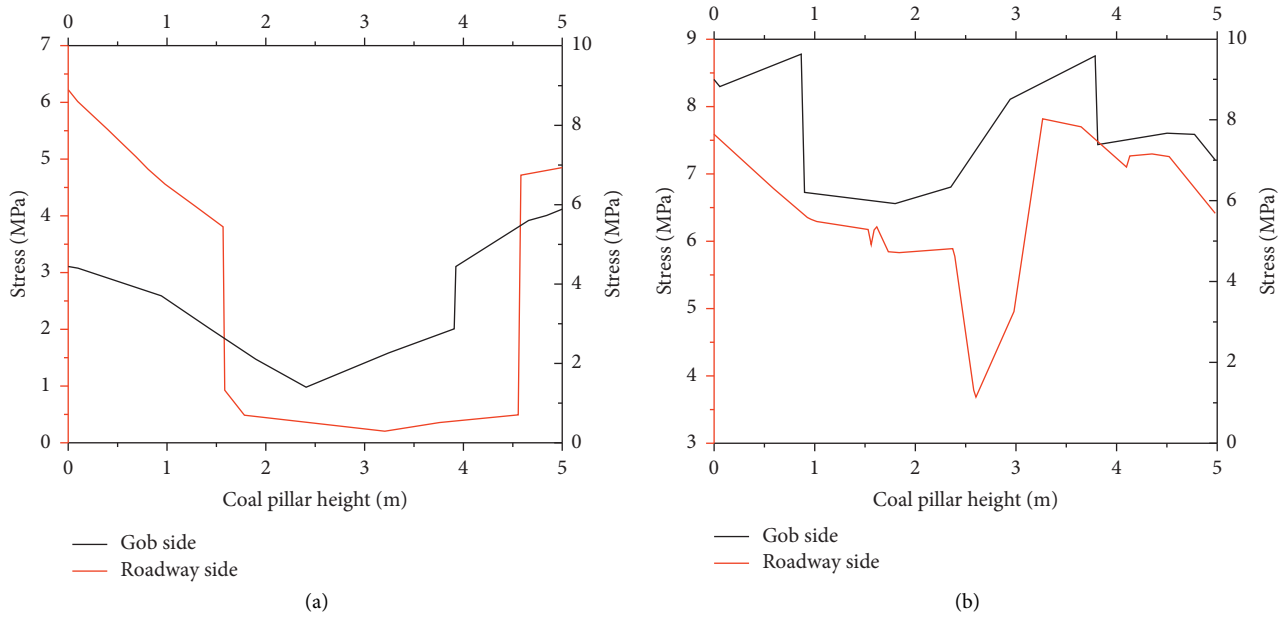

Figure 8: Horizontal stress distribution of coal pillar. (a) Excavation of 21015 entry. (b) Excavation of 21015 working face mine.

than that of the bottom, and the deformation of the entry-side coal pillar is obviously larger than that of the gob-side coal pillar. (2) Mining stage: similar to the entry excavation stage, the deformation in the middle of the coal pillar was significantly lower than that of the top and bottom, and the deformation on both sides of coal pillar is basically the same.

The analysis was as follows:

(1) During the entry excavation, the overlying strata have not broken, and the abutment pressure was carried by the gob and solid coal. The horizontal stress of the coal pillar basically showed a low degree. With the mining of working face, the overlying strata gradually fractured and rotated, and the pressure of Key block B was carried by the coal pillar and solid coal as shown in Figure 10. The horizontal stress decreased and then increased from the shallow part of roof to coal pillar, which presented an obvious uneven stress distribution. Moreover, because of the crushing and expending effect of immediate roof, the gob was sufficiently filled and relatively decrease breaking and deflection degrees of the gob-side coal pillar.

(2) Comparing the variations of horizontal stress and deformation of coal pillar during entry excavation and working face mining, when the inclination

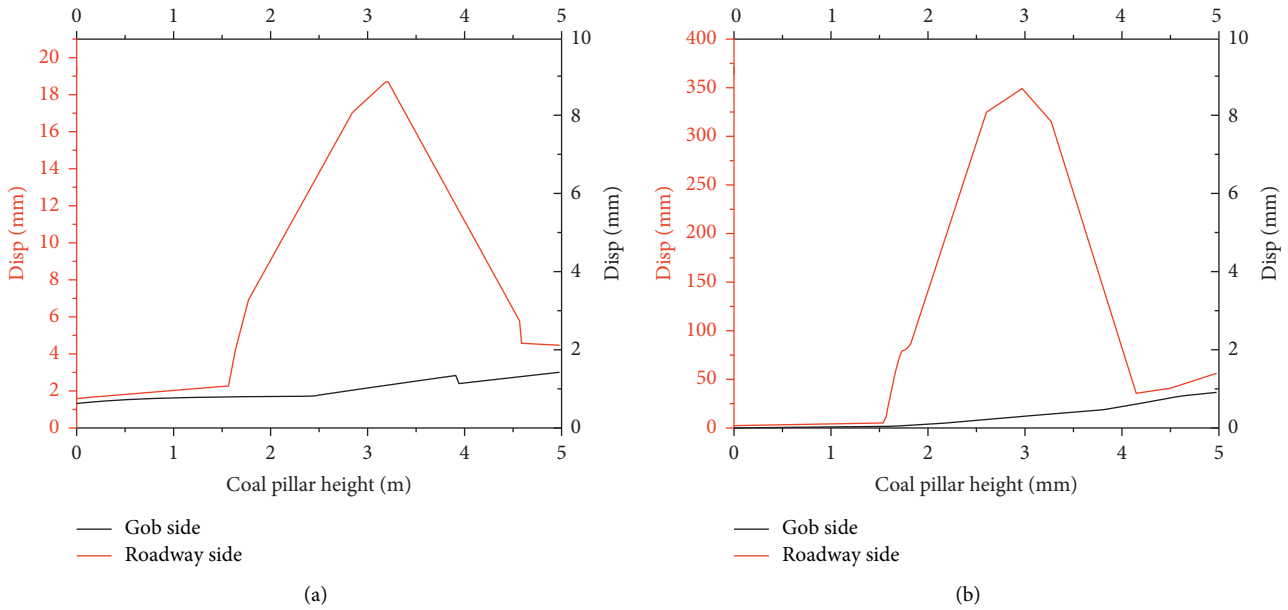

Figure 9: Horizontal displacement distribution of coal pillar. (a) Excavation of 21015 entry. (b) Excavation of 21015 working face.

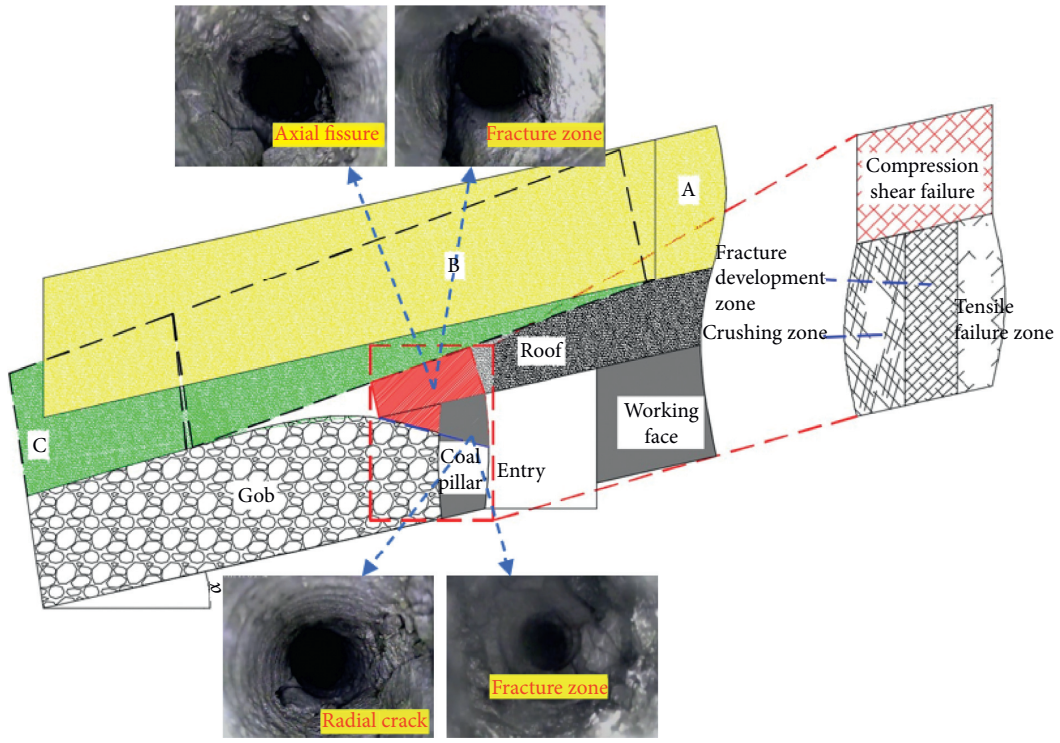

Figure 10: Plastic damage diagram of the coal pillar.

increases, the key block B may be deformed and unstable, which results in coal pillar expansion, squeezing, breaking, and deformation. It is clear that the inclination directly affects the rotation motion of the overlying strata and intensifies the uneven stress and deformation situation of the surrounding rock of the entry, which was basically consistent with the stress characteristics obtained from Section 4.3.

5. Stability Control Technique of Entry Influenced by Inclination

The asymmetric deformation failure characteristics of entry surrounding rock in gently inclined coal seam were caused by uneven external forces. The symmetric supporting structures have high bearing capacity under the uniform external force, but it will fail under the action of uneven

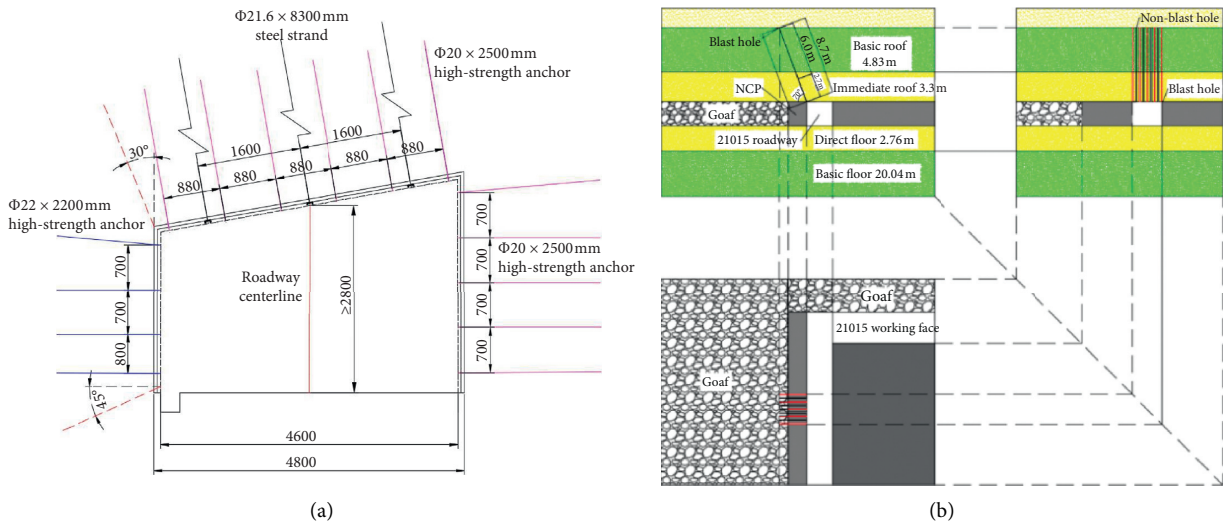

Figure 11: Stability control arrangement of entry. (a) Optimized support schemes and parameters. (b) Layout of the blast hole.

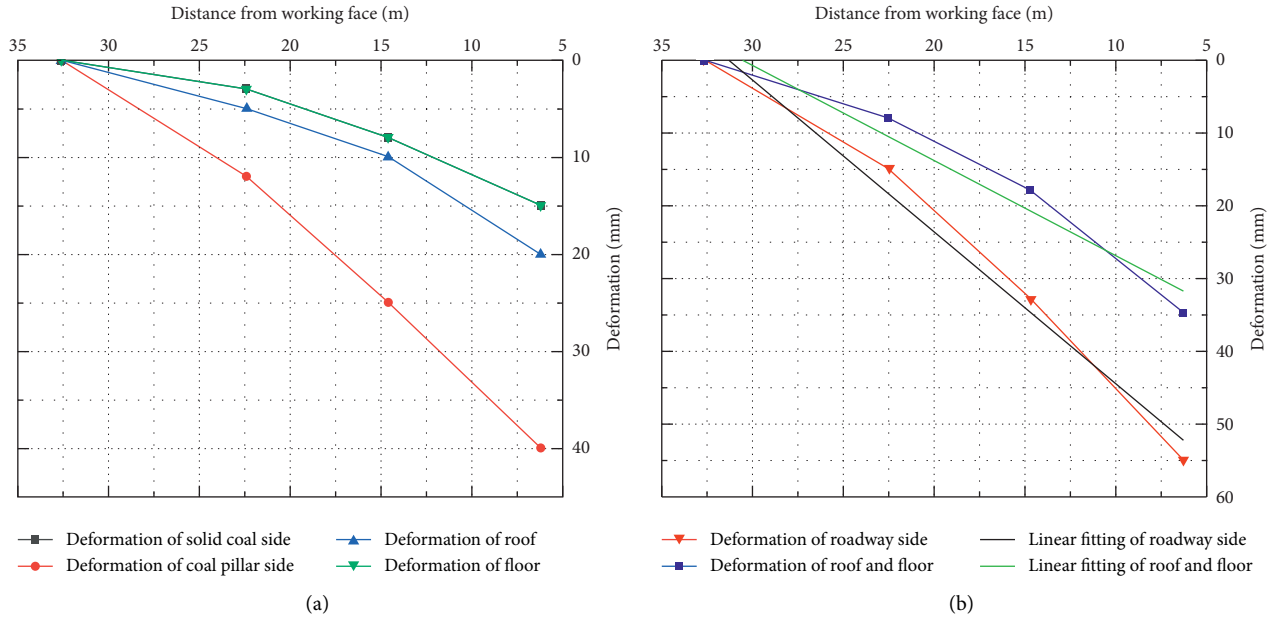

Figure 12: Deformation monitoring of surrounding rock.

external force [25]. The asymmertric control that can be effectively coordinated with roadway surrounding rock influenced by inclination should be put forward. Moreover, human intervention in the evolution of the roof overburden structure was an effective technique for reducing the stress and deformation of the entry influenced by inclination.

5.1. Entry Stability Control Method. To ensure the normal use of the mining entry under the influence of gently inclined coal seam, it is necessary to adopt a collaborative control technology of roof cutting for pressure relief and support strengthening. According to the instability mechanism of the entry under the influence of gently inclined coal seam, the following methods were proposed for controlling entry stability: ① relieve the uneven external forces of entry surrounding rock; ② improve the support strength of weak structure such as coal pillars and solid coal rib; and ③ strengthen the overall structure of the roof and deep rock formations.

5.2. Entry Stability Control Technology. According to the foregoing entry stability control method, the optimized

support schemes and parameters are presented in Figure 11(a). Considering the roof and the advancing speed of the working face, the cutting height was 8.13 m, the drilling depth was 8.70 m, the diameter was 38 mm, the angle was 20°, the spacing was 600 mm, the sealing length was 2.7 m, the loaded length was 6 m, the explosive load per meter was 0.45 kg, and the shaped charge tube was used for forward blasting and series detonation.1#, 3#, 5#, 7#, 9# were blasting holes and 2#, 4#, 6#, 8# were pilot holes, as shown in Figure 11(b).

5.3. Application Effect. To verify the effect of the entry asymmetric control form of the surrounding rock, surface displacement monitoring was set up to monitor the deformation of roadway surrounding rock during the mining process. The measurement results are shown in Figure 12. The maximum convergence of the coal pillar rib was 40 mm, the solid coal rib was 15 mm, the roof was 20 mm, and the floor was 15 mm, respectively. Compared with the control effect before repairing, the maximum deformation of coal pillar rib has been reduced by 38%, the maximum deformation of solid coal rib has been reduced by 53%, and the deformation of roof and floor was basically unchanged. It can be seen that entry deformation was significantly reduced and there was no surge in deformation rate, which showed that the collaborative control method of roof cutting for pressure relief and support strengthening satisfied the long-term stability of entry. In addition, no roof fall, collapse, or rib spalling occurred during the service period of the entry. The surrounding rock control method provides a reference for similar asymmetric deformation entry affected by inclination.

6. Conclusions

Based on the above field investigation, theoretical analysis, and numerical simulation results, the conclusions can be summarized as follows:

(1) In gently inclined coal seam, the fracture line of the main roof was positioned above the coal pillar. Under the influence of inclination, horizontal stress was transferred to the coal pillar which was the main load carrier.

(2) Due to the influence of inclination, the overlying strata fracturing and rotation occur severely, the front abutment stress increases sharply, which is the internal cause of entry asymmetric deformation failure.

(3) According to asymmetric failure characteristics of entry, collaborative control technology of roof cutting for pressure relief and support strengthening is put forward.

Data Availability

The experimental test data used to support the findings of this study are included within the article.

Conflicts of Interest

The authors declare that they have no conflicts of interest.

Acknowledgments

The authors gratefully acknowledge the financial support provided by the National Natural Science Foundation of China (51674242 and 52074266).

References

[1] W. J. Guo, H. L. Wang, and S. J. Chen, "Coal pillar safety and surface deformation characteristics of wide strip pillar mining in deep mine," *Arabian Journal of Geosciences*, vol. 9, no. 2, p. 9, 2016.

[2] B. Du, C. Liu, J. Yang et al., "Abutment pressure distribution pattern and size optimization of coal pillar under repeated mining: a case study," *Arabian Journal of Geosciences*, vol. 13, no. 23, 2020.

[3] Z. Ma, C. Chen, X. Liang et al., "Field and numerical investigation on the stability of coal pillars of gob-side entry driving with top coal," *Arabian Journal of Geosciences*, vol. 13, no. 22, pp. 1–11, 2020.

[4] W. D. Wu, J. B. Bai, X. Y. Wang et al., "Numerical study of failure mechanisms and control techniques for a gob-side yield pillar in the sijiazhuang coal mine, China," *Rock Mechanics and Rock Engineering*, vol. 52, no. 6, 2018.

[5] Z. Xia, Q. L. Yao, G. S. Meng et al., "Numerical study of stability of mining roadways with 6.0-m section coal pillars under influence of repeated mining," *International Journal of Rock Mechanics and Mining Sciences*, vol. 138, 2021.

[6] H. W. Zhang, Z. J. Wan, Z. Y. Ma et al., "Stability control of narrow coal pillars in gob-side entry driving for the LTCC with unstable overlying strata: a case study," *Arabian Journal of Geosciences*, vol. 11, no. 21, 2018.

[7] Y. Zhang, Z. J. Wan, C. L. I. Fu et al., "Large deformation mechanism of roadway driving along goaf under unstable overlying rock strata," *Journal of Mining & Safety Engineering*, vol. 29, no. 4, pp. 451–458, 2012.

[8] B. Yu, Z. Zhang, T. Kuang, and J. Liu, "Stress changes and deformation monitoring of l coal pillars located in weak ground," *Rock Mechanics and Rock Engineering*, vol. 49, no. 8, pp. 3293–3305, 2016.

[9] E. Esterhuizen, C. Mark, and M. M. Murphy, "Numerical model calibration for simulating coal pillars, gob and overburden response," in *Proceedings of the 29th international conference on ground control in mining*, pp. 46–57, Morgantown, WV, USA, July 2010.

[10] A. J. Das, P. K. Mandal, P. S. Paul, and R. K. Sinha, "Generalised analytical models for the strength of the inclined as well as the flat coal pillars using rock mass failure criterion," *Rock Mechanics and Rock Engineering*, vol. 52, no. 10, pp. 3921–3946, 2019.

[11] W. Gao and M. Ge, "Stability of a coal pillar for strip mining based on an elastic-plastic analysis," *International Journal of Rock Mechanics and Mining Sciences*, vol. 87, pp. 23–28, 2016.

[12] S. H. Prassetyo, M. A. Irnawan, G. M. Simangunsong, R. K. Wattimena, I. Arif, and M. A. Rai, "New coal pillar strength formulae considering the effect of interface friction," *International Journal of Rock Mechanics and Mining Sciences*, vol. 123, Article ID 104102, 2019.

[13] J. J. Dai, P. F. Shan, and Q. Zhou, "Study on intelligent identification method of coal pillar stability in fully mechanized caving face of thick coal seam," *Energies*, vol. 13, no. 2, 2020.

[14] S. F. Liu, Z. J. Wan, Y. Zhang et al., "Research on evaluation and control technology of coal pillar stability based on the fracture digitization method," *Measurement*, vol. 158, 2020.

[15] W. Gao, "Influence of interaction between coal and rock on the stability of strip coal pillar," *Geomechanics and Engineering*, vol. 16, no. 2, pp. 151–157, 2018.

[16] A. J. Das, P. K. Mandal, P. S. Paul, R. K. Sinha, and S. Tewari, "Assessment of the strength of inclined coal pillars through numerical modelling based on the ubiquitous joint model," *Rock Mechanics and Rock Engineering*, vol. 52, no. 10, pp. 3691–3717, 2019.

[17] A. J. Das, P. S. Paul, P. K. Mandal et al., "Investigation of failure mechanism of inclined coal pillars: numerical modelling and tensorial statistical analysis with field validations," *Rock Mechanics and Rock Engineering*, vol. 54, pp. 3263–3289, 2021.

[18] P. X. Zhao, G. Li, S. G. Li et al., "Analysis of size effect of mechanical characteristics of coal pillars gob-side entry in inclined thick coal seam," *Journal of Mining & Safety Engineering*, vol. 36, no. 6, pp. 1120–1127, 2019, in Chinese.

[19] X. Z. Chen and M. Wang, "Research on surrounding rock deformation characteristics of gob-side entry driving in deep inclined coal seam and its control technology," *Journal of Mining & Safety Engineering*, vol. 32, no. 3, pp. 485–490, 2015, in Chinese.

[20] S. Zhang, X. Wang, G. Fan, D. Zhang, and C. Jianbin, "Pillar size optimization design of isolated island panel gob-side entry driving in deep inclined coal seam-case study of Pingmei No. 6 coal seam," *Journal of Geophysics and Engineering*, vol. 15, no. 3, pp. 816–828, 2018.

[21] W. X. Huang, *Study on the Mechanism of Water Breakout in the Mining Floor on High Pressurized Water in Chen Silou Coal mine*, China University of Mining and Technology, Xuzhou, China, 2017, in Chinese.

[22] M. G. Qian, P. W. Shi, and J. L. Xu, *Mine Pressure and Strata Control*, China University of Mining and Technology Press, Xuzhou, China, 2010, in Chinese.

[23] J. L. Xu and J. F. Ju, "Structural morphology of key stratum and ITS influence on strata behaviors in fully-mechanized face with super-large mining height," *Chinese Journal of Rock Mechanics and Engineering*, vol. 30, pp. 1547–1556, 2011, in Chinese.

[24] Q. Y. Xu, Q. G. Huang, and G. C. Zhang, "Fracture and instability mechanism and control technology of a narrow coal pillar in an entry in fully mechanized caving mining under intense effect mining," *Journal of Mining & Safety Engineering*, vol. 941, pp. 941–948, 2019, in Chinese.

[25] X. Xu, F. He, X. Li, and W. He, "Research on mechanism and control of asymmetric deformation of gob side coal roadway with fully mechanized caving mining," *Engineering Failure Analysis*, vol. 120, Article ID 105097, 2021.

Hindawi
Advances in Civil Engineering
Volume 2021, Article ID 9464225, 21 pages
https://doi.org/10.1155/2021/9464225

Research Article

Three-Dimensional Finite Difference Analysis on the Ground-Sequential Tunneling-Superstructure Interaction

Ali Lakirouhani,[1] **Reyhaneh Jafari**,[2] **and Hadi Hasanzadehshooiili**[3]

[1]*Department of Civil Engineering, Faculty of Engineering, University of Zanjan, Zanjan, Iran*
[2]*Department of Civil Engineering, Faculty of Engineering, University of Zanjan, Zanjan, Iran*
[3]*Department of Civil and Water Engineering, Laval University, Quebec, Canada*

Correspondence should be addressed to Ali Lakirouhani; rou001@znu.ac.ir

Received 9 April 2021; Revised 20 May 2021; Accepted 1 June 2021; Published 14 June 2021

Academic Editor: Chunshun Zhang

In this paper, a three-dimensional finite difference analysis is presented to investigate the interactive effects of sequential tunneling and the superstructure on the settlement profile of the ground. To simulate the practical sequential tunneling procedure, tunnel excavation is conducted in a step-by-step framework; tunnel excavation starts from the beginning of the model and is updated in a continuous manner, and the installation of the tunnel support system is done with a delay step compared to tunnel excavation. The numerical modeling accuracy is validated using the available analytical and numerical solutions for both two-dimensional and three-dimensional simplified cases. The well-validated modeling procedure is adopted to investigate effects of tunnel diameter, depth of tunneling, and number of superstructure stories on the profile of occurring settlements. Two cases of free-field and three-dimensional superstructural modeling are compared with regard to the effect of tunneling. In addition, the effect of tunneling advancement on the generation of excess structural forces and moments are studied as another important factor in the soil-tunneling-superstructure interaction problem. It is observed that, in the free-field case, with advancing the tunnel face, the longitudinal settlement profiles approach the steady-state condition and the maximum ground settlement tends to converge to a specific value, whereas as the tunnel passes under a structure, the settlement increases steadily as the tunnel progresses. There is a direct relationship between the depth and diameter of the tunnel and the settlement. In addition, the effect of the number of superstructure stories on the maximum settlement is more considerable compared to the free-field condition. According to the results, when the tunnel passes under 8-story and 12-story structures, the maximum settlement increases by 40% and 70%, respectively, compared to the free-field condition. It is also shown that tunneling-induced settlements result in the regeneration of structural forces.

1. Introduction

Due to the occurrence of settlements and settlement-induced displacements in surface structures, excavating tunnels in urban areas has always been of a great importance. Besides, structures constructed on the ground may be affected by the advancements in the tunneling in terms of displacements, drifts, and excess internal and structural forces/moments. This interactive nature makes it a coupled interaction problem, in which not paying enough and proper consideration to its modeling can be conducive to severe and intolerable consequences. Ground-tunneling-superstructure interaction problem can be analyzed from two different aspects. In the first approach, effects of the superstructure on the tunneling-induced displacements and stress fields are evaluated, while the second one deals with the vulnerability of superstructures against the displacements and stresses that emerged from the tunneling. In this regard, proper and accurate design of tunneling projects needs an in-depth understanding of this interaction nature. In recent years, such an investigation has been carried out based on empirical [1, 2], analytical [3], and numerical [4–10] methods. Among these methods, numerical techniques with the ability to model the more complicated problems (in forms of

geometry, stress field, material property, etc.) have gained more attention. Mroueh and Shahrour showed that it is essential to adopt a three-dimensional modeling approach, which considers simultaneous effects of tunneling and superstructure. It was due to three-dimensional nature of the tunnel excavation and the nonlinear behavior of the soil [11]. In some other numerical investigations, to decrease the calculation time and efforts, the superstructure was assumed to be an elastic beam/plate with flexural and bending stiffness equal to the corresponding stiffness of the original superstructure [12–16]. Displacements and settlements that occurred were then assessed with advancing the tunnel face. Some researchers addressed low modeling accuracies and not presenting structural damages as shortcomings available in this approach. Despite those researchers, other studies showed that, with calibrating simplified numerical models (in the form of simplified superstructure) with the field cases, there can be more accurate numerical results [17, 18]. But there was not still a general agreement in view of the simplified or detailed superstructural modeling. A need for properly characterizing the model using real field cases, not assuring its suitability for modeling more complicated cases and a need for the structural vulnerability analysis were the main reasons that three-dimensional modeling of the superstructure was further developed in recent years. Dias and Kastner conducted a case study on the effects of the superstructure (in the form of a structural frame) on the tunneling-induced ground settlements. They presented a comparison between the obtained results with the observations from a 6-story building located on the line 2 of Cairo metro. Compared to the results obtained from the field, their transverse settlement profile was wider, and the maximum settlement value was increased in the vicinity of the superstructure. Also, internal structural forces were affected by the tunneling operations [19]. Mroueh and Shahrour studied effects of the weight and the stiffness of a multistory frame on the transverse settlement profile and the internal structural forces using the three-dimensional modeling. As the first approach, they calculated the tunneling-induced settlements for the free-field state and as the next solution step, and they exerted the calculated settlement values to the superstructure. The second approach was a more accurate one, in which the tunnel advancement and the effect of the superstructure were considered simultaneously. It was concluded that the simplified model overestimates internal structural forces and moments as it neglects the stiffness of the superstructure in the calculation of settlements. They also investigated effect of the weight of the superstructure and found that not considering the structural weight will result in higher internal structural forces compared to the reality [11]. Jenck and Dias three-dimensionally studied the tunneling problem considering a structural frame as the superstructure (using columns and slabs elements, founded on a raft); evaluating effects of the weight and the stiffness of the structure on the settlement profiles, they found that the stiffness of the structure plays an important role in the modeling accuracy. They showed that the transverse settlement profile of the free field and the model with the consideration of the superstructure follow a relatively similar behavior [20]. Maleki et al. modeled a tunnel and the superstructure in a decoupled manner and did not take the simultaneous effects of tunneling and superstructure into consideration in their three-dimensional models. To model the superstructure, they analyzed two cases of an elastic plate as the foundation and the three-dimensional geometry of the superstructure. Results obtained from the three-dimensional geometry for the superstructure were more acceptable. Although values of the settlement obtained from two approaches were different, there were still common trends in the settlement profiles for both cases. Observed differences were believed to be attributed to the uniform distribution of the weight of the structure in the plate model compared to the dead column loads in the three-dimensional model of the superstructure [21]. What has not yet been considered in the earlier studies is the sensitivity of the settlement profiles to the size of the studied numerical model. Among the conducted studies, there is not a common agreement on the selection of the proper model sizes. As a matter of fact, the size of the numerical model should be adopted in a way to avoid the boundary effects on the results. Most researchers selected $6D$ and $3D$ values, respectively, for the minimum distance between the center of the tunnel and the vertical boundaries and the minimum distance between the center of the tunnel and the bottom boundary (D represents the tunnel diameter). Franzius studied an excavation length of more than 21 times of the tunnel diameter in his three-dimensional investigation and the distance between the last tunnel face and the vertical side boundary was selected to be 11.5 times of the tunnel's diameter. Focusing on the longitudinal settlement profiles, it was observed that, with advancing tunnel face, steady-state settlement situation was not satisfied, emphasizing that the size of the model affects results [22]. Franzius et al. investigated the effect of the model size on the settlement and suggested that, to minimize the boundary effect, there should be at least a distance from the first excavation facing to the vertical side boundary equal to the 13 times of the tunnel diameter. But there was not still a steady-state situation in their longitudinal settlement profiles [23]. Some other researchers introduced $(H + 4D)$, $(H + 3D)$, and $(3H)$, respectively, as the minimum required height, length, and width of the model, where H and D, respectively, represent depth of the tunnel and its diameter. In addition to the model size, proper selection of the suitable constitutive law plays an important role in the determination of the tunneling-induced settlements. Chow (1994) selected two linear-elastic and elastoplastic constitutive models to numerically analyze the tunneling problem. The performance of the linear-elastic model with a linearly increasing soil stiffness was realized to be more accurate [24]. Calabresi et al. presented that numerical models developed based on the simple and elastoplastic constitutive laws lead to a wider settlement profile and are not suitable for studying the soil inelastic behavior in small strain conditions [25]. Guedes and Santos Pereira adopted a linear elastoplastic constitutive law to model the second line of Shanghai metro and observed that their settlement profiles were not in close agreement with the field observations [26]. Hence, in this study, special consideration is paid to the proper selection of

the model size, also the appropriate constitutive law. In addition, as described, there are some studies on the two- and three-dimensional numerical analysis of the settlements induced by the tunnel advancement considering the tunnel-structure interaction available in the literature [7, 8, 10, 11, 15, 20–23]. But there are limited ones when introducing a detailed, three-dimensional geometry for the superstructure into the problem. As far as the authors know, there is not such an investigation which adopts the described advantages and employs a finite difference method to investigate the longitudinal settlement profile. Fargnoli et al. focusing on a case study shed some light on the problem [27]. But, to come into a comprehensive and accurate conclusion, such a study should be accompanied by an in-depth parametric study to investigate effects of different parameters of the tunnel and the superstructure. Thus, this paper presents a parametric study to show the role of the depth of tunneling, tunnel diameter, and the geometry of the superstructure using a well-validated three-dimensional finite difference investigation. As there has not been a three-dimensional finite difference framework in the literature to parametrically assess effects of the tunnel advancement on the performance of structural members of the superstructure, this study presents such evaluations as an important novelty.

2. Definition of the Problem and Research Significance

This paper utilizes finite difference modeling approach and FLAC 3D [28] software to comprehensively investigate the soil-sequential tunneling-superstructure interaction problem. Like the previous studies on the sequential TBM tunneling in urban areas, it is assumed that the whole tunnel cross section is excavated in a single step and the tunnel advancement is carried out in a staged construction manner with a constant round length. The thickness of the installed concrete lining is assumed to be 40 cm and the installation of the permanent support system has a delay step relative to the excavation steps. As there was not a common agreement between researchers on the suitable model size and the constitutive law, as the preliminary phase, a considerable number of numerical models with different sizes and governing constitutive laws were built, to evaluate the sensitivity of the settlement profile to these two factors. In this regard, free-field analyses are carried out for a variety of model sizes; also constitutive laws and then longitudinal settlement profiles with the advancement of tunneling are calculated and analyzed for each of the studied cases as a basis for the selection of the proper size of the model and for the preliminary assessment of the selected constitutive law prior to its characterization (due to the large number of the studied cases, the results are not presented here). Model dimensions and constitutive parameters presented in the paper are those attained from the intensive preliminary investigations. Longitudinal settlement profile of the ground with the sequential tunneling advancement is also developed with the consideration of the effect of the real geometry of the superstructure as a contribution of the present study. Besides, the impact of tunnel advancement on the structural elements of the superstructure is comprehensively investigated. In this regard, developed numerical models are first well validated against available theoretical and other numerical methods. Next, parametric studies are done to fill the gap between available studies, each assessing one or more of the affecting factors. To do this, effects of depth of tunneling, diameter of the tunnel, and the geometry (number of stories) of the superstructure on the longitudinal settlement profile are all addressed in a unique study. In addition, generation of the excess internal structural forces and moments in the superstructure due to sequential tunneling is evaluated.

3. Validation of Numerical Models

Validation of the conducted numerical studies is carried out in three different phases. The first following section deals with two-dimensional verifications (both analytical and numerical ones), while the second one compares the results obtained from the three-dimensional numerical studies with the available theoretical relationships.

3.1. Two-Dimensional Validation of Models with Simplified Cases. In this section, two-dimensional models are developed to validate the accuracy of the numerical modeling with available theoretical and numerical solutions.

3.1.1. Comparison of Ground Reaction Curve with Hoek's Analytical Solution. Due to tunnel excavation, existing stress field will be disturbed and redistributed around the excavated tunnel and, consequently, excavated area can converge. The first validation phase investigates displacements occurring at the tunnel crown, sidewalls, and floor based on the dimensionless internal tunnel pressure (ratio of tunnel support pressure, P_i , to the initial field stress, P_0), known as the convergence-confinement graph of tunnels. Calculated graphs are then compared to the analytical solution presented by Hoek [29]. According to Hoek, soil failure can be addressed using the following relationship based on the classical Mohr–Coulomb criterion [29]:

$$\sigma = \sigma_{\text{cm}} + K, \tag{1}$$

where

$$\sigma_{\text{cm}} = \frac{2c\cos\phi}{1-\sin\phi}, \qquad K = \frac{1+\sin\phi}{1-\sin\phi}, \tag{2}$$

where σ_{cm} is the uniaxial compressive strength of materials (in MPa), c is the cohesion (in MPa), and ϕ represents the friction angle. The minimum internal lining pressure (critical pressure, P_{cr}), where the material behavior changes from elastic to plastic, can be calculated using Equation (3). For a tunnel with the radius of R and under isotropic, far-field in situ stress of p_0 and an inner pressure of P_i (from the internal support to the tunnel wall), if $P_i > P_{\text{cr}}$ (Figure 1), the

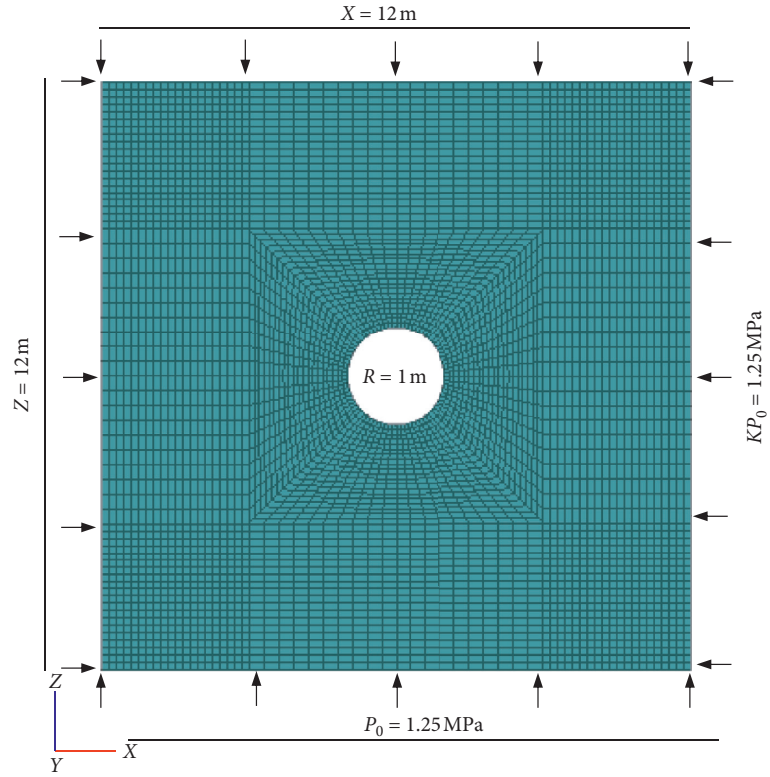

Figure 1: The geometry of the two-dimensional model used to perform the validation.

behavior of materials around the tunnel will be elastic and the radial displacement around the tunnel can be calculated as presented in the following equation:

$$P_{cr} = a\left(\frac{2P_0 - \sigma_{cm}}{1 + K}\right), \tag{3}$$

$$u_{ie} = \frac{R(1+\upsilon)}{E}(P_0 - P_i), \tag{4}$$

where υ and E, respectively, represent Poisson's ratio and Young's modulus of material.

According to Figure 1, a two-dimensional model with the dimensions of $12^m \times 12^m$ with a 2 m in diameter circular tunnel is considered for the modeling purposes. Poisson's ratio and Young's modulus of materials, respectively, were assumed to be $\upsilon = 0.22$ and $E = 60$ MPa. Far-field, in situ stress is $P_0 = 1.25$ MPa. Regarding the comparison presented in Figure 2, there are suitable consistency between results of the numerical analysis and the analytical relationship.

3.1.2. Comparison of Settlements with the Research Conducted by Dragojević. In this section, a two-dimensional model is developed to model the problem previously solved by Dragojević as the second validation phase. Geotechnical and geomechanical properties of the layered studied soil are presented in Table 1. Dragojević, using finite element Diana software, studied the longitudinal and transverse surface settlements and compared two-dimensional and three-dimensional modeling results and found that the suitable stress release percentage should be $\beta = 63\%$ for his two-dimensional models [30]. Like dimensions and features of the original problem, a $50^m \times 80^m$ model is developed (Figure 3), in which the depth of tunneling and the tunnel diameter are, respectively, 15 m and 6 m and the stress release factor is 63%. Also materials are assumed to follow an elastoplastic behavior with the Mohr–Coulomb criterion.

After tunnel excavation, the concrete lining is installed. A linear-elastic model is used as the governing constitutive law for the support system. The thickness of concrete is 0.35 m and other mechanical properties of the support system are $\upsilon = 0.15$, $E = 15$ GPa, and $P = 2500$ kg/m^3. As presented in Figure 4, there is a suitable agreement between the results of the finite difference modeling of the present study and the finite element modeling of Dragojević [30].

3.2. Three-Dimensional Validation of the Model with Analytical Relationships. As the free-field analysis is the preliminary step of all the analyses conducted in the present study, the three-dimensional model of a tunnel is built and compared to the analytical relationship of the longitudinal ground settlement presented by Panet and Guento as shown in the following equation:

$$S_v(x) = S_{v\max}(x)\left(0.28 + 0.72\left(1 - \left(\frac{0.84}{0.84 + x^*}\right)^2\right)\right), \tag{5}$$

where X is the distance between the desired section and the tunnel face, $S_v(X)$ presents the longitudinal ground settlement across the excavation direction, $S_{v\max}(X)$ is the

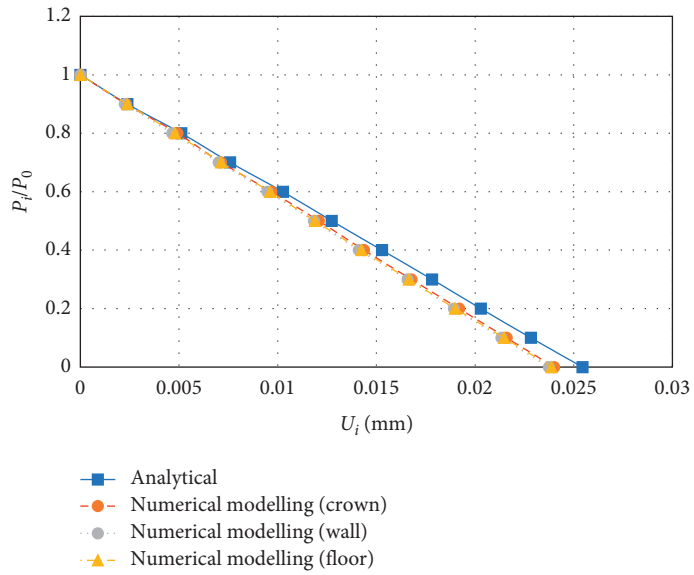

Figure 2: Comparison between the ground reaction curves calculated from the two-dimensional finite difference modeling and the analytical relationships of Hoek.

Table 1: Geotechnical and geomechanical properties of the material [30].

Parameter	Index	Unit	First layer (h_1)	Second layer (h_2)	Third layer (h_3)
Coefficient of lateral soil pressure	k	—	0.65	0.85	0.58
Density	ρ	kg/m^3	1850	2000	2000
Friction angle	ϕ	($\circ$)	23	20	25
Cohesion	c	kPa	18	20	60
Young's modulus	E	MPa	10	15	60
Poisson's ratio	v	—	0.4	0.3	0.3

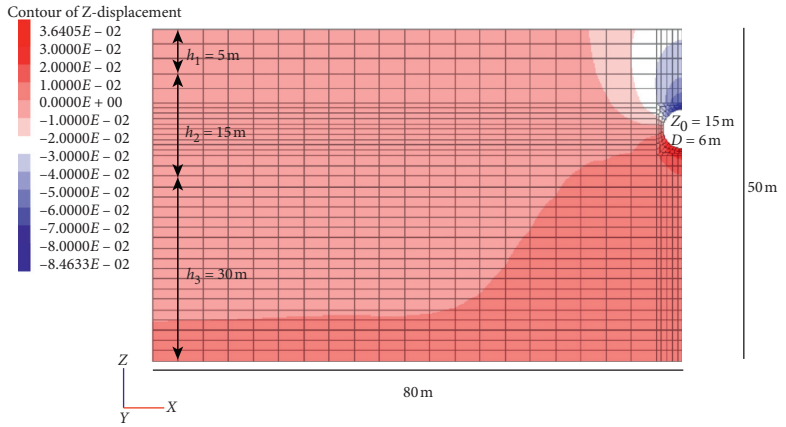

Figure 3: Geometry and meshing of the two-dimensional model used for validation, as well as vertical displacement contour.

maximum longitudinal ground settlement at the steady state condition, and $X^* = (X/R)$ (R is the tunnel radius).

Unlu and Gercek presented a continuous function for the prediction of the longitudinal settlement in the elastic condition as shown in Equation (6). In Equation (6), $X^* = 0$ represents the position of the tunnel face; also, negative and positive X values, respectively, stand for the points in front and behind the tunnel face [32].

$$S_v(x) = S_{v\max}(x)\left[(0.22v + 0.19) + A_b\left(1 - \left(\frac{B_b}{(B_b + x^*)}\right)^2\right)\right], \quad (x^* > 0), \tag{6}$$

where v is Poisson's ratio of the ground and

$$A_a = -(0.22v + 0.19),$$
$$B_b = 0.39v + 0.65. \tag{7}$$

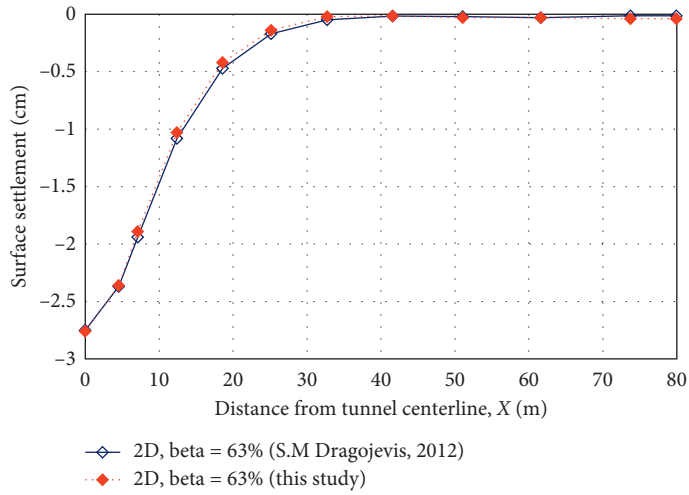

Figure 4: Comparison between the ground's transverse settlement profile of the present study and Dragojević [30].

Geometry of the model is discretized using 8-node, quadratic grids. Model dimensions are, respectively, 80 m, 140 m, and 85 m in width, length, and height. The depth and the diameter of the tunnel are, respectively, 30 m and 6 m. Vertical side boundaries are fixed in the horizontal direction, while the bottom boundary is fixed in both horizontal and vertical directions. After the generation of in situ stresses, the tunnel excavation is conducted in 2 m intervals and continues to the last section, which has 80 m distance from the initial side boundary. Mechanical behavior of the concrete support system is linear elastic. Its thickness is 0.4 m, and other elastic parameters of the support system, which is installed with a delay step: $\upsilon = 0.15$, $E = 20$ GPa, and $P = 2500\,\text{kg/m}^3$. Figure 5 compares the results obtained from the numerical modeling of the present study with the analytical relationships proposed in (6) and (7). X direction is considered as the excavation direction. It should be noted that the relationship suggested by Panet and Guento (1982) is only applicable for the estimation of the settlements behind the tunnel face and cannot predict values of the settlement for those points located in front of the tunnel face. As shown in Figure 5, results are in a good agreement and the superiority of the numerical model in tracking the gradual settlement calculation near to the tunnel face is obvious.

4. Consideration of Superstructure: Three-Dimensional Modeling versus Free-Field Case

In this section, the free-field case, in which the effect of superstructure on the tunneling-induced ground settlement is disregarded, is compared to the case of the detailed three-dimensional modeling of the superstructure. As the common features used in all the cases, model dimensions are, respectively, 140 m, 140 m, and 85 m in X, Y, and Z directions (Figure 6). Bottom boundary is fixed in both horizontal and vertical directions, while side boundaries are restricted from displacements in the horizontal direction. In the cases of the presence of the structure, the structure is symmetrically placed over the tunnel (with regard to the tunnel axis across X-direction). Three-dimensional geometry of the superstructure is built using structural beam elements and beam-to-column connections are considered rigid. All the modeled beams and also all the columns (in different stories) have the same cross-sectional shape and features. All the spans are 6 m in length and the height of all stories is 3 m. Table 2 presents geotechnical and geometrical properties of the studied ground and tunnel, while Table 3 shows mechanical and geometrical specifications of the beam-column elements used in the modeling of 8-story concrete building (applied as a benchmark for studying the real geometry of the superstructure).

The longitudinal ground profiles of the settlement for the two cases of existence of the structure and the free field obtained from numerical analysis are shown in Figure 7. In this figure, the longitudinal profiles of the settlement are shown for every ten meters of the tunnel advance and by arrow, and the position of the tunnel front surface is marked on each graph. Based on the results obtained for the tunneling in the free-field condition, with the tunnel advancements, longitudinal settlement profiles reach a steady state and all the profiles tend to a peak settlement value. In contrast, the results gained from the case of the three-dimensional superstructure modeling show that, with the tunnel advancement, there is a progressive trend in settlements until the tunnel face passes through the location of the superstructure. With advancing the tunnel face toward the location of the structure, differences between free-field settlements and the superstructure's case increase and the maximum difference corresponds to the middle of the superstructure. In this state, the superstructure experiences an unbalanced settlement with respect to the tunnel face. After that, with passing the tunnel face through the location of the superstructure, this unbalanced settlement decreases. Also, the maximum occurring settlement refers to the state that the tunnel face completely passes through the superstructure. In addition, despite the case of free-field settlements, there is not a steady state condition prior to passing through the structure. GF and STSI, respectively, refer to the "Ground-Free-Field" and "Soil-Tunnel-Superstructure-

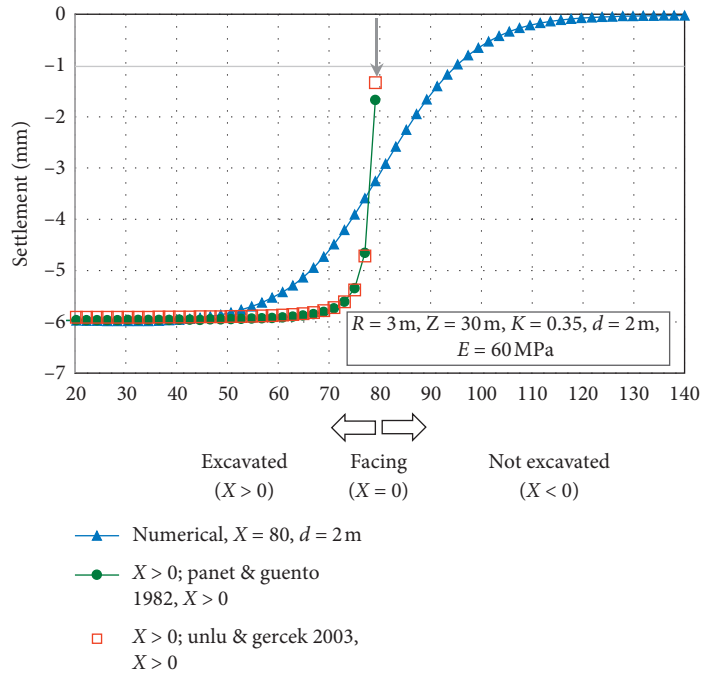

Figure 5: Comparison between the longitudinal ground settlement obtained from the numerical model and the analytical relationships.

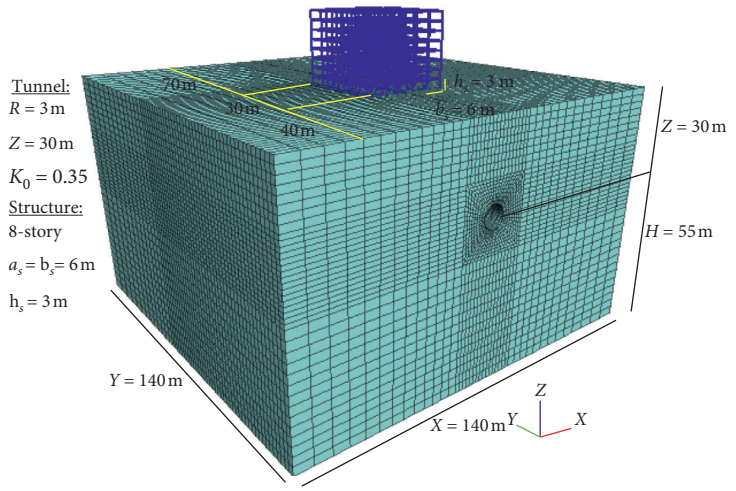

Figure 6: Geometry and meshing of three-dimensional models and surface structures.

Table 2: Geotechnical and geometrical properties of the studied ground and tunnel.

Parameter	Index X	Unit	Value
Coefficient of lateral earth pressure	k	–	0.35
Density of the ground	ρ	kg/m^3	1700
Ground friction angle	ϕ	($\circ$)	30
Ground cohesion	c	kPa	30
Ground Young's modulus	E	MPa	60
Ground Poisson's ratio	υ	—	0.25
Radius of tunnel	R	m	3
Depth of tunnel	Z	m	30
Round length	L_{exc}	m	22
Density of support system	P	kg/m^3	2500
Young's modulus of support system	E	GPa	25
Poisson's ratio of support system	υ	—	0.15
Thickness of support system	t	m	0.4

Table 3: Geometrical and mechanical properties of the concrete beam and column elements.

Parameter	Index	Unit	Value
Young's modulus	E	GPa	25
Poisson's ratio	υ	–	0.25
Cross section of beams	$B \times H$	cm^2	20×20
Cross section of columns	$B \times L$	cm^2	20×40
Moment of inertia of the beams (y)	I_y	cm^4	106666.7
Moment of inertia of the beams (z)	I_z	cm^4	26666.7
Moment of inertia of the columns	$I_y = I_Z$	cm^4	213333.3

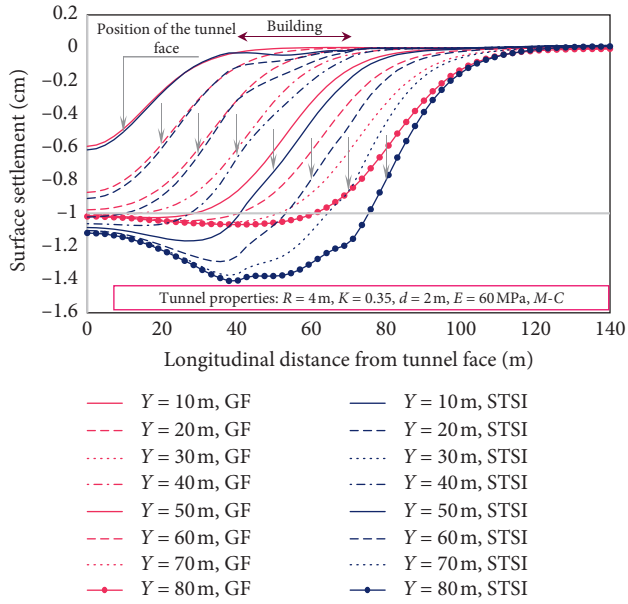

Figure 7: Comparison between longitudinal tunneling-induced settlement profiles of the free-field and three-dimensional superstructure cases with regard to the tunnel advancement.

Interaction" cases. Figures 8 and 9 present displacement and stress contours in the vertical direction for the case of an 8-story concrete structure, respectively.

5. Results and Discussion

As described, proper consideration of the superstructure plays an important role in the solution of the soil-tunnel-superstructure problem. In this regard, the three-dimensional approach for the modeling of the superstructure is considered for the parametric analyses. Hence, the well-validated three-dimensional finite difference model described in the previous sections is adopted to study effects of the diameter of tunnel, the depth of tunneling, and the geometry of the superstructure on the tunneling-induced ground settlements. Moreover, the vulnerability of the superstructure against tunneling effects is discussed characterizing internal forces and moments of its structural elements.

5.1. Effect of the Tunnel Diameter on the Longitudinal Settlement Profile. In this section, assuming that all other parameters are kept constant, the problem is solved for three different tunnel diameters, 8 m, 12 m, and 16 m. As shown in Figures 10–12 , with increasing the tunnel diameter, settlements increase considerably. As Figures 10–12 simultaneously show settlements of both free-field and superstructure-included cases, it is understood that, with increasing the diameter of the tunnel, the effect of the superstructure on the tunneling-induced settlements increases.

Comparing different cases, effects of the diameter of the tunnel on the tunneling-induced settlements are clearly shown in Figure 13. As depicted, its effect is even more considerable below the superstructure.

5.2. Effect of the Depth of Tunneling on the Longitudinal Settlement Profiles. To investigate the effect of the depth of the tunneling, three different tunneling depths are modeled (15 m, 30 m, and 45 m) and the obtained results are separately presented in Figures 14–16 considering both free-field and soil-superstructure interaction conditions.

Figure 17 compares settlement profiles for different tunneling depths. It is shown that, with increasing the depth of tunneling, settlement increases, but the effect of the superstructure on the tunneling-induced settlements decreases. In other words, for the tunneling depths higher than 45 m, the interaction effects of the tunnel excavation and the superstructure decrease and the general trends of STSI cases will be like those observed for free-field cases.

5.3. Effect of the Geometry (Number of Stories) of the Superstructure on the Longitudinal Settlement Profile. 6-, 8-, 12-, and 17-story structures are considered for evaluating the impact of the geometry (number of stories) of the superstructure on the longitudinal settlement profiles. Dimensions of foundations for these 6-, 8-, 12-, and 17-story structures are, respectively, $18^m \times 18^m$, $30^m \times 30^m$, $30^m \times 30^m$, and $42^m \times 42^m$. Settlement profiles are presented in Figures 18–21 . Also, Figure 22 compares effects of all four studied cases (different numbers of stories) in a single figure. It is observed that when the tunnel face completely passes through the superstructure, longitudinal settlement profile of the 6-story building shows a slight heaving behavior, which can be attributed to the low number of stories and, hence, the enhanced stiffness of the superstructure. In such condition, the settlement profile is quite identical to the free-field graph. With increasing the number of stories and the weight of the structure, maximum settlement of the ground significantly increases and the heaving behavior (under the structure) decreases. Also, for structures with more than 17 stories, there is a considerable difference between the settlement profiles of free-field and soil-superstructure interaction cases.

5.4. Effect of Sequential Tunneling on the Internal Forces and Displacements of the Superstructure. Tunneling-induced ground settlements cause excess internal forces and moments in the structural elements of the superstructure. In this section, the benchmark model geometry and properties described in the previous sections are used to evaluate

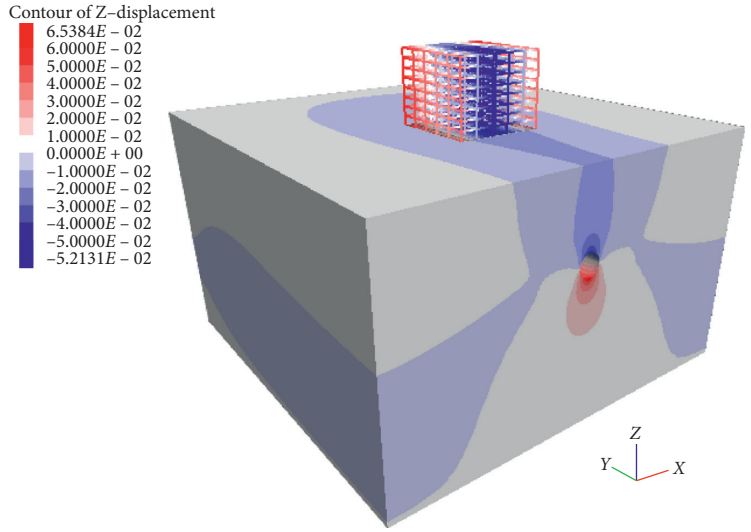

Figure 8: Displacement contours in the vertical direction induced by the tunnel advancement for the model of the tunnel with an 8-story concrete structure.

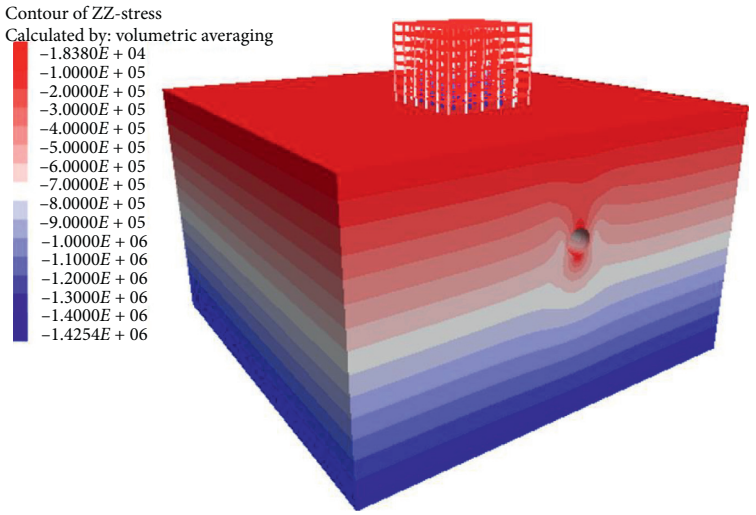

Figure 9: Stress contours in the vertical direction induced by the tunnel advancement for the model of tunnel with an 8-story concrete structure.

internal forces, bending moments and displacements of beams and columns of the superstructure with the tunnel advancement. Figure 23 shows the geometry of the tunnel and the 8-story superstructure, which is symmetric in the X-direction with respect to the tunnel axis. Benchmark structural elements investigated in this paper, which are selected from the ground floor, are located above the tunnel axis and in the point with the coordination of $Y = 40$ m (distance of the element from the tunnel opening). The studied beam and columns are, respectively, shown using B_1 and C_2, C_3, C_4 symbols (Figure 23) and the variation of the axial force and the vertical displacement of the columns C_2, C_3, C_4; also, the bending moment and the vertical displacement of the beam B_1 (at the beginning, middle, and the end of the beam) with the tunnel advancement are then depicted.

Vertical displacement of the column C_2, C_3, C_4 while the tunnel passes through the structure is shown in Figures 24–26 , respectively. As expected from the settlement profiles, with advancing the tunnel face, the vertical displacement of the column increases. The rate of this increase will be even more, while the tunnel face is under the superstructure. Comparing the diagrams of these three figures, it can be seen that the shorter the distance from the column to the axis of the tunnel, the more the column settles. For example, the maximum vertical displacement of column C_2 has the shortest distance to the axis of the tunnel, 1.4 cm, while for columns C_3 and C_4 it is 1.1 cm and 0.83 cm, respectively.

The diagrams in Figures 27–29 show the changes in the axial force of these three columns against the advance of the tunnel. It is observed that the C_2 column settlement causes

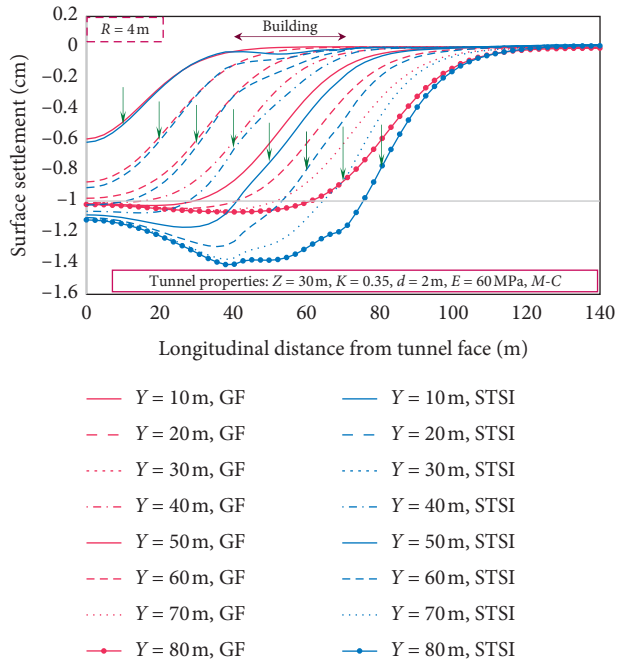

Figure 10: Comparison of longitudinal settlement profiles between free-field and superstructure-included cases for the tunnel with the diameter of 8 m.

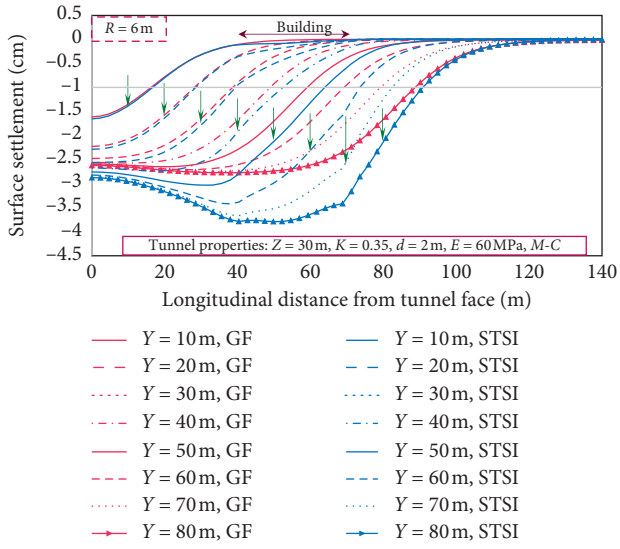

Figure 11: Comparison of longitudinal settlement profiles between free-field and superstructure-included cases for the tunnel with the diameter of 12 m.

some of the axial force of this column to be released and the absolute value of the axial force decreases as the tunnel progresses (Figure 27). The axial force released from this column is transmitted by beams to adjacent columns. In the case of column C_3 in Figure 28, it can be seen that as the tunnel progresses, there is a decreasing trend in absolute axial force in this column, but when the tunnel is placed under the structure, this trend slows down and is almost constant. This is because the transfer of axial load from column C_2 to this column modulates the decreasing trend of the axial force of this column. Next, for column C_4, it can be seen in Figure 29 that, unlike the two adjacent columns, the absolute magnitude of its axial force increases as the tunnel progresses. In other words, although the subsidence of this column reduces its

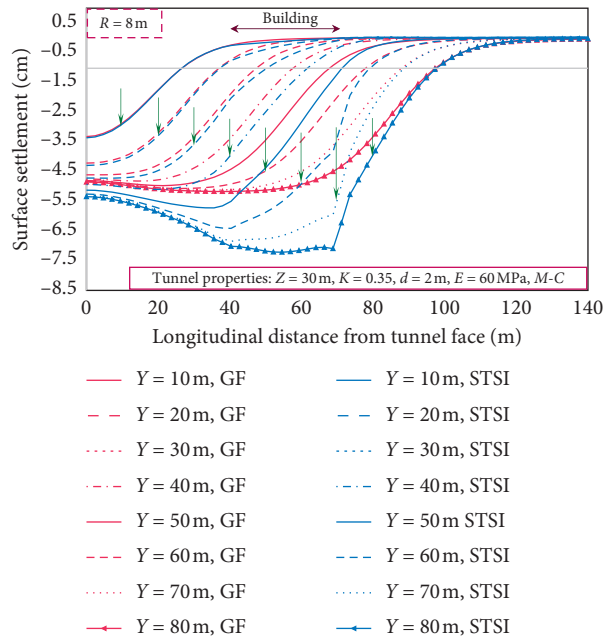

Figure 12: Comparison of longitudinal settlement profiles between free-field and superstructure-included cases for the tunnel with the diameter of 16 m.

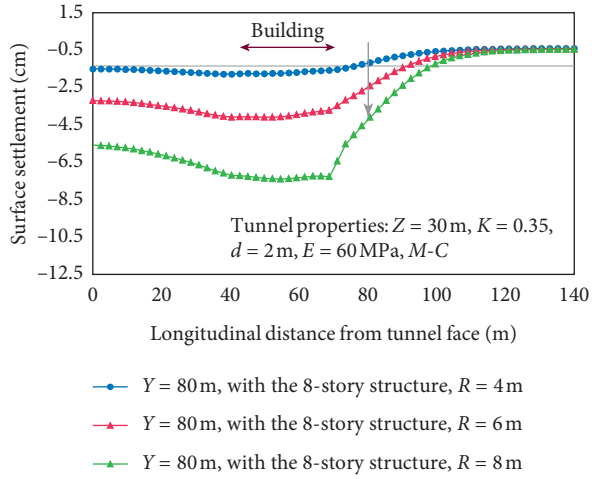

Figure 13: Comparison of the longitudinal tunneling-induced settlement profiles under the structure for different diameters of the tunnel.

axial force, the share of axial force from the two columns C_2 and C_3 ultimately increases its axial force.

The axial force transmission is done by the middle beam; because of this transmission, the middle beam will experience a higher bending moment to carry on the force from the side column to the other ones. Figure 30 shows the variation of the bending moment at three different points of the beam versus the tunnel advancement.

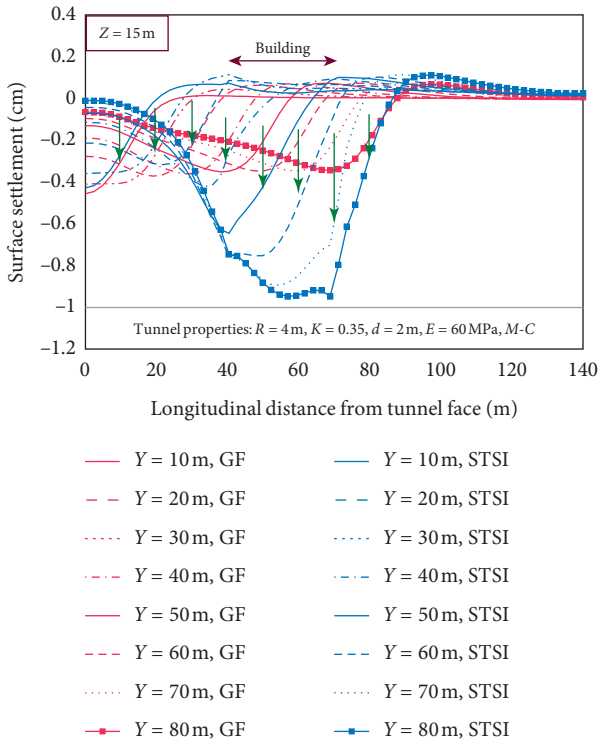

Figure 14: Comparison of longitudinal settlements between free-field and superstructure-included cases for the tunneling depth of 15 m.

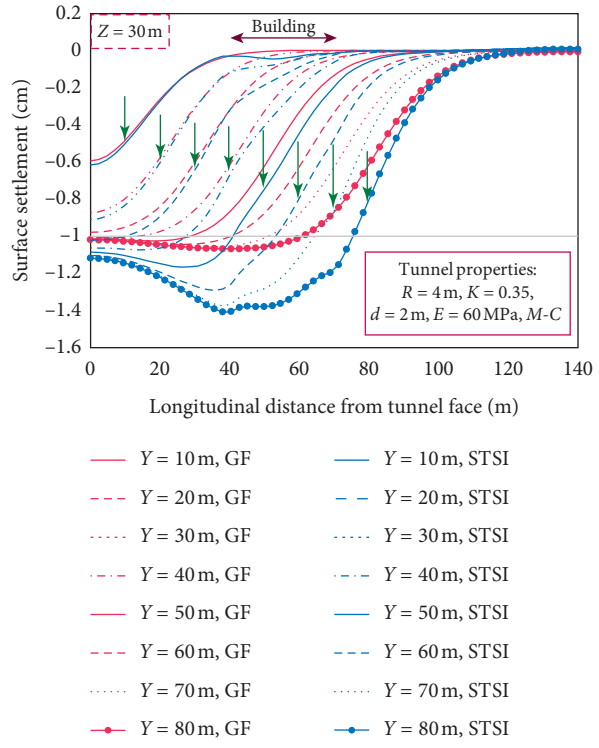

Figure 15: Comparison of longitudinal settlements between free-field and superstructure-included cases for the tunneling depth of 30 m.

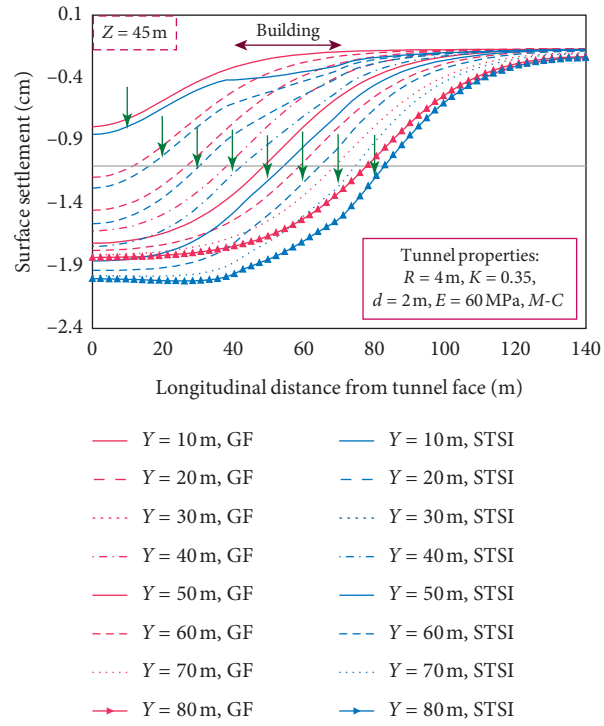

Figure 16: Comparison of longitudinal settlements between free-field and superstructure-included cases for the tunneling depth of 45 m.

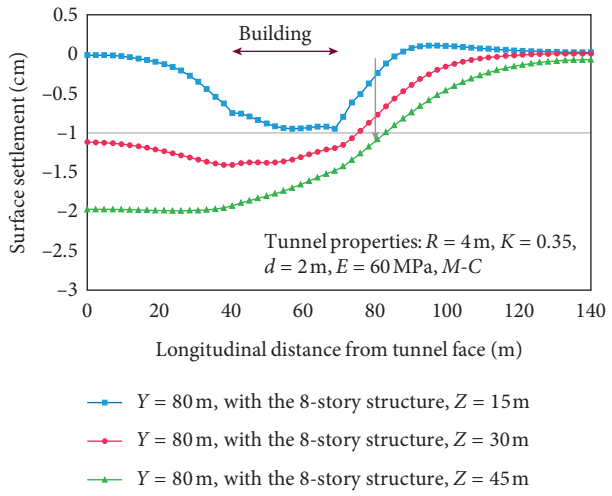

Figure 17: Comparison of the longitudinal tunneling-induced settlement profiles for different depths of tunneling.

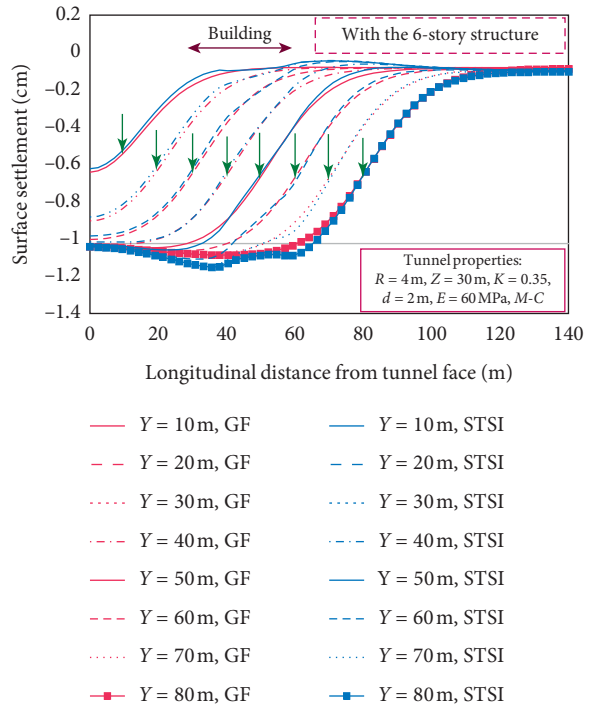

Figure 18: Comparison of longitudinal settlements between free-field and superstructure-included cases for the 6-story structure.

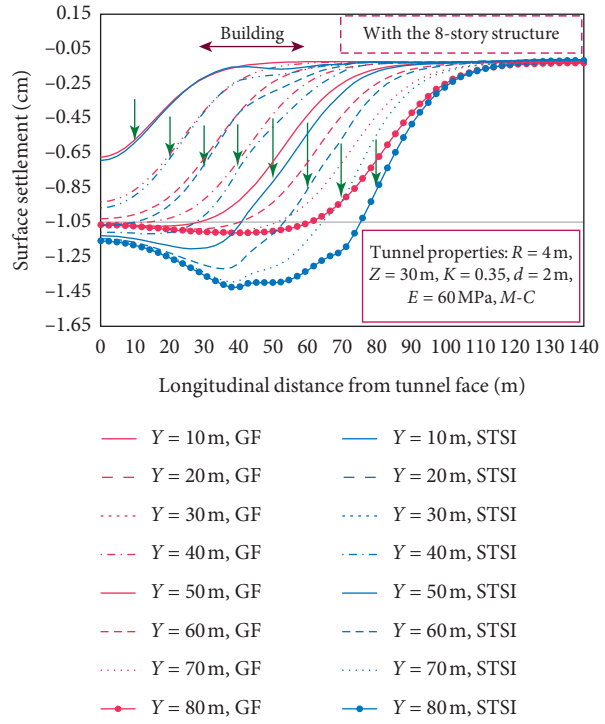

Figure 19: Comparison of longitudinal settlements between free-field and superstructure-included cases for the 8-story structure.

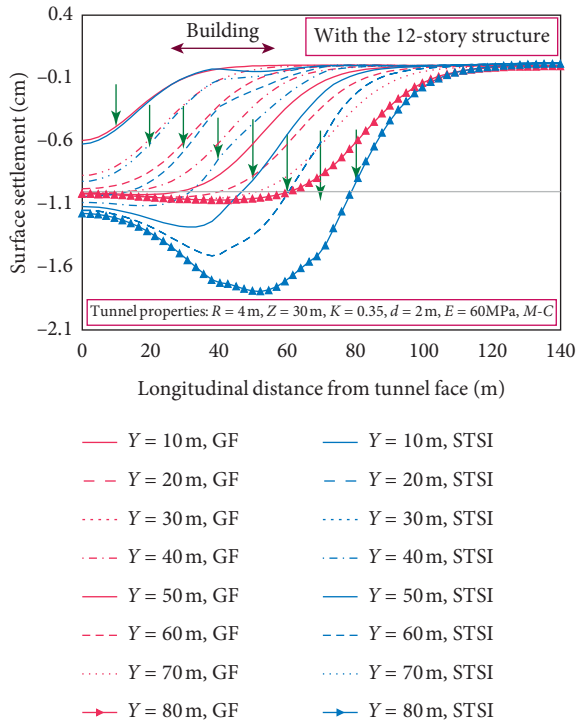

Figure 20: Comparison of longitudinal settlements between free-field and superstructure-included cases for the 12-story structure.

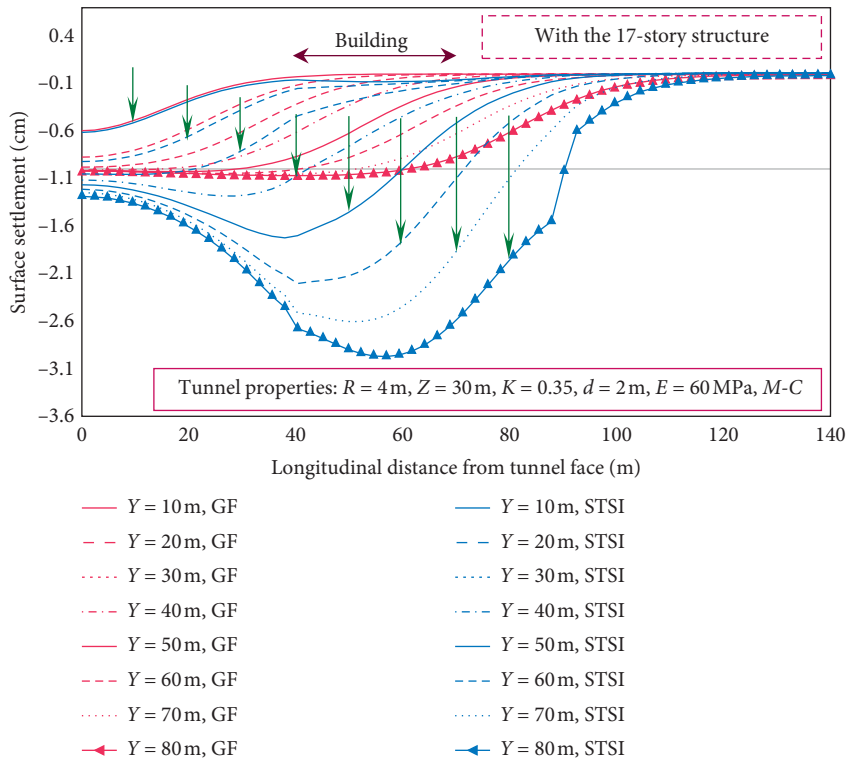

Figure 21: Comparison of longitudinal settlements between free-field and superstructure-included cases for the 17-story structure.

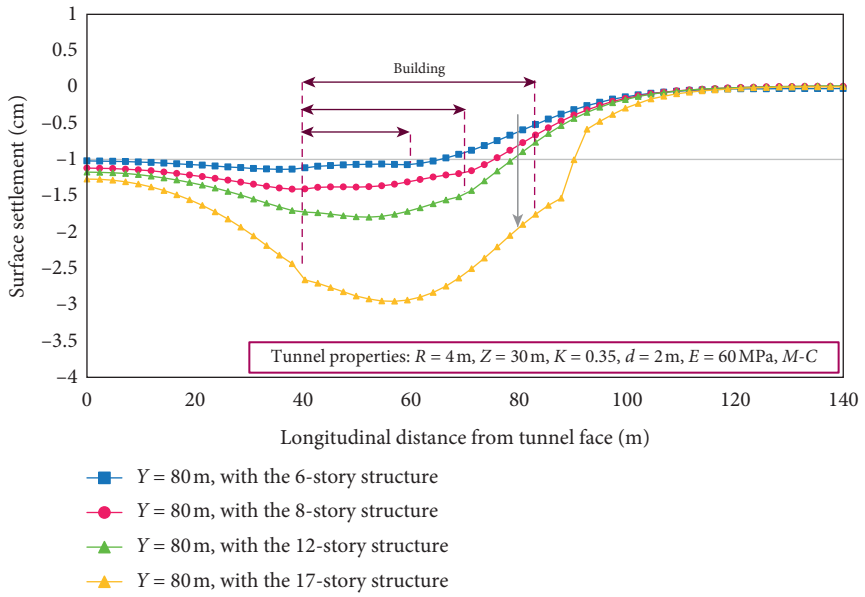

FIGURE 22: Comparison of the longitudinal tunneling-induced settlement profiles under the structure for different numbers of stories of the superstructure.

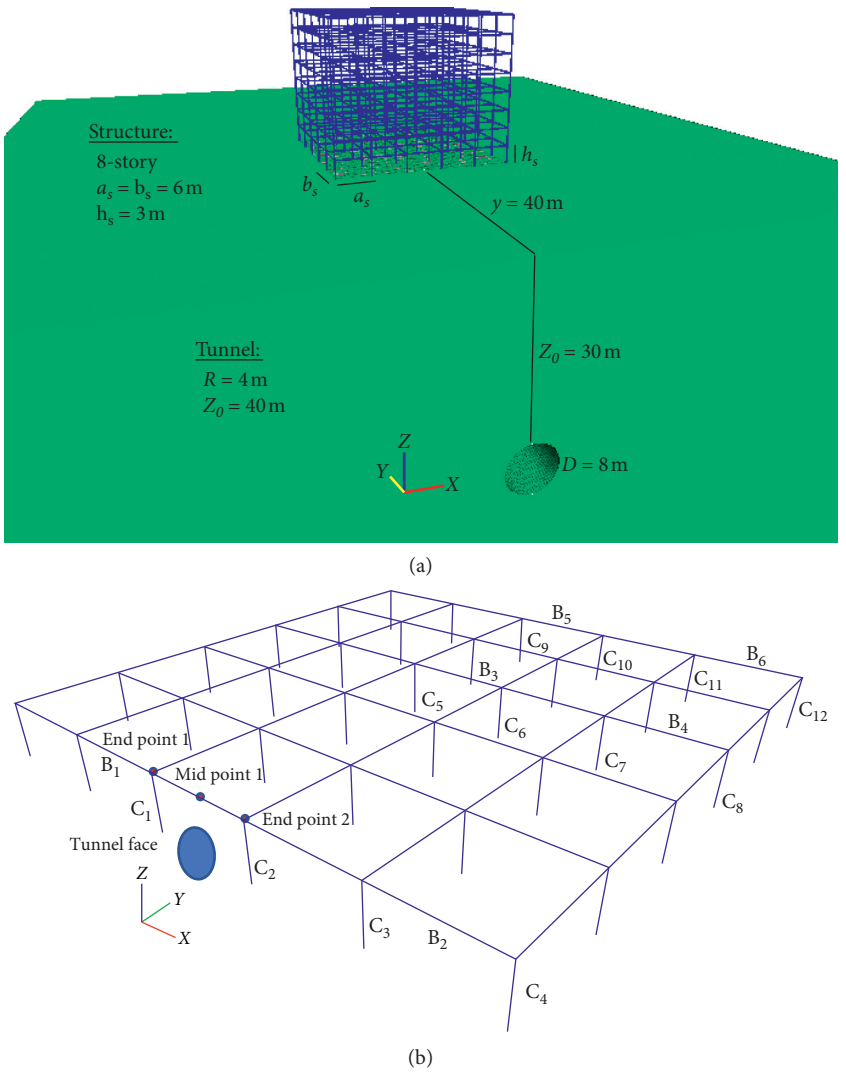

FIGURE 23: (a) Geometry of the tunnel and the superstructure. (b) Location of the studied beams and columns on the ground floor of the superstructure.

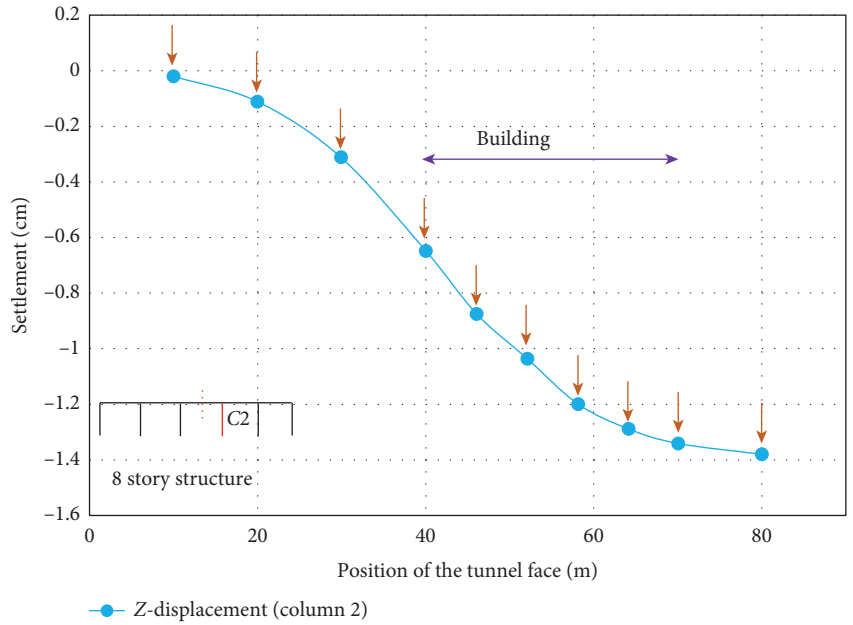

Figure 24: Variation of the vertical displacement of column C_2 versus the tunnel advancement.

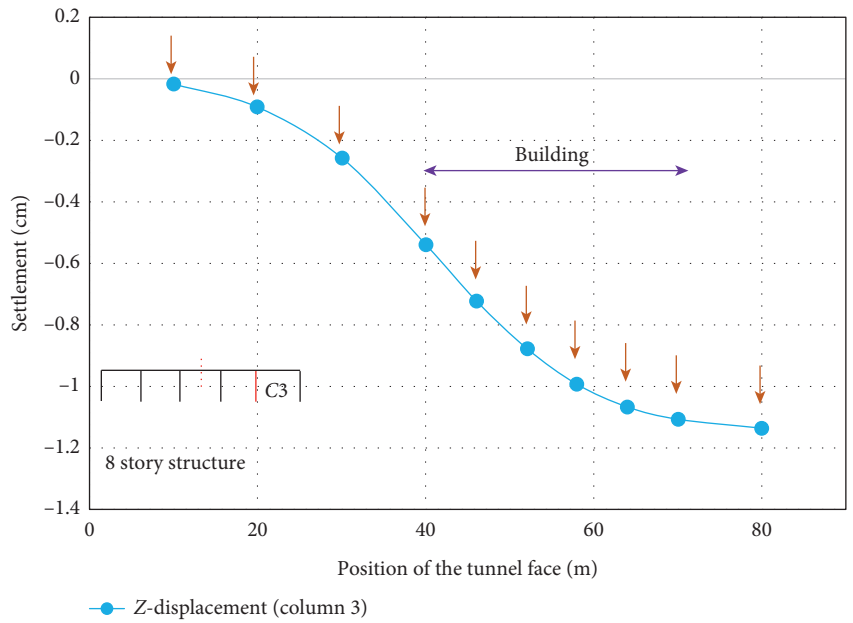

Figure 25: Variation of the vertical displacement of column C_3 versus the tunnel advancement.

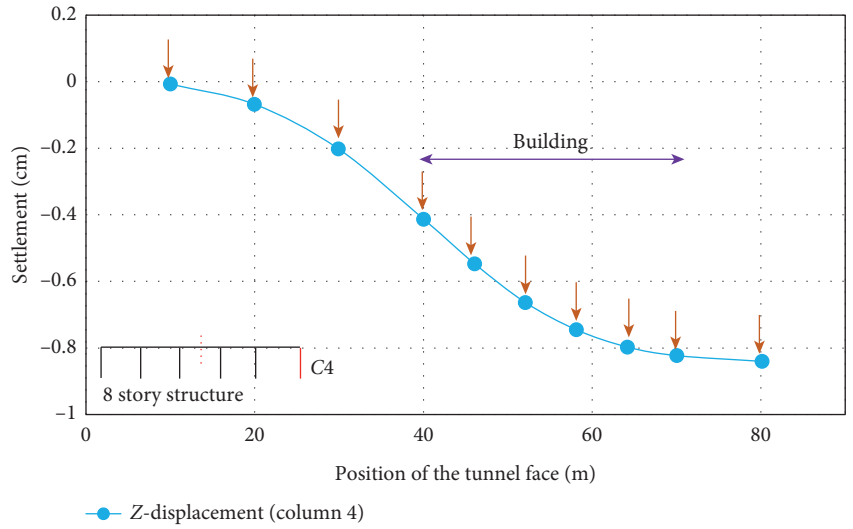

Figure 26: Variation of the vertical displacement of column C_4 versus the tunnel advancement.

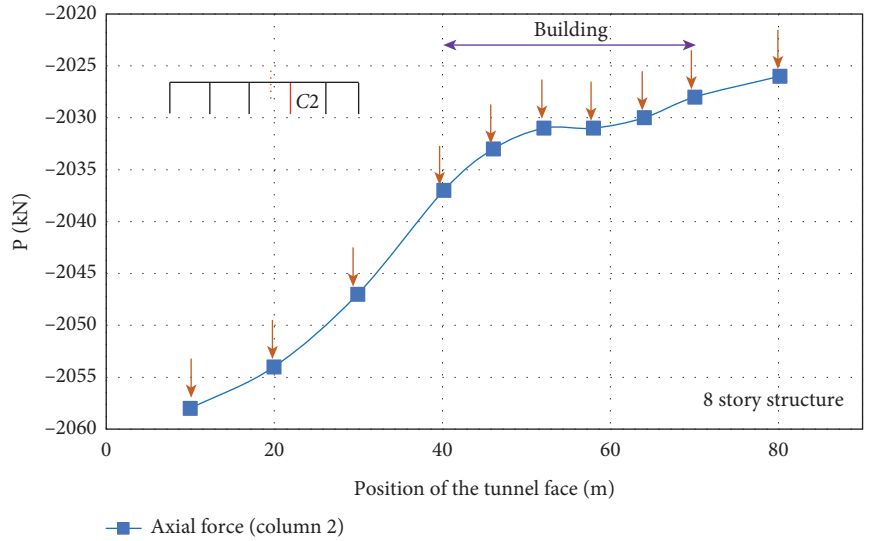

Figure 27: Variation of the axial force of column C_2 versus the tunnel advancement.

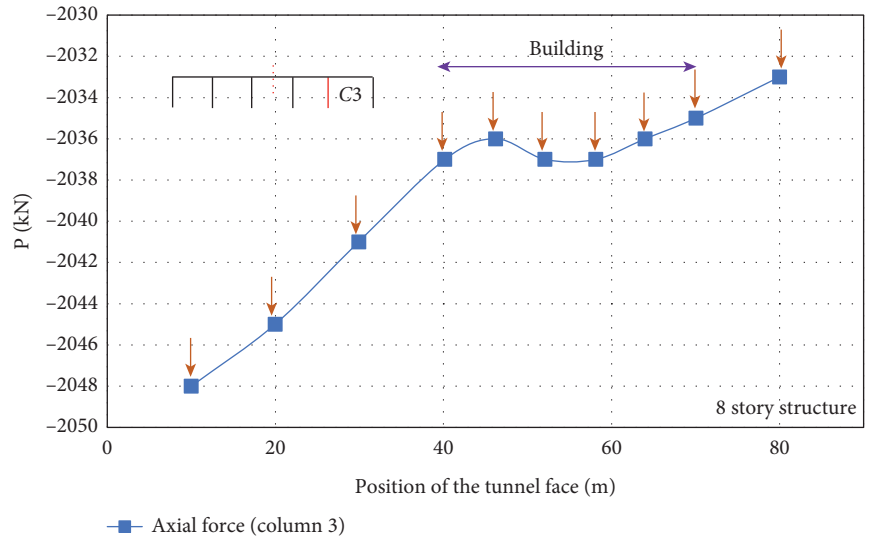

Figure 28: Variation of the axial force of column C_3 versus the tunnel advancement.

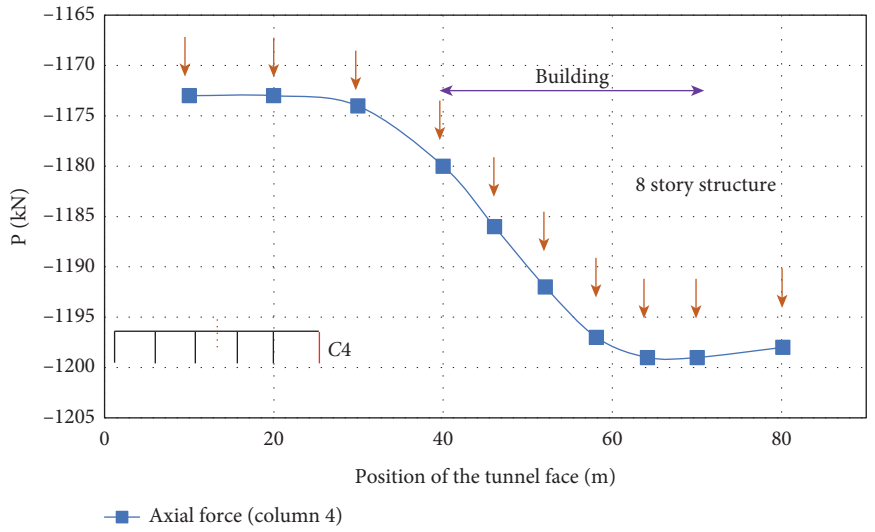

Figure 29: Variation of the axial force of column C_4 versus the tunnel advancement.

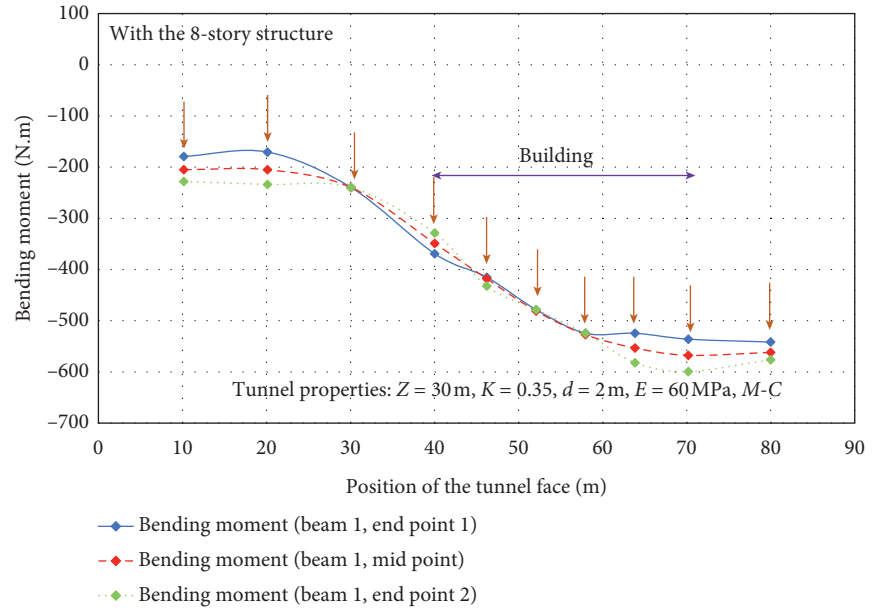

Figure 30: Variation of the bending moment of beam B_1 with the tunnel advancement.

6. Conclusion

In this paper, the ground-tunnel-superstructure interaction problem is studied based on the three-dimensional finite difference modeling and using Flac 3D software. To investigate effects of the sequential tunneling, the excavation of the whole section in the tunnel face is done in a single step, while the tunnel advancement is carried out in a stepwise, sequential manner. Also, the installation of concrete support is done with a delay step toward the progress of the tunnel. The developed numerical model is first validated against available two-dimensional and three-dimensional, analytical, and numerical models. Then, the well-validated numerical approach is adopted for conducting parametric studies on the effects of different parameters. It should be noted that, considering the meaningful impact of the proper selection of the material constitutive law and the model size on the shape and the values of the longitudinal settlement profile, an intensive sensitivity analysis is conducted prior to the final analyses. Based on the sensitivity of the longitudinal, tunneling-induced settlement profiles to different selected sizes and behaviors, proper model size and constitutive law are adopted. As another contribution of the present paper, effects of the diameter and the depth of the tunnel and also the number of the stories of the superstructure on the tunneling-induced longitudinal ground settlements are investigated. Excess internal forces and moments caused in the elements of the structure because of the tunnel advancement are also

evaluated and further discussed. Based on the results obtained, the following can be concluded:

(i) For the free-field case, with advancing the tunnel face, longitudinal settlement profiles tend to a steady state, and steady state means that, in the longitudinal profiles, the vertical settlement will no longer exceed a maximum value.

(ii) Models with the superstructure behave differently; superstructure causes a considerable change in both figures and values of the longitudinal settlement profiles. Settlements increase as the tunnel face advances until the facing passes through the location of the superstructure. With advancing the facing toward the location of the structure, differences between free-field settlements and the superstructure's case increase. Maximum difference corresponds to the midpoint of the superstructure; in this state, the superstructure experiences an unbalanced settlement with respect to the tunnel face. After that, with passing the tunnel face through the location of the superstructure, this unbalanced settlement decreases. Maximum occurring settlement refers to the state that the tunnel face completely passes through the superstructure. In addition, despite the case of free-field settlements, there is not a steady-state condition prior to passing through the structure.

(iii) With increasing the diameter of the tunnel, tunneling-induced settlements significantly increase. In other words, the increased diameter of the tunnel enhances the effect of the superstructure on the settlements. This is the main reason why there is a higher difference between the settlements of the free-field and superstructure included cases. Increasing the tunnel diameter increases both maximum ground settlement and the value of the settlement at the tunnel opening (at the beginning of the model).

(iv) With increasing the depth of tunneling, values of the settlement increase; however, effects of the interaction between tunnel excavation and the superstructure decrease. For example, when a tunnel is excavated at a depth of 15 meters under an 8-story structure, the maximum settlement on the ground increases by more than 130% compared to the free-field condition, but when the tunnel is at a depth of 45 meters under an 8-story structure, only a 15% increase in settlement occurs.

(v) In creasing the depth of the tunneling increases both maximum ground settlement and the value of the settlement at the tunnel opening.

(vi) When the tunnel face completely passes through the superstructure, the longitudinal settlement profile of the 6-story building shows a slight heaving behavior, which can be attributed to the low number of stories and, hence, the enhanced stiffness of the superstructure. In such a condition, the settlement profile is quite identical to the free-field graph. With increasing the number of stories and the weight of the structure, maximum settlement of the ground significantly increases and the heaving behavior under the structure (shown for the low-story buildings) decreases. For example, when the number of stories increases to 8, the maximum settlement relative to the ground without a surface structure increases by 40%, and when the surface structure is 12 stories, it is about 70%. For structures with more than 17 stories, there is a considerable difference between the settlement profiles of free-field and superstructure-soil interaction cases.

(vii) It is observed that the effect of number of stories of the superstructure on the maximum settlement is more noticeable compared to its impact on the settlement value at the opening of the tunnel.

(viii) The most important impact of the tunnel excavation on the superstructure is redistribution of the internal, structural forces and moments in the beams and columns. Due to the ground settlement and the vertical displacements observed in the beams/columns, the stress release occurs, and the axial force of the columns decreases or increases. The closer the column is to the tunnel axis, the greater its settlement, and the steeper the column settlement curve as the tunnel face passes under the structure. Due to the subsidence of the columns adjacent to the axis of the tunnel, their axial force increases, but the axial force of the columns farther from the axis of the tunnel increases due to the redistribution of force between the columns, even if they are settled. For example, numerical analysis performed in this paper showed that the passage of a tunnel with a diameter of 8 meters under an 8-story building and at a depth of 30 m causes the column located at a distance of 3 m from the axis of the tunnel (C_2) to settle 1.4 cm and its axial force is reduced by 31 kN, and the column, located 9 m from the axis of the tunnel (C_3), settles 1.1 cm and its axial force is reduced by 14 kN and column located 15 m from the axis of the tunnel (C_4) will settle 0.82 cm, but its axial force will increase by 25 kN.

Data Availability

No data were used to support this study.

Conflicts of Interest

The authors declare that they have no conflicts of interest.

References

[1] R. B. Peck, "Deep excavations and tunneling in soft ground," in *Proceeding of the 7th International Conference.SMFE, State of the Art*, pp. 225–290, Mexico, MX, USA, July 1969.

[2] M. O'reilly and B. New, *Settlements above Tunnels in the United Kingdom-their Magnitude and Prediction*, Institution of Mining & Metallurg, London, UK, 1982.

[3] N. Loganathan and H. G. Poulos, "Analytical prediction for tunneling-induced ground movements in clays," *Journal of Geotechnical and Geoenvironmental Engineering*, vol. 124, no. 9, pp. 846–856, 1998.

[4] P. Vermeer, P. Bonnier, and S. Möller, "On a smart use of 3D-FEM in tunnelling," in *Proceeding of Eighth International Symposium on Numerical Models in Geomechanics*, pp. 361–366, Rome, Italy, April 2002.

[5] S. C. Möller, *Tunnel Induced Settlements and Structural Forces in Linings*, University. Stuttgart Institute of Geotechnik, Stuttgart, Germany, 2006.

[6] A. Ghorbani and H. Hasanzadehshooiili, "A comprehensive solution for the calculation of ground reaction curve in the crown and sidewalls of circular tunnels in the elastic-plastic-EDZ rock mass considering strain softening," *Tunnelling and Underground Space Technology*, vol. 84, pp. 413–431, 2019.

[7] R. Katzenbach, S. Leppla, M. Vogler, M. Seip, and S. Kurze, "Soil-structure-interaction of tunnels and superstructures during construction and service time," *Procedia Engineering*, vol. 57, pp. 35–44, 2013.

[8] G. Giardina, M. J. DeJong, and R. J. Mair, "Interaction between surface structures and tunnelling in sand: centrifuge and computational modelling," *Tunnelling and Underground Space Technology*, vol. 50, pp. 465–478, 2015.

[9] A. H. Akhaveissy, "Analysis of tunnel and super structures for excavation," *Scientia Iranica*, vol. 18, no. 1, pp. 1–8, 2011.

[10] A. Mirhabibi and A. Soroush, "Three-dimensional simulation of interaction between surface buildings and twin tunnelling regarding the surface settlement," *Geotechnical Geological Engineering*, vol. 38, pp. 5143–5166, 2020.

[11] H. Mroueh and I. Shahrour, "A full 3-D finite element analysis of tunneling-adjacent structures interaction," *Computers and Geotechnics*, vol. 30, no. 3, pp. 245–253, 2003.

[12] C. Wroth and J. Burland, "Settlement of buildings and associated damage," in *SOA Review, Conf. Settlement of Structures*Pentech Press, Cambridge, UK, 1974.

[13] R. Mair, "Prediction of ground movements and assessment of risk of building damage due to bored tunnelling," in *Proceedings of the. Geotechnical Aspects of Underground Construction in Soft Ground*, London, UK, April 1996.

[14] D. Potts and T. Addenbrooke, "A structure's influence on tunnelling-induced ground movements," in *Proceedings of the Institution of Civil Engineers*, Geotechnical Engineering, Muscat, Oman, April 1997.

[15] J. Franzius and T. Addenbrooke, "The influence of building weight on the relative stiffness method of predicting tunnelling-induced building deformation," in *Proceedings of the Third International Symposium (IS-Toulouse 2002) Geotechnical Aspects of Underground Construction in Soft Ground*, pp. 53–57, Cambridge, UK, October 2002.

[16] C. Leung, J. Yu, Y. Chow, Y. Ng, H. Tan, and C. Hua, "Tunneling beneath existing buildings supported on shallow foundations," in *Proceedings of the 4th Geo-China International Conference*, pp. 251–258, Shandong, China, July 2016.

[17] H. Burd, G. Houlsby, C. Augarde, and G. Liu, "Prediction of tunnel-induced settlement damage to masonry Structures," OUEL Report 2162/98, Department of Engineering Science, Oxford, UK, 1998.

[18] J. Pickhaver, H. Burd, and G. Houlsby, "An equivalent beam method to model masonry buildings in 3D finite element analysis," *Computers & Structures*, vol. 88, no. 19-20, pp. 1049–1063, 2010.

[19] D. Dias and R. Kastner, "Tunneling in soils-ground movements, and damage to buildings," in *Proceedings of the Planning and Engineering for the Cities of Tomorrow. Second International Conference on Soil Structure Interaction in Urban Civil Engineering Swiss*, Federal Institute of Science and Technology, Mookkannoor, India, January 2002.

[20] O. Jenck and D. Dias, *Tunnelling on Urban Areas: 3D Numerical Analysis of Soil/structure Interaction*, Is Amsterdam'05, Amsterdam, Netherland, 2006.

[21] M. Maleki, H. Sereshteh, M. Mousivand, and M. Bayat, "An equivalent beam model for the analysis of tunnel-building interaction," *Tunnelling and Underground Space Technology*, vol. 26, no. 4, pp. 524–533, 2011.

[22] J. N. Franzius, *Behaviour of Buildings Due to Tunnel Induced Subsidence*, University of London, London, UK, 2003.

[23] J. N. Franzius, D. M. Potts, and J. B. Burland, "The influence of soil anisotropy andK0on ground surface movements resulting from tunnel excavation," *Géotechnique*, vol. 55, no. 3, pp. 189–199, 2005.

[24] L. Chow, *The Prediction of Surface Settlements Due to Tunnelling in Soft Ground*, University of Oxford, Oxford, UK, 1994.

[25] G. Calabresi, S. Rampello, and L. Callisto, "Prediction of tunnel-induced displacements in historic buildings: the case of castel S.angelo," in *Proceedings of the Twelf European Conference on Soil Mechanics and Geotechnical Engineering (Proceedings) The Netherlands Society of Soil Mechanics and Geotechnical Engineering*, Ministry of Transport, Amsterdam, Netherlands, June 1999.

[26] P. Guedes and C. Santos Pereira, "The role of the soil K_0 value in numerical analysis of shallow tunnels," in *Proceeding of the International Symposium on Geotechnical Aspects of Underground Construction in Soft Ground*, CRC Press, Boca Raton,FL, USA, December 2000.

[27] V. Fargnoli, C. G. Gragnano, D. Boldini, and A. Amorosi, "3D numerical modelling of soil-structure interaction during EPB tunnelling," *Géotechnique*, vol. 65, no. 1, pp. 23–37, 2015.

[28] Itasca Consulting Group, Inc, *FLAC3D — Fast Lagrangian Analysis of Continua in Three-Dimensions*, Itasca, Minneapolis, MN, USA, 7.0 edition, 2019.

[29] E. Hoek, "Support for very weak rock associated with faults and shear zones," in *Proceedings of the Rock Support and Reinforcement Practice in Mining*, Routledge, Kalgoorlie,Australia, March 1999.

[30] S. Dragojević, "Analysis of ground settlement caused by tunnel construction," *Građevinar*, vol. 64, no. 7, pp. 573–581, 2012.

[31] M. Panet and A. Guento, "Analysis of convergence behind the face of a tunneli," in *Proceeding of the International Symposium Tunneling*, pp. 197–204, IMM, London, UK, June 1982.

[32] T. Unlu and H. Gercek, "Effect of Poisson's ratio on the normalized radial displacements occurring around the face of a circular tunnel," *Tunnelling and Underground Space Technology*, vol. 18, no. 5, pp. 547–553, 2003.